GPS　QZSS

A STUDY ON INTEGRATION OF GPS AND

QUASI-ZENITH SATELLITE SYSTEM

MARCH 2008

Graduate School of Marine Science and Technology
Tokyo University of Marine Science and Technology
Doctor Course of Applied Marine Environmental Studies

Yun　Zhang

Deeply thanks for my parents and my wife

GPS　　QZSS

A STUDY ON INTEGRATION OF GPS AND

QUASI-ZENITH SATELLITE SYSTEM

2008.3

Graduate School of Marine Science and Technology
Tokyo University of Marine Science and Technology
Doctor Course of Applied Marine Environmental Studies

Yun　Zhang

LIST OF CONTENTS

LIST OF TABLES

LIST OF FIGURES

ABSTRACT

A Study on Integration of GPS and Quasi-zenith Satellite System

GPS　　QZSS

0462035 Yun Zhang

Course of Applied Marine Environmental Studies

Tokyo University of Marine Science and Technology

QZSS

GPS　　　　　　　　　Galileo

GPS

L1C/A　　　L1C　　　L2C　　　　L5

QZSS

/　　　　　　　　　　　　　　　　100%

QZSS

1.

GPS　L5　　　　　　　QZSS

L1　L2　L5

Klobuchar

Saastamoinen　　　　　　　　DLL　PLL

QZSS

2.

QZSS　　　　　　　　　　　　60ºE-152ºE　　　10ºS-60ºN

: 125ºE-145ºE　　　25ºN-45ºN

QZSS　　　　　95%

15　　　24　　　　　　minNVS　5　　　　　　　　24

PDOP 2.3% 28%　　　　　　　　　　　　　　　　　　　　　　　　minNVS

6　　　　　　　PDOP　25%

/　　　　　　　　　　/

/　　　　　　　　　　　　　L1　　　DGPS

24　　　　　　　　　　　　　4% 47%

16% 47%　　　　　　　　RTK　　　24

ASR　99.0%

QZSS

3.　　　　8
QZSS　　　　　　　8　　　　　　　　　　　　　　8
　　　　　8

8　　　　　　8
　　　　24　　PDOP

8

4.　　　DGPS
　　　　　　QZSS　　　L1　　　DGPS
　　　　　/　　　　　　　　　　　　/
14.167km　　　　　/　　　　　　180.871km
/　(　　　521.715km　　QZSS
9.0　　　　10.0　　　　　　　10.64
13.46　　　　　　　　15.83　　16.92
19.21　　26.32　　　　　　QZSS
DGPS　　　　　　　　　DGPS

5.　　RTK　　　　　　　AR　/　　ASR
QZSS　　　　　　　　　AR
　　　　　　AR

QZSS　　　　　　　24　　　　　5

RTK

24   ASR   99.8%   ASR   97.6%

                                                              GF

                        AR   ASR

85   70%

            QZSS   AR

ACKNOWLEDGEMENTS

CHAPTER 1
INTRODUCTION

1.1 BACKGROUND

From last decade, the US has implemented several improvements for both civil and military applications. In GPS modernization, a second civil signal (L2C), and a third civil signal on an additional frequency L5 would be offered for civil users. The first modernized Block IIR (designated as the IIR-M) with L2C was launched on 26 September 2005, and L5 will be broadcast from the first IIF satellite (the next generation of GPS satellite) in the new future. Therefore, future GPS users can receive three frequency signals on L1, L2 and L5, which could improve the accuracy and reliability of GPS positioning. [Yun Zhang, Nobuaki Kubo, Akio Yasuda. (2005)]

The dual-frequency Global Positioning System (GPS) has found widespread use for many precision applications. However, there are still some situations where using GPS only cannot provide the required precision and reliability. For GPS complementation and augmentation, Japan has started Quasi-zenith Satellite System (QZSS) project since 2002. The basic design and manufacturing of the engineering models of the on-board equipment started in 2004. [Kogure, S., Kawano, I., and Kajii, M., 2003].

Japanese QZSS is a regional space-based positioning system that used constellation of satellites placed in multiple orbital planes. QZSS consists of three satellites, the system covers regions in East Asia and Oceania centering and at least one satellite stays around the zenith for about 8 hr and is visible with high elevation. [Yun Zhang, Falin Wu, Akio Yasuda (2007)]. The first QZSS satellite will be launched in 2009. That GPS and QZSS have complete compatibility and interoperability has been agreed in the 5th TWG (Technical Working Group), on January 26, 2006. [Satoshi Kogure, Mikio Sawabe, Motohisa Kishimoto, (2006)] QZSS satellites will use modernized GPS signals as a base, transmitting six navigation signal, including L1C/A signal, L1C signal, L2C signal L5 signal, L1-SIRF signal and LEX signal [Japan Aerospace of Exploration Agency, (2007)].

For the purpose of QZSS, with integrating QZSS with GPS, the number of visible satellites (NVS) and dilution of precision (DOP) could be improved not only in Japan, but also throughout most of the East Asian region, therefore satellite availability and environment for satellite positioning are expected to be greatly improved, moreover, triple frequency measurement can also substantially aid in the process of carrier phase ambiguity resolution (AR). [Yun Zhang, Nobuaki Kubo, Akio Yasuda. (2005)] Reliability and efficiency of the system were also expected to be improved.

1.2 RESEARCH OBJECTIVE

The main purpose of this research is to ensure performance of integrating QZSS with GPS. The specific objectives are as follows:

- Develop triple frequency simulator to perform numerical measurement

- Study impact from triple frequency in AR

- Study the feature of QZSS orbit

- Study the advantage of GPS with QZSS in NVS, Position Dilution of Precision (PDOP) analysis

- Study the improvement of GPS with QZSS in Differential GPS positioning (DGPS) in different baseline

- Study the impact of GPS with QZSS in Double Differential (DD) carrier phase AR in different baseline

1.3 ARTICLE OUTLINE

The thesis is composed of 6 chapters. Background and purpose of research were introduced in chapter 1.

In chapter 2, modernization GPS and QZSS was overviewed. Program of two systems were described, and new civil signals and constellation were given here. Expected of impact in integrating QZSS with GPS was also shown here.

In chapter 3, several linear combination signals with triple frequency signals were discussed, three linear combination algorisms for carrier based AR with triple frequency were offered, wide-lane (WL) method, geometry-free (GF) method and ionosphere-free (IF) method for long-base method were introduced.

In chapter 4, triple frequency simulator was introduced in brief. Error models and noise parameters were shown here. Using the simulator, numerical estimating was performed with four QZSS constellation options or without QZSS. NVS, PDOP, short-baseline L1 DGPS positioning and short-baseline primary signal Ambiguity Success Rate (ASR) were measured. Region for spatial estimation was East Asia Region. Six cities, Sapporo, Tokyo, Naha in Japan, Shanghai, Kashi in China, and Jakarta in Indonesia were chosen for temporal estimation.

In chapter 5, positioning with QZSS or without QZSS was studied. QZSS Option 3 constellation was used here because it was decided as the formal orbit in QZSS. Five Japanese cities were chosen as reference and rover stations to positioning in short distance (about 0.7km), medium distance (about 14.2km), long distance (about 190.9km) and extra-long distance (521.7km). Several AR algorisms for each baseline introduced in chapter 3 were used here.

In chapter 6, the whole research works was summarized with conclusions and recommendations.

In this chapter, programs of modernization GPS and QZSS program are introduced respectively. A discussion on the compatibility and interoperability of the two systems is also included, and the expected impacts of the systems for improving performance are presented here.

2.1 GPS MODERNIZATION

In this section, modernization GPS program, new satellite and new signal were introduced.

2.1.1 Modernization GPS Program

The United States' Global Positioning System (GPS), having reached "Fully Operational Capability" on July 17, 1995, completed its original design goals. However, additional advances in technology and new demands on the existing system led to the effort to modernize the GPS system. Announcements from the Vice President and the White House in 1998 initiated these changes. In 2000, U.S. Congress authorized the effort, referred to as GPS III. The project involves new ground stations and new satellites, with additional navigation signals for both civilian and military users, and aims to improve the accuracy and availability for all users. The target date is 2013 with incentives offered to the contractors if they can complete it by 2011.

The goals of the program are to protect the military user's services and enhance civil use. [Swider, (2001)] For these reasons, the modernization should:
● For the military user: add new signals with spectral separation and increased signal power to improve protection, prevention and preservation capacity
● For the civil user: add new signals to improve accuracy, availability and signal redundancy.

For civil GPS users worldwide, the first real step of GPS modernization was removing the degradation capability, known as Selective Availability (SA) from GPS signal, The amount of error added was "set to zero" [THE WHITE HOUSE, (2000)] at midnight on May 1, 2000, which could improve the accuracy of measurement data and navigation result.[Miyano Tomoyuki, Kawano Isao, Mokuno Masaaki, Suzuki Takashi, (2000)]. On 19 Sep. 2007, United States Department of Defense announced that they would not procure any more satellites capable of implementing SA. [U.S. DoD., (2007)]

2.1.2 GPS Satellite Modernization

Four generations of satellites have flown in the GPS constellation: Block I, Block II, Block IIA (Augmentation), and Block IIR.

Block IIRs began replacing older Block II and IIAs in 1997. Block IIR satellites provided dramatic improvements over previous blocks. They could determine their own position by performing inter-satellite ranging with other IIR vehicles. They also had reprogrammable satellite processors enabling problem fixes and upgrades in flight, increased satellite autonomy, and radiation hardness.

The first modernized Block IIR (designed as IIR-M) with L2C (1227.60MHz) was launched on 26 September 2005. The fourth Block IIR-M satellite was launched successfully on 17 Oct, 2007. Currently 12 IIR and 4 IIR-M satellites are on orbit. It will be maneuvered into the F2 slot in the sixth of the six GPS orbital planes, near to a 16-year-old Block IIA space vehicle (SV29, PRN29) on which three of the satellite's four atomic clocks have ceased functioning. [Inside GNSS, (2007)] Recently, Lockheed Martin-led team has begun production activities to reconfigure a Block IIR-M to include a new demonstration payload that will transmit a third civil signal, which was located on L5 frequency (1176.45MHz). [GPS World, (2007)]

Block IIF satellites are the next generation of GPS space vehicles. The Block IIF system allows affordable technology insertion and block upgrades, while emphasizing compatibility and interoperability with the current space vehicles, ground control system, and user equipment GPS Block IIF satellites will feature extended design life more than 12 years, faster processors with more memory, and a new civil signal on a third frequency (L5). Boeing confirmed what the Air Force announced in August: the satellite is on track for launch sometime in 2008. [GPS World, (2007)]

Figure 2.1 shows the image of GPS Block IIR (on the left) and Block IIF (on the right) satellites.
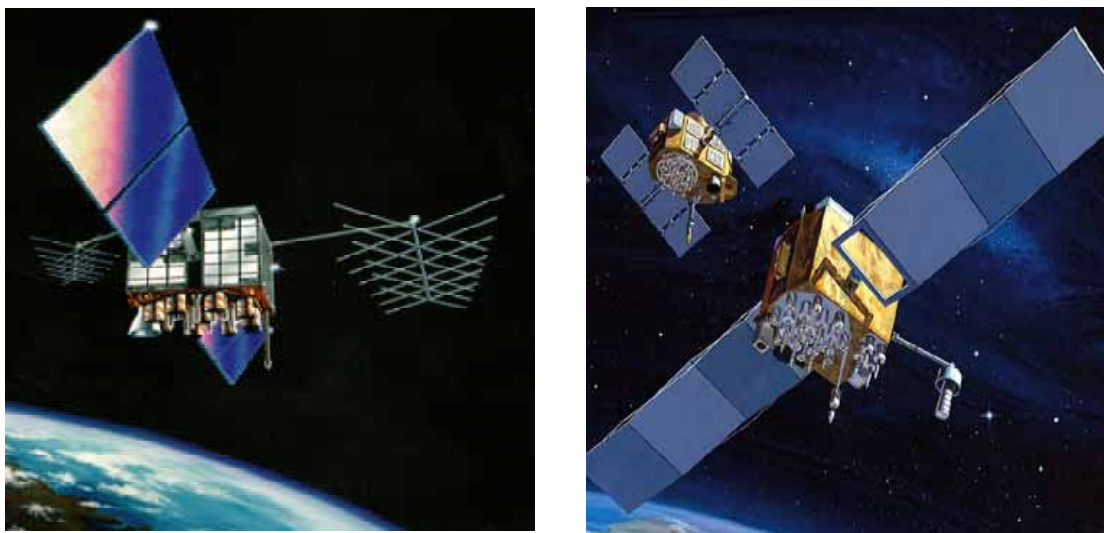
Figure 2.1 GPS Block IIR Satellite (Left) and IIF Satellite (Right) [Lt Col John Wilt, (2001)]

2.1.3 New GPS Civil Signals

Figure 2.2 shows the modernized GPS signals from [U.S. Dot, (2003)].
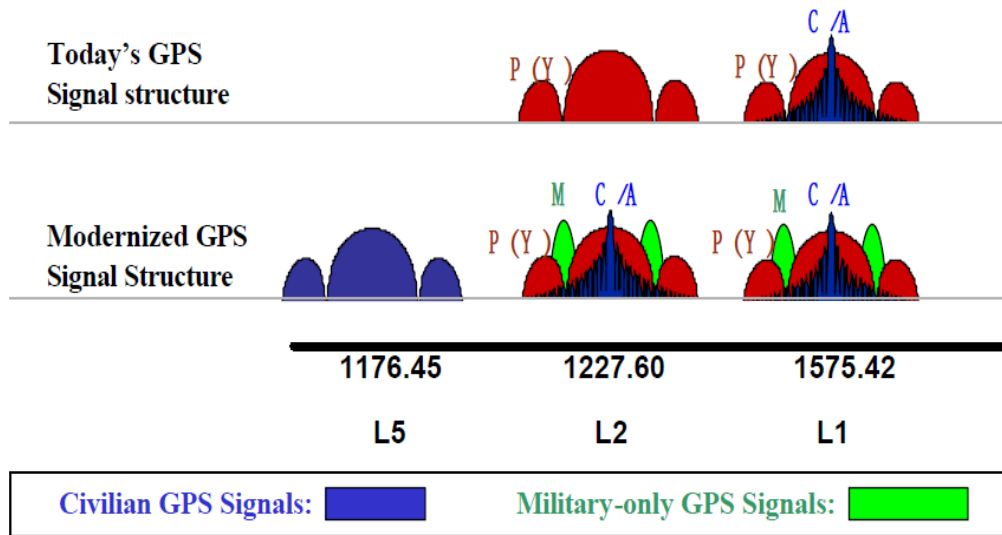
Figure 2.2 Modernization GPS signal [U.S. Dot, (2003)]

◆ **L2C (1227.6MHz)**

A White House press release on March 30, 1998, announces that a civil signal would be added to the GPS L2 frequency. Block IIR-M satellites firstly launched in 2005 broadcast L2C signals. The most important object was to L2C enable the development of low-cost, dual frequency civil GPS receivers that allow for correction of ionosphere error. [Sakai Takeyasu, Fukushima Sonosuke, Takeichi Noboru, Aramaki, Masae, Ito Ken, (2007)]

◆ **L5 (1176.45MHz)**

L5 signal will be broadcast beginning with the first IIF satellite, and demo signal will be with IIR–M satellite. It will transmit at a high power than current civil GPS signals, and have a wider bandwidth. Because of the lower frequency, indoor users could also be enhanced reception.

◆ **L1C (1575.42MHz)**

On June 26th, 2004, the United States of America and European Community established the "Agreement on the Promotion, Provision and Use of GALILEO and GPS Satellite Based Navigation Systems and Related Applications" (form "http://pnt.gov/public/docs/2004-US-EC-agreement.pdf") It was to adopt a common baseline signal to be transmitted in the future by GALILEO and GPS on L1 center frequency. L1C signal will

build on improved characteristics of other modernized GPS signal. The detail of L1C project could be found from "http://www.navcen.uscg.gov/gps/modernization/L1/L1C-report-short.pdf".

2.2 JAPANESE QZSS

In this section, program, constellation and signal of QZSS were introduced, augmentation GPS with QZSS was also presented.

2.2.1 QZSS Program

The Quasi-zenith Satellite System is a satellite navigation system in Japan which is designed to complement and augment global-positioning satellites (GPS). On Jan 2007, JAXA (Japan Aerospace of Exploration Agency) released the initial version of the "Interface Specifications for the Quasi Zenith Satellite System (QZSS)"(IS-QZSS Version 0.0.). [Japan Aerospace of Exploration Agency, (2007)] This document summarizes the specifications of positioning signals and messages sent from the QZSS, its service outline, and performance. The second draft was also released on June 8, 2007.

According to the document, QZSS project will be promoted incrementally in accord with the official policy of the Government of Japan released on March 31, 2006 as follows:

- Phase One: the first QZSS satellite will be launched in 2009. Technical validation and application demonstration will be conducted.
- Phase Two: following the successful completion of Phase One, the 2nd and 3rd QZSS satellites will be launched. Full system operation will be demonstrated.

2.2.2 QZSS Constellation

◆ **QZS design**

Figure 2.3 shows image of QZS-1. QZS has two deployable solar cell array panels, an L-band transmission antenna (L-ANT), an L1-SAIF transmission antenna (LS-ANT), and a TTC antenna. The QZS utilizes fixed (non-steerable) antennas mounted on one side of the spacecraft. The QZS attitude is controlled is controlled to ensure that these antennas always point toward the center of the Earth. Yaw steering controls the orientation of the solar cell arrays to optimize reception of sunlight. [Japan Aerospace of Exploration Agency, (2007)]

Figure 2.3 Image of QZS-1 (Source: IS-QZSS Ver. 0.1)

◆ **Orbit**

Table 2.1 indicates the parameters of three operational satellites for Asymmetric QZSS Satellite orbit In the option, argument of perigee is set to 270º to enable the placement of the apogee in the northern hemisphere. The feature of asymmetric QZSS satellite orbit will be discussed in chapter 4 in details.

Semi-major Axis	42,164km (average)
Eccentricity	0.099
Inclination	45 °±5 °
Argument of perigee	270 °±1 °
Mean Motion	120 °
Longitude of ascending node (LAN	146.3 ° East ±5 °

Table 2.1 QZSS satellite orbit parameters

◆ **Constellation**

The baseline QZSS constellation will consist of initially one satellite, and ultimately three (or more) satellites. Figure 2.4 illustrates the ground tracks of the QZSS constellation [Petrovski, I. G., Ishii, M., Torimoto, H., Kishimoto, H., Furukawa, T., Saito, M., Tanaka, T., and Maeda, H., (2003)] and [Wu, F., Kubo, N., and Yasuda, A, (2004)]. All QZS are in orbits, which are the same as "8-shape" ground track, as shown in figure 2.4. The average central longitude of the QZS ground track is 135ºEast.

8
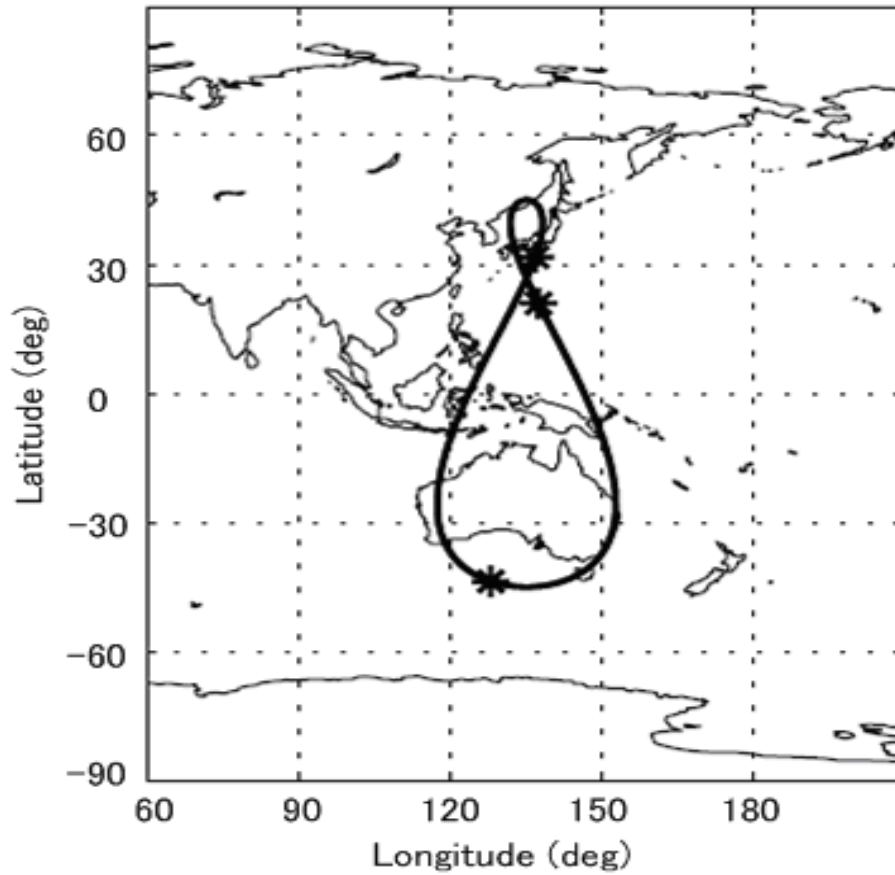
Figure 2.4 Ground track of Asymmetric 8-shape QZSS satellite orbit

2.2.3 QZSS Signal

QZSS will transmit six positioning signal: L1C/A signal, L1-SAIF signal, L1C signal, L2C signal, LEX signal and L5 signal. L1C/A signal, L1C signal, L2C signal and L5 signal are to ensure compatibility and interoperability with existing and modernized GPS signal. This will minimizes changes to specifications and receiver designs. L1-SAIF signal and LEX signal are known as sub-meter class performance enhanced signal to improve of reliability of the system. In this research L1, L2 and L5 signal are interested.

Signal	Frequency [MHz]	Wavelength [m]	Note
L1-C/A, L1-C	1575.42	0.1903	Compatibility and interoperability
L2-Civil	1227.60	0.2442	with existing and modernized GPS
L5-Civil	1176.45	0.2548	signal
L1-SAIF	1575.42	0.1903	Compatibility with GPS-SBAS
LEX	1278.75	0.2344	Compatibility withGALILEO-E6

Table 2.2 Planned QZSS signals

Table 2.2 gives an overview of planed QZSS signals with corresponding frequencies and wavelengths [Satoshi KOGURE, (2007)]. Figure 2.5 shows the QZSS navigation signal spectrum.
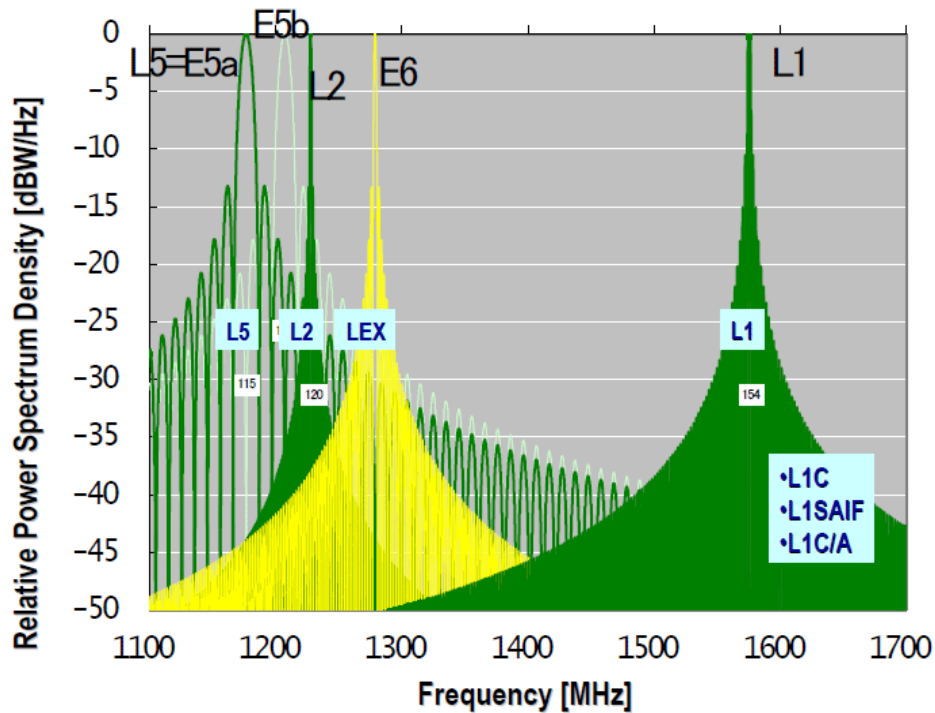
Figure 2.5 QZSS navigation signal spectrum (Source: IS-QZSS Ver. 0.1)

Table 2.3 summarized schedule of modernized GPS and QZSS signals. [Richard D. Fontana, Wai Cheung, Tom Stansell, (2001)] and [Japan Aerospace of Exploration Agency, (2007)]

Signal/SV	GPS/IIR	GPS/IIR-M	GPS/IIF	GPS/III	QZSS
L1 C/A					
L1 P/Y					
L1 M					
L1 C					
L1-SAIF					
L2 Civil					
L2 P/Y					
L2 M					
L5 Civil					
LEX					

Table 2.3 GPS and QZSS signals

2.2.4 GPS Augmentative with QZSS

In the open environment, the position of the receiver can be easily and accurately determined using GPS signal, however, in the center of city or canyons in the mountainous terrain, accurate position could not be estimated accurately because the GPS signal path was obstructed, performance of system was limited because narrow roads and high building around. Integrating QZSS with GPS, availability and accuracy of satellite positioning are expected to be improved using extra high elevation QZSS satellites, especially in urban environment.

In QZSS, accuracy of SIS (Signal in Space) URE (User Range Error) is excepted approximately 30cm (1-sigma), and the User Positioning Error (UPE) with GPS-QZSS combination is to be almost equivalent or slightly better than UPE by only GPS signals [Satoshi Kogure, Mikio Sawabe, Motohisa Kishimoto, (2006)]. Performance in carrier phase-based positioning in QZSS with modernization GPS was expected to be enhanced, because

- using more linear combinations with extra signal;
- using better initial receiver accuracy with modernization signal;
- using better constellation geometry with extra satellites.

ASR in DD carrier phase AR could be estimated more precisely. Resolving time of AR was expected to be reduced. Efficiency and reliability were also expected to be improved. Impact from triple frequency system will be studied in chapter 3 and QZSS positioning will be discussed in chapter 5 in details.

TRIPLE FREQUENCY AMBIGUITY RESOLUTION

The imminent triple frequency systems, including QZSS and modernization GPS, will enable **more linear combinations** of the carrier phase observations. The purpose here is in an attempt to seek proper candidates with good features for better AR performance.

In this chapter, double difference (DD) code and carrier measurement equations were discussed. Several ambiguity resolution (AR) methods with various linear combinations (LC) of three signals, L1 (1575.42MHz), L2 (1227.60MHz) and L5 (1176.45MHz), were developed. Wide-Lane (WL) for shorter baseline, Geometry-Free (GF) and Ionosphere-Free (IF) methods for longer baseline were introduced here. Excepted impact from triple frequency was also presented in this chapter.

3.1 OBSERVATION MEAUREMENTS

There are two types of GPS observations: pseudorange (code) and carrier phase. Pseudorange is often used in navigation, and carrier phase is favored in high precision surveying. [Alfred Leick, (1995)] In QZSS and modernization GPS, there will be two more civil GPS signals in addition to the current one at the L1 frequency (1575.42 MHz). The second civil signal will be broadcast at the L2 frequency (1227.60 MHz), and the third civil signal will be broadcast at L5 frequency (1176.45 MHz).

In this section, single and double difference (DD) code, carrier measurements were introduced. DD LC signals with three primary signals were discussed, measurement noise, ionosphere error and geometry error in LC signal and AR with LC signal were also studied here.

3.1.1 Single Observation

◆ **Single code observation**

Pseudorange is a measurement of the distance between the satellite and the receiver's antenna, referring to the epochs of emission and reception of the code. Single position range between one satellite i and one receiver α was given as:

$$P_{\kappa\alpha}^{i} = \rho + \frac{f_{L1}^{2}}{f_{\kappa}^{2}} I_{L1\alpha}^{i} + T_{\alpha}^{i} + c\mu_{\alpha} - c\mu^{i} + b_{\kappa\alpha} + b_{\kappa}^{i} + \delta_{\kappa} \quad (m) \qquad (3.1.1)$$

where,

ρ : geometric range

f_{κ} : means frequency of L1, L2 and L5 signals

I_{L1} : ionosphere ranger error on L1 signal

T : troposphere range error

μ : clock error in receiver α or in satellite i

b : hardware bias in receiver α or in satellite i

δ : noise in code measurement

◆ **Single carrier phase observation**

The phase observable is the difference between the received satellite carrier phase (as sensed by the receiver's antenna) and the phase of the internal receiver oscillator. Single carrier phase range in unit m between one satellite i and one receiver α was given as:

$$\Phi_{\kappa\alpha}^i = \rho - \frac{f_{L1}^2}{f_\kappa^2} I_{L1\alpha}^i + T_\alpha^i + \lambda_\kappa N_\alpha^i + c\mu_\alpha - c\mu^i + b_{\kappa\alpha} + b_\kappa^i + \varepsilon_\kappa \quad (\text{m}) \tag{3.1.2}$$

where,

ρ : geometric range

f_κ : frequency of signal

λ_κ : wavelength of signal

N : unknown cycle integer ambiguity

I_{L1} : ionosphere ranger error on L1 signal

μ : clock error in receiver α or in satellite i

b : hardware bias in receiver α or in satellite i

ε : noise in carrier phase measurement.

Carrier phase range in unit cycles was also given:

$$\phi_{\kappa\alpha}^i = \frac{1}{\lambda_\kappa}\rho - \frac{\lambda_\kappa}{\lambda_{L1}^2} I_{L1\alpha}^i + \frac{1}{\lambda_\kappa}T_\alpha^i + N_\alpha^i + f_\kappa\mu_\alpha - f_\kappa\mu^i + \frac{1}{\lambda_\kappa}b_{\kappa\alpha} + \frac{1}{\lambda_\kappa}b_\kappa^i + \frac{1}{\lambda_\kappa}\varepsilon_\kappa \quad (\text{cycle}) \tag{3.1.3}$$

3.1.2 Double Difference (DD) Observation

In single observable from equations (3.1.1), (3.1.2) and (3.1.3), the clock error μ_α and hardware bias $b_{\kappa\alpha}$ in the receiver α can be cancelled by single difference between two satellites, and the clock error μ^i and hardware bias b_κ^i in the satellite i can be cancelled by single difference between two receivers. So both hardware bias and clock error can all be removed using DD method.

In this research, DD measurements were interested, because the most important feature of DD observation is the cancellation of the large receives clock error. Residual DD ionosphere range error, DD troposphere range error and DD ephemeris error were neglected in short baseline, however, they will become worse when

baseline are longer. Because multipath error is a function of the specific receiver-satellite-reflector geometry, it does not cancel in the double-difference observable.

◆ **DD Code observation**

DD code measurement between two satellites i, j and two receivers α, β were written as:

$$\nabla\Delta P_\kappa = \nabla\Delta\rho + \left(\frac{f_{L1}}{f_\kappa}\right)^2 \nabla\Delta I_{L1} + \nabla\Delta T + \nabla\Delta\delta_\kappa \text{ (m)} \tag{3.2}$$

where,

$\nabla\Delta$: double differencing operator between two satellites and two receivers:

$$\nabla\Delta(\bullet) = (\bullet)_{\alpha\beta}^{ij} = (\bullet)_\alpha^i - (\bullet)_\alpha^j - \left((\bullet)_\beta^i - (\bullet)_\beta^j\right)$$

◆ **DD carrier phase observation**

DD carrier phase measurement was estimated from phase observations with a pair of satellites and a pair of receivers. DD carrier phase measurement equation between two satellites i, j and two receivers α, β was written in unit m as equation (3.4).

$$\nabla\Delta\Phi_\kappa = \nabla\Delta\rho - \left(\frac{f_{L1}}{f_\kappa}\right)^2 \nabla\Delta I_{L1} + \nabla\Delta T + \lambda_\kappa \nabla\Delta N_\kappa + \nabla\Delta\varepsilon_\kappa \text{ (m)} \tag{3.3}$$

where:

$\nabla\Delta$: double differencing operator between two satellites and two receivers

$\nabla\Delta N$: unknown DD cycle integer ambiguity, which plays an important role in double differencing.

DD carrier phase measurement could also be expressed in unit cycle:

$$\nabla\Delta\phi_\kappa = \frac{1}{\lambda_\kappa}\nabla\Delta\rho - \frac{\lambda_\kappa}{\lambda_{L1}^2}\nabla\Delta I_{L1} + \frac{1}{\lambda_\kappa}\nabla\Delta T + \nabla\Delta N_\kappa + \frac{1}{\lambda_\kappa}\nabla\Delta\varepsilon_\kappa \text{ (cycle)} \tag{3.4}$$

Signal	Frequency (MHz)	Wavelength	Iono. error on L1 single (m)	Std of noise (cycle)	Std of noise (m)
$\nabla\Delta$ L1	1575.42	0.1903	1.0	0.014	0.0027
$\nabla\Delta$ L2	1227.60	0.2442	1.31	0.018	0.0044
$\nabla\Delta$ L5	1176.45	0.2538	1.36	0.009	0.0023
$\nabla\Delta$ P1	1575.42	0.1903	1.0	1.58	0.20

Table 3.1 Characters in the primary signals in triple frequencies

14

Table 3.1 shows characters in the DD signals in triple frequencies system in this research. [Yun Zhang, Nobuaki Kubo, Akio Yasuda. (2005)]

3.1.3 Linear Combination with Triple Frequency DD Carrier Phase Observations

General DD carrier phase linear combination (LC) signal for triple frequency in unit cycles was given as:

$$\nabla\Delta\phi_{LC} = k_1\nabla\Delta\phi_{L1} + k_2\nabla\Delta\phi_{L2} + k_3\nabla\Delta\phi_{L5} \quad \text{(cycle)} \tag{3.5.1}$$

where ϕ_{L1}, ϕ_{L2} and ϕ_{L5} means carrier phase measurements in unit cycles on L1, L2 and L5 frequency, respectively.

Basing on DD carrier phase observation from equation (3.4), LC signal in unit cycles was also expressed:

$$\nabla\Delta\phi_{LC} = \left(\frac{k_1}{\lambda_{L1}} + \frac{k_2}{\lambda_{L2}} + \frac{k_3}{\lambda_{L5}}\right)(\nabla\Delta\rho + \nabla\Delta T) - \left(k_1\frac{1}{\lambda_{L1}} + k_2\frac{\lambda_{L2}}{\lambda_{L1}^2} + k_3\frac{\lambda_{L5}}{\lambda_{L1}^2}\right)\nabla\Delta I_{L1}$$
$$+ \nabla\Delta N_{LC} + \left(\frac{k_1}{\lambda_1}\nabla\Delta\varepsilon_{L1} + \frac{k_2}{\lambda_2}\nabla\Delta\varepsilon_{L2} + \frac{k_3}{\lambda_{L5}}\nabla\Delta\varepsilon_{L5}\right) \quad \text{(cycle)} \tag{3.5.2}$$

where,
LC signal ambiguity $\nabla\Delta N_{LC}$ was given as:
$$\nabla\Delta N_{LC} = k_1\nabla\Delta N_{L1} + k_2\nabla\Delta N_{L2} + k_3\nabla\Delta N_{L5} \tag{3.5.3}$$

where N_{L1}, N_{L2} and N_{L5} means ambiguity on L1, L2 and L5 carrier phase measurement, respectively.

Frequency of LC signal was: $f_{LC} = k_1 f_{L1} + k_2 f_{L2} + k_3 f_{L5}$ \qquad (3.5.4)

Wavelength of LC signal was: $\lambda_{LC} = \dfrac{c}{k_1 f_{L1} + k_2 f_{L2} + k_3 f_{L5}} = \dfrac{1}{\dfrac{k_1}{\lambda_{L1}} + \dfrac{k_2}{\lambda_{L2}} + \dfrac{k_3}{\lambda_{L5}}}$ \qquad (3.5.5)

where the basic requirement to be met is that $(k_1 f_{L1} + k_2 f_{L2} + k_3 f_{L5}) > 0$ or $\dfrac{k_1}{\lambda_{L1}} + \dfrac{k_2}{\lambda_{L2}} + \dfrac{k_3}{\lambda_{L5}} > 0$. Using

equation (3.5.4) and (3.5.5), frequency and wavelength of LC signal could be calculated.

◆ **Measurement noise in LC signal**

Measurement noise in LC signal in unit m was expressed as equation (3.5.6), and which in unit cycles was expressed in equation (3.5.7).

$$\nabla\Delta\sigma_{LC} = \sqrt{k_1^2\nabla\Delta\sigma_{\varepsilon L1}^2 + k_2^2\nabla\Delta\sigma_{\varepsilon L2}^2 + k_3^2\nabla\Delta\sigma_{\varepsilon L5}^2} \quad \text{(m)} \tag{3.5.6}$$

$$\nabla\Delta\sigma_{LC} = \frac{\sqrt{k_1^2\nabla\Delta\sigma_{\varepsilon L1}^2 + k_2^2\nabla\Delta\sigma_{\varepsilon L2}^2 + k_3^2\nabla\Delta\sigma_{\varepsilon L5}^2}}{\lambda_{LC}} \quad \text{(cycle)} \tag{3.5.7}$$

where $\nabla\Delta\sigma$ shows standard deviation of carrier phase measurement noise in unit m.

◆ **Ionosphere error in LC signal**

According to equation (3.5.2), ionosphere error corresponding on L1 signal in LC signal in unit cycle was:

$$\nabla\Delta I_{LC} = \lambda_{L1}\left(k_1\frac{1}{\lambda_{L1}} + k_2\frac{\lambda_{L2}}{\lambda_{L1}^2} + k_3\frac{\lambda_{L5}}{\lambda_{L1}^2}\right) \times \frac{\nabla\Delta I_{L1}}{\lambda_{L1}} = \left(k_1 + k_2\frac{\lambda_{L2}}{\lambda_{L1}} + k_3\frac{\lambda_{L5}}{\lambda_{L1}}\right) \times \frac{\nabla\Delta I_{L1}}{\lambda_{L1}} \quad \text{(cycle)} \quad (3.5.8)$$

DD ionosphere error in LC signal in unit m was:

$$\nabla\Delta I_{LC} = \lambda_{LC}\left(k_1\frac{1}{\lambda_{L1}} + k_2\frac{\lambda_{L2}}{\lambda_{L1}^2} + k_3\frac{\lambda_{L5}}{\lambda_{L1}^2}\right)\nabla\Delta I_{L1} \quad \text{(m)} \quad\quad\quad (3.5.9)$$

In equations (3.5.8) and (3.5.9) ionosphere error in LC signal expressed to be compared to the DD ionosphere influence on the L1 signal. LC signal Ionosphere error $\nabla\Delta I_{L1}$ was equal to be zero when $\left(k_1 + k_2\frac{\lambda_{L2}}{\lambda_{L1}} + k_3\frac{\lambda_{L5}}{\lambda_{L1}}\right) = 0$, LC signal is refer to as **ionosphere-free (IF)** signal.

◆ **Geometry error in LC signal**

According to equation (3.5.2), geometry error in LC signal in unit cycle was:

$$\nabla\Delta G_{LC} = \left(\frac{k_1}{\lambda_{L1}} + \frac{k_2}{\lambda_{L2}} + \frac{k_3}{\lambda_{L5}}\right)\left(\nabla\Delta\rho + \nabla\Delta T\right) \quad \text{(cycle)} \quad\quad\quad (3.5.10)$$

If λ_{LC} could be calculated from equation (3.5.5), geometry error in LC signal could also be expressed as:

$$\nabla\Delta G_{LC} = \frac{1}{\lambda_{LC}}\left(\nabla\Delta\rho + \nabla\Delta T\right) \quad \text{(cycle)} \quad\quad\quad (3.5.11)$$

Equation (3.5.11) indicated that the LC signal geometry error in cycle will be decreased when LC signal wavelength is greater. Assuming that $\left(\frac{k_1}{\lambda_{L1}} + \frac{k_2}{\lambda_{L2}} + \frac{k_3}{\lambda_{L5}}\right) = 0$, the influence of the geometrical error on LC signal in cycle is not existed, so this LC signal was refer to as a **geometry-free (GF)** signal.

◆ **AR in LC signal**

From measurement noise, ionosphere error and geometry error in LC signal analysis in above, standard deviation of total error in LC signal was given as:

$$\nabla\Delta\sigma_{ErrorLC} = \nabla\Delta\sigma_{LC} + \nabla\Delta\sigma_G + \nabla\Delta\sigma_I \quad (m) \qquad\qquad (3.5.12)$$

where, $\nabla\Delta\sigma_{LC}$ means standard deviation of measurement noise in LC signal in unit m, $\nabla\Delta\sigma_I$ means standard deviation of ionosphere error in LC signal in unit m, $\nabla\Delta\sigma_G$ means standard deviation of geometry error in LC signal in unit m.

If the total error in unit m is under the half of LC signal wavelength $\nabla\Delta\sigma_{ErrorLC} < \frac{1}{2}\lambda_{LC}$, $\nabla\Delta N_{LC}$ could be rounded correct from float ambiguity in AR. [Jung, J, P. Enge, and B. Pervan, (2000)]

From the next section, LC signals, including WL signal, GF signal and IF signal, were discussed in details, and several AR method using LC signals were also proposed. Because DD measurements were interested in this research, DD carrier phase measurements liner combinations were discussed directly. "$\nabla\Delta$" will be neglected in the equation.

3.2 WIDE-LANE (WL) METHOD

WL method with triple frequency has been provided by [Ronald R. Hatch, (1982)] early. This section is a summary of the aforementioned WL method for triple frequency system.

3.2.1 WL Combination Signal

In three frequencies system, a user can generate three beat frequency signals. The L1 and L2 carrier frequencies are processed to create the Wide-Line (WL) signal with wavelength 86 centimeters. The combination of L1 and L5 could offer the second beat frequency with 75 centimeters in wave length. The combination of the L2 and L5 carrier frequencies could create the third beat frequency with 5.9 meter in wavelength.

In unit meters, WL linear combination can be given as following:

$$\Phi_{w\kappa\lambda} = \frac{\lambda_{w\kappa\lambda}}{\lambda_\kappa}\Phi_\kappa - \frac{\lambda_{w\kappa\lambda}}{\lambda_\lambda}\Phi_\lambda = \rho + \frac{f_{L1}^2}{f_\kappa f_\lambda}I_{L1} + \lambda_{w\kappa\lambda}N_{w\kappa\lambda} + T + \varepsilon_{w\kappa\lambda} \, (m) \qquad (3.6.1)$$

where,

frequency of WL signal is $f_{w\kappa\lambda} = f_\kappa - f_\lambda$;

wave length of EWL is: $\lambda_{w\kappa\lambda} = \dfrac{c}{f_\kappa - f_\lambda} = 1/\left(\dfrac{1}{\lambda_\kappa} - \dfrac{1}{\lambda_\lambda}\right)$ (m);

c means light velocity.

WL signal could also be expressed in unit cycles:

$$\phi_{w\kappa\lambda} = \phi_\kappa - \phi_\lambda = \frac{\Phi_{w\kappa\lambda}}{\lambda_{w\kappa\lambda}} \quad \text{(cycle)} \tag{3.6.2}$$

$\varepsilon_{w\kappa\lambda}$ is the noise in the WL signal, if assuming no correlation between the primary signals, standard deviation of noise in unit m can be calculated in equation (3.7.1), and equation (3.7.2) show standard deviation of WL signal noise $\varepsilon_{w\kappa\lambda}$ in unit cycle.

$$\sigma_{w\kappa\lambda} = \sqrt{\frac{\lambda_{w\kappa\lambda}^2}{\lambda_\kappa^2}\sigma_\kappa^2 + \frac{\lambda_{w\kappa\lambda}^2}{\lambda_\lambda^2}\sigma_\lambda^2} \quad \text{(m)} \tag{3.7.1}$$

$$\sigma_{w\kappa\lambda} = \frac{\sqrt{\frac{\lambda_{w\kappa\lambda}^2}{\lambda_\kappa^2}\sigma_\kappa^2 + \frac{\lambda_{w\kappa\lambda}^2}{\lambda_\lambda^2}\sigma_\lambda^2}}{\lambda_{w\kappa\lambda}} \quad \text{(cycle)} \tag{3.7.2}$$

where, σ shows noise in primary carrier signal in unit m.

Ionosphere error in WL signal in unit m was expressed in equation (3.7.3), and that in unit cycle was expressed in equation (3.7.4).

$$I_{w\kappa\lambda} = -\frac{f_{L1}^2}{f_\kappa f_\lambda}I_{L1} \quad \text{(m)} \tag{3.7.3}$$

$$I_{w\kappa\lambda} = -\frac{\lambda_{L1}}{\lambda_{w\kappa\lambda}}\frac{f_{L1}^2}{f_\kappa f_\lambda} \times \frac{I_{L1}}{\lambda_{L1}} \quad \text{(cycle)} \tag{3.7.4}$$

WL combination signals with L1, L2 and L5 signal could be written in unit m were given in equations (3.8), (3.9) and (3.10), respectively.

$$\Phi_{w12} = \rho + \frac{f_{L1}^2}{f_{L1}f_{L2}}I_{L1} + T + \lambda_{wL1L2}N_{wL1L2} + \varepsilon_{wL1L2\Phi} \quad \text{(m)} \tag{3.8}$$

$$\Phi_{w15} = \rho + \frac{f_{L1}^2}{f_{L1}f_{L5}}I_{L1} + T + \lambda_{wL1L5}N_{wL1L5} + \varepsilon_{wL1L5\Phi} \quad \text{(m)} \tag{3.9}$$

$$\Phi_{w25} = \rho + \frac{f_{L1}^2}{f_{L2}f_{L5}}I_{L1} + T + \lambda_{wL2L5}N_{wL2L5} + \varepsilon_{wL2L5\Phi} \quad \text{(m)} \tag{3.10}$$

In the research, Φ_{w12} is called WL single, Φ_{w15} is called medium WL (MWL) single, and Φ_{w25} is called extra WL signal (EWL). Basing on measurement noise of primary signal noise given in table 3.1, table 3.2 summarized the ionosphere error and measurement noise in three WL signals.

	WL (L1-L2)	MWL (L1-L5)	EWL (L2-L5)
Frequency (MHz)	347.82	398.97	51.15
Wavelength	0.86	0.75	5.86
Ionosphere error (m)	-1.28 I_{L1}	-1.34 I_{L1}	-1.72 I_{L1}
Measurement noise (m)	0.020	0.013	0.118
Ionosphere error (cycles)	-0.28 $\dfrac{I_{L1}}{\lambda_{L1}}$	-0.33 $\dfrac{I_{L1}}{\lambda_{L1}}$	-0.06 $\dfrac{I_{L1}}{\lambda_{L1}}$
Measurement noise (cycles)	0.0228	0.0166	0.020

Table 3.2 Influence of ionosphere errors and measurement noise in three WL signals

Figure 3.1 shows flow char of WL methods in dual frequencies (left) or triple frequencies (right) AR. There are two steps in WL method for dual frequency system. The first step in approach for AR was estimating ambiguity N_{wL1L2} of WL Φ_{wL1L2} signal. With the result from the first step, N_{L1} of L1 signal is resolved using estimated Φ_{wL1L2} signal in the second step.
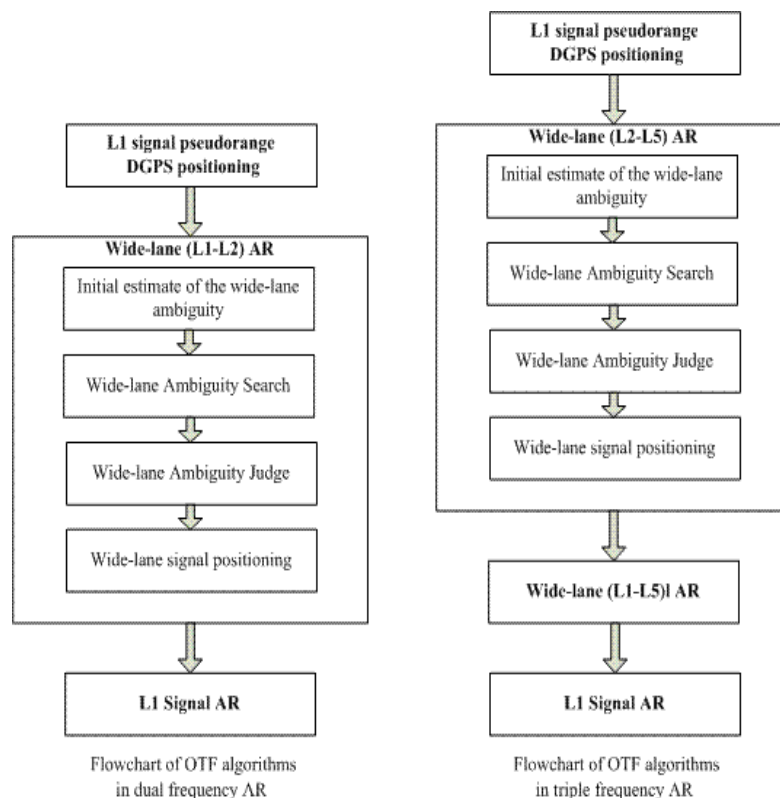
Figure 3.1 Flowchart of WL Method in dual (left) and triple (right) frequency AR

There are three steps in WL method for triple frequency system. The first step in approach for AR was estimating ambiguity N_{wL2L5} of EWL Φ_{w25} signal. This combination has a wavelength of 5.86 m and the ambiguity is resolved by rounding "float" solution to the nearest integer. With the result from the first step, N_{wL1L5} of WL Φ_{w15} signal is resolved in the second step. Using the results of the first two steps, ambiguity of primary signal could be estimated.

3.2.2 AR with WL signals for Dual Frequency

◆ **First Step for dual frequency WL method**

Combination code observation from equation (3.2) and WL signal from equation (3.8), the float WL ambiguities $\tilde{N}_{wL1L2}$ could be resolved using L1 pseudorange:

$$\tilde{N}_{wL1L2} = \frac{\Phi_{wL1L2} - P_{L1} + \left(-\frac{f_{L1}^2}{f_{L1}f_{L2}} + 1\right)I_{L1}}{\lambda_{wL1L2}} \qquad (3.11)$$

Ionosphere error in the first step is:

$$I_{FS} = \left(-\frac{f_{L1}^2}{f_{L1}f_{L2}} + 1\right)I_{L1} \quad \text{(m)} \qquad (3.12.1)$$

$$I_{FS} = \frac{\left(-\frac{f_{L1}^2}{f_{L1}f_{L2}} + 1\right)\lambda_{L1}}{\lambda_{wL1L2}} \times \frac{I_{L1}}{\lambda_{L1}} \quad \text{(cycle)} \qquad (3.12.2)$$

Measurement noise in the first step is:

$$\sigma_{FS} = \sqrt{\sigma_{PL1}^2 + \sigma_{\varepsilon L1L2}^2} \quad \text{(m)} \qquad (3.13.1)$$

$$\sigma_{FS} = \frac{\sqrt{\sigma_{PL1}^2 + \sigma_{\varepsilon L1L2}^2}}{\lambda_{wL1L2}} \quad \text{(cycle)} \qquad (3.13.2)$$

where, σ_{PL1} shows standard deviation of L1 pseudorange noise in unit m, and $\sigma_{\varepsilon L1L2}$ shows the standard deviation of WL signal noise in unit m.

If the condition that the sum of ionosphere errors and the measurement noise in equation (3.13) is within half of MWL wavelength, the integer WL ambiguity can be successfully obtained by rounding the float ambiguity to the nearest integer:

$$N_{wL1L2} = {}_{round}\left(\tilde{N}_{wL1L2}\right) \qquad (3.14)$$

After the WL ambiguity is fixed, the MWL becomes the most precise range and therefore can be used in the estimation of the L1 ambiguity.

◆ **Second Step for dual frequency WL method**

Combination WL from equation (3.8) and carrier phase observation from equation (3.3), the float L1 ambiguities $\tilde{N}_{L1}$ could be resolved using MWL range:

$$\tilde{N}_{L1} = \frac{\Phi_{L1} - \Phi_{w12} + \lambda_{wL1L2} N_{wL1L2} + \left(1 + \frac{f_{L1}^2}{f_{L1} f_{L2}}\right) I_{L1}}{\lambda_{L1}} \qquad (3.15)$$

Ionosphere error in the second step is:

$$I_{SS} = -\left(1 + \frac{f_{L1}^2}{f_{L1} f_{L2}}\right) I_{L1} \quad \text{(m)} \qquad (3.16.1)$$

$$I_{SS} = -\left(1 + \frac{f_{L1}^2}{f_{L1} f_{L2}}\right) \times \frac{I_{L1}}{\lambda_{L1}} \quad \text{(cycle)} \qquad (3.16.2)$$

Measurement noise in the second step is:

$$\sigma_{SS} = \sqrt{\sigma_{\varepsilon L1}^2 + \sigma_{\varepsilon L1L2}^2} \quad \text{(m)} \qquad (3.17.1)$$

$$\sigma_{SS} = \frac{\sqrt{\sigma_{\varepsilon L1}^2 + \sigma_{\varepsilon L1L2}^2}}{\lambda_{L1}} \quad \text{(cycle)} \qquad (3.17.2)$$

where, $\sigma_{\varepsilon L1}$ shows standard deviation of L1 carrier phase measurement noise in unit m, and $\sigma_{\varepsilon L1L2}$ shows the standard deviation of WL signal noise in unit m.

The integer L1 ambiguity can be obtained in equation (3.18) assuming that the sum of ionosphere error and measurement noise in equation (3.17) does not exceed half of an L1 cycle.

$$N_{L1} = {}_{round}\left(\tilde{N}_{L1}\right) \qquad (3.18)$$

There are two mainly error sources in WL method:
1) ionosphere error depending on baseline distance;
2) Amplified measurement noise in combination signals, including multipath error

Basing on measurement noise of primary signal noise given in table 3.1 and which of WL signal in table 3.2, table 3.3 indicates influence of ionosphere errors and measurement noise on each step using WL method for dual frequency.

Steps	Ionosphere error	Measurement noise
	in meters	
1	$-0.28\,I_{L1}$	0.201
2	$-2.28\,I_{L1}$	0.020
	in cycles	
1	$-0.07\dfrac{I_{L1}}{\lambda_{L1}}$	0.234
2	$-2.28\dfrac{I_{L1}}{\lambda_{L1}}$	0.104

Table 3.3 Influence of ionosphere errors and measurement noise on each step using dual frequency WL method

The further information of WL method for dual frequency could also be found in [T. Tsujii, M. Murata, M. Harigae, T. Ono and T. Inagaki, (1998)].

3.2.3 AR with WL signals for Triple Frequency

◆ **First Step**

Combination code observation from equation (3.1) and EWL signal from equation (3.10), the float EWL ambiguities $\tilde{N}_{wL2L5}$ could be resolved using L1 pseudorange:

$$\tilde{N}_{wL2L5} = \frac{\Phi_{25} - P_{L1} + \left(-\dfrac{f_{L1}^{\;2}}{f_{L2}f_{L5}} + 1 \right) I_{L1}}{\lambda_{wL2L5}} \qquad (3.19)$$

Ionosphere error in the first step is:

$$I_{FS} = \left(-\frac{f_{L1}^{\;2}}{f_{L2}f_{L5}} + 1 \right) I_{L1} \quad \text{(m)} \qquad (3.20.1)$$

$$I_{FS} = \frac{\left(-\dfrac{f_{L1}^{\;2}}{f_{L2}f_{L5}} + 1 \right)\lambda_{L1}}{\lambda_{wL2L5}} \times \frac{I_{L1}}{\lambda_{L1}} \quad \text{(cycle)} \qquad (3.20.2)$$

Standard deviation of measurement noise in the first step was given as:

$$\sigma_{FS} = \sqrt{\sigma_{PL1}^{\;2} + \sigma_{\varepsilon L2L5}^{\;2}} \quad \text{(m)} \qquad (3.21.1)$$

$$\sigma_{FS} = \frac{\sqrt{\sigma_{PL1}{}^2 + \sigma_{\varepsilon L2L5}{}^2}}{\lambda_{wL2L5}} \quad \text{(cycle)} \tag{3.21.2}$$

where, σ_{PL1} shows standard deviation of L1 pseudorange noise in unit m, and $\sigma_{\varepsilon L2L5}$ shows the standard deviation of EWL signal noise in unit m.

As the EWL wavelength are 5.861m, the influence of residual ionosphere error and the measurement noise on EWL AR in equation (3.21) should be limited, so the integer EWL ambiguity can obtained:

$$N_{wL2L5} =_{round} \left(\tilde{N}_{wL2L5} \right) \tag{3.22}$$

where $_{round}(x)$ indicates the nearest integer number to x.

Once the EWL ambiguity is resolved, the fixed EWL range becomes the most precise range and therefore can be used to resolve the WL ambiguity in the second step.

◆ **Second Step**

Combination MWL from equation (3.9) and EWL signal from equation (3.10), the float MWL ambiguities $\tilde{N}_{wL1L5}$ could be resolved using EWL range:

$$\tilde{N}_{wL1L5} = \frac{\Phi_{w15} - \Phi_{w25} + \lambda_{wL2L5}N_{wL2L5} + \left(-\dfrac{f_{L1}{}^2}{f_{L1}f_{L5}} + \dfrac{f_{L1}{}^2}{f_{L2}f_{L5}} \right)I_{L1}}{\lambda_{wL1L5}} \quad \text{(m)} \tag{3.23}$$

Ionosphere error in the second step is:

$$I_{SS} = \left(-\frac{f_{L1}{}^2}{f_{L1}f_{L5}} + \frac{f_{L1}{}^2}{f_{L2}f_{L5}} \right)I_{L1} \quad \text{(m)} \tag{3.24.1}$$

$$I_{SS} = \frac{\left(-\dfrac{f_{L1}{}^2}{f_{L1}f_{L5}} + \dfrac{f_{L1}{}^2}{f_{L2}f_{L5}} \right)\lambda_{L1}}{\lambda_{WL1L5}} \times \frac{I_{L1}}{\lambda_{L1}} \quad \text{(cycle)} \tag{3.24.2}$$

Standard deviation of measurement noise in the second step is:

$$\sigma_{SS} = \sqrt{\sigma_{\varepsilon L1L5}{}^2 + \sigma_{\varepsilon L2L5}{}^2} \quad \text{(m)} \tag{3.25.1}$$

$$\sigma_{SS} = \frac{\sqrt{\sigma_{\varepsilon L1L5}{}^2 + \sigma_{\varepsilon L2L5}{}^2}}{\lambda_{wL1L5}} \quad \text{(cycle)} \tag{3.25.2}$$

where, $\sigma_{\varepsilon L1L5}$ shows the standard deviation of MWL signal noise in unit m, and $\sigma_{\varepsilon L2L5}$ shows the standard deviation of EWL signal noise in unit m.

If the condition the sum of ionosphere range errors and the measurement noise in equation (3.25) is within half of MWL wavelength, the integer MWL ambiguity can be successfully obtained by rounding the float ambiguity to the nearest integer:

$$N_{wL1L5} = _{round}\left(\tilde{N}_{wL1L5}\right) \tag{3.26}$$

After the MWL ambiguity is fixed, the MWL becomes the most precise range and therefore can be used in the estimation of the L1 ambiguity.

◆ **Third Step**

Combination MWL from equation (3.9) and carrier phase observation from equation (3.4), the float L1 ambiguities $\tilde{N}_{L1}$ could be resolved using MWL range:

$$\tilde{N}_{L1} = \frac{\Phi_{L1} - \Phi_{w15} + \lambda_{wL1L5}N_{wL1L5} + \left(1 + \frac{f_{L1}^2}{f_{L1}f_{L5}}\right)I_{L1}}{\lambda_{L1}} \tag{3.27}$$

Ionosphere error in the third step is:

$$I_{TS} = -\left(1 + \frac{f_{L1}^2}{f_{L1}f_{L5}}\right)I_{L1} \quad \text{(m)} \tag{3.27.1}$$

$$I_{TS} = -\left(1 + \frac{f_{L1}^2}{f_{L1}f_{L5}}\right) \times \frac{I_{L1}}{\lambda_{L1}} \quad \text{(cycle)} \tag{3.27.2}$$

Standard deviation of measurement noise in the third step is:

$$\sigma_{TS} = \sqrt{\sigma_{\varepsilon L1}^2 + \sigma_{\varepsilon L1L5}^2} \quad \text{(m)} \tag{3.28.1}$$

$$\sigma_{TS} = \frac{\sqrt{\sigma_{\varepsilon L1}^2 + \sigma_{\varepsilon L1L5}^2}}{\lambda_{L1}} \quad \text{(cycle)} \tag{3.28.1}$$

where, $\sigma_{\varepsilon L1L5}$ shows the standard deviation of MWL signal noise in unit m., and $\sigma_{\varepsilon L1}$ shows the standard deviation of L1 carrier phase signal noise in unit m.

The integer L1 ambiguity can be obtained in equation (3.29) assuming that the sum of ionosphere error and measurement noise in equation (3.28) does not exceed half of an L1 cycle.

$$N_{L1} = _{round}\left(\tilde{N}_{L1}\right) \tag{3.29}$$

Once N_{L1}, N_{wL1L5} and N_{wL2L5} are fixed, the other primary signal ambiguities could also be derived as:

$$N_{L5} = N_{L1} - N_{wL1L5} \qquad\qquad (3.30.1)$$
$$N_{L2} = N_{L1} - N_{wL1L5} - N_{wL2L5} \qquad\qquad (3.30.2)$$

Similar to dual frequency WL method, there are two mainly error sources, ionosphere error and amplified measurement noise, in WL method. Basing on measurement noise of primary signal noise given in table 3.1 and which of WL signal in table 3.2, table 3.4 indicates influence of ionosphere errors and measurement noise on each step using WL method for triple frequency.

Steps	Ionosphere error	Measurement noise
	in meters	
1	$-0.72\,I_{L1}$	0.232
2	$0.38\,I_{L1}$	0.119
3	$-2.34\,I_{L1}$	0.013
	in cycles	
1	$-0.023\,\dfrac{I_{L1}}{\lambda_{L1}}$	0.04
2	$-0.096\,\dfrac{I_{L1}}{\lambda_{L1}}$	0.16
3	$-2.34\,\dfrac{I_{L1}}{\lambda_{L1}}$	0.07

Table 3.4 Influence of ionosphere errors and measurement noise on each step
using triple frequency WL method

According to table 3.4, the influence of ionosphere error on EWL AR in the first step could be almost negligible. In the second step, the influence of ionosphere error on WL AR increases significantly, but still no more than 0.1 time of I_{L1} in unit cycles. However, ionosphere error in L1 AR in the third step is amplified over 2.0 time of I_{L1} in unit cycles. Among three steps AR, step3 is the worst in ionosphere error, and step 2 is the worst in measurement noise. Step 1 is the best in ionosphere error and measurement noise.

3.2.4 Limitation in Triple Frequency WL Method

In this part, probability of success rounding in three steps in triple frequency WL method was estimated to evaluate AR performance.

◆ **Probability of success rounding of EWL signal in triple frequency WL method**

In the first step, the difference x between float EWL ambiguity $\tilde{N}_{wL2L5}$ and corresponding correct ambiguity N_{wL2L5} is:

$$x = \tilde{N}_{wL2L5} - N_{wL2L5} \qquad (3.25.1)$$

The difference follows a normal distribution as:

$$f(x \mid \mu_x, \sigma_x) = \frac{1}{\sqrt{2\pi}\sigma_x} \exp\left[-\frac{x^2}{2\sigma_x{}^2} \right] \qquad (3.25.2)$$

where, μ_x is the mean value of x, and σ_x is the standard deviation in unit cycle, which could estimated as:

$$\sigma_x = \sqrt{\sigma_I^2 + \sigma_\Phi^2} \text{ (cycle)} \qquad (3.25.3)$$

where σ_I^2 means the variance of the residual ionosphere error in unit cycle, and σ_Φ^2 means the variance of the measurement noise in unit cycle, which has been listed in table 3.2 In order to fix correct integer through rounding, it should be satisfied with $|x| < 0.5$,[Jung, J, P. Enge, and B. Pervan, (2000)] so the probability in the first step $P_{correct\ N_{EWL}}$ could calculated in equation (3.25.4) when **means of** x **is zero**.

$$P_{correct\ N_{EWL}} = \int_{-0.5}^{0.5} f(x)dx \qquad (3.25.4)$$

◆ **Probability of success rounding of MWL signal in triple frequency WL method**

Similar to the first step, the difference y between float $\tilde{N}_{wL1L5}$ and corresponding correct ambiguity N_{wL1L5} in the second step was give as:

$$y = \tilde{N}_{wL1L5} - N_{wL1L5} \qquad (3.26.1)$$

$$P_{correct\ N_{MWL}} = \int_{-0.5}^{0.5} f(y)dy \times P_{correct\ N_{EWL}} = \int_{-0.5}^{0.5} f(y)dy \int_{-0.5}^{0.5} f(x)dx \qquad (3.26.2)$$

when **means of** y **is zero**.

◆ **Probability of success rounding of L1 signal in triple frequency WL method**

Similar to the first step, the difference z between float $\tilde{N}_{L1}$ and corresponding correct ambiguity N_{L1} in the third step was give as:

$$z = \tilde{N}_{L1} - N_{L1} \tag{3.27.1}$$

$$P_{correct\ N_{L1}} = \int_{-0.5}^{0.5} f(z)dz \times P_{correct\ N_{MWL}} \times P_{correct\ N_{EWL}} = \int_{-0.5}^{0.5} f(z)dz \int_{-0.5}^{0.5} f(y)dy \int_{-0.5}^{0.5} f(x)dx \tag{3.27.2}$$

when **means of** z **is zero**.

According to derived ionosphere error and measurement noise with triple frequency WL AR in table 3.4, figure 3.2 gives the probability of success rounding $P_{correct\ N_{EWL}}$, $P_{correct\ N_{MWL}}$ and $P_{correct\ N_{L1}}$ in 3 steps with increase of the residual DD ionosphere range errors, assuming **zero mean of** x , y , z .

(a)

(b)

(c)
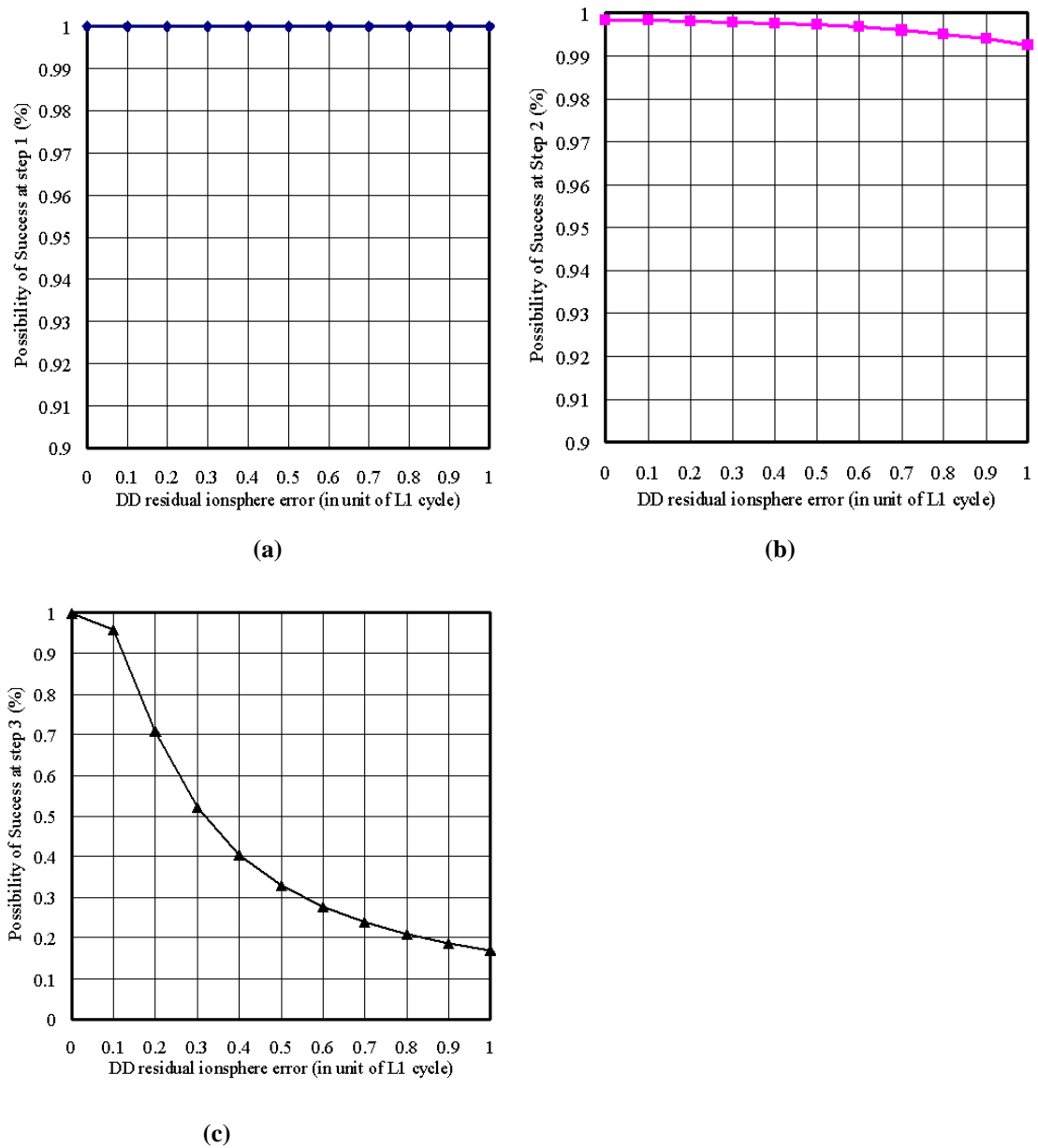
Figure 3.2 Success rate of rounding in three steps using triple frequency WL method.

In figure 3.2, figure 3.2(a) gives the success rate of rounding in step 1 $P_{correct\ N_{EWL}}$, figure 3.2(b) gives the success rate of rounding in step 2 $P_{correct\ N_{MWL}}$, and figure 3.2(c) gives the success rate of rounding in step 3 $P_{correct\ N_{L1}}$. With the increasing in ionosphere error from 0.0 to 1.0, the probability of correct rounding for EWL in step 1 was all 100.0%. It means that ionosphere error could not affect the performance in EWL ambiguity estimation. Though the probability of correct rounding for MWL in step 2 was worse than which in step 1, it could also more than 99.0%. However, probability of the correct rounding on L1 signal in step 3 drops to a very low level when ionosphere became greater, it means that L1 ambiguity estimation in step 3 is very sensitive to the growth of the ionosphere error.

From figure 3.2, over short distance, ionosphere error can be effectively cancelled by double differencing, so the ambiguity estimation is mainly subject to measurement noise, ambiguity could be estimated perfectly using WL method. However, with increasing baseline distance, the residual ionosphere error increases gradually. The increased ionosphere error may lead to failures of integer round in longer baseline. Limitation of WL method was concluded, Therefore, AR with WL method is generally possible over short baseline. In this research, **WL method was proposed in short and medium baseline**.

3.2.5 Impact from Triple Frequency WL Method

In this part, expected impact form triple frequency WL method was discussed. Probability of success rounding on L1 signal using triple frequency WL method was compared to which using dual frequency WL method.

◆ **Probability of success rounding of L1 signal in dual frequency WL method**

Using acknowledges introduced in the last part, probability of success rounding on L1 signal using dual frequency WL method was given as:

$$P_{correct\ N_{L1}} = \int_{-0.5}^{0.5} f(y)dy\, P_{correct\ N_{WL}} = \int_{-0.5}^{0.5} f(y)dy \int_{-0.5}^{0.5} f(x)dx \qquad (3.27.3)$$

where:
difference x between float $\tilde{N}_{wL1L2}$ and corresponding correct ambiguity N_{wL1L2} in the first step was given as:
$x = \tilde{N}_{wL1L2} - N_{wL1L2}$, when **means of** x **is zero**.

difference y between float $\tilde{N}_{L1}$ and corresponding correct ambiguity N_{L1} in the second step was give as:

$y = \tilde{N}_{L1} - N_{L1}$, when **means of** y **is zero**.
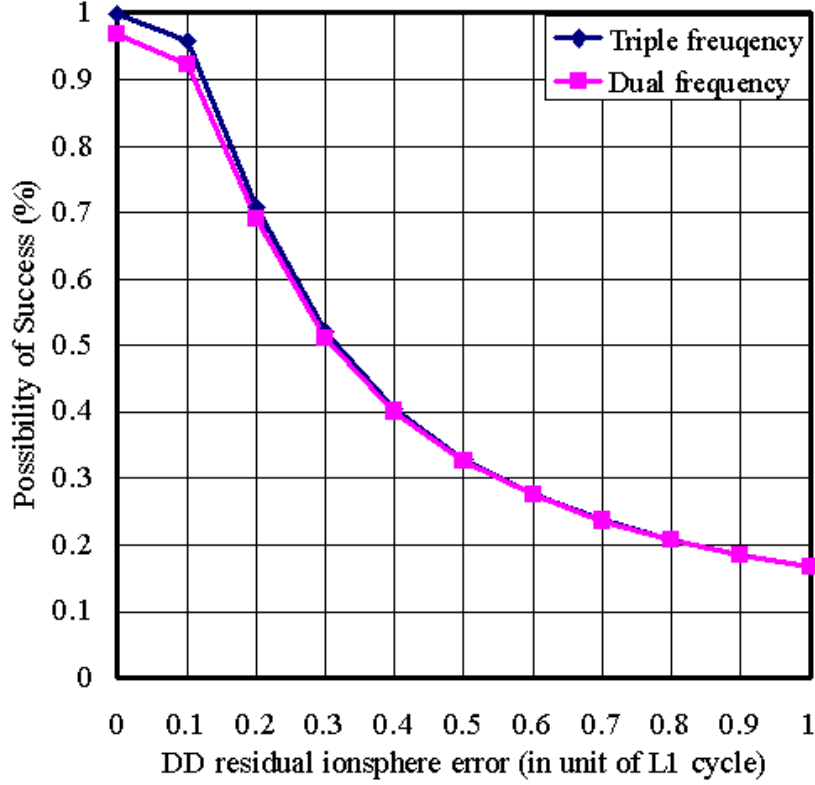
Figure 3.3 L1 signal success rate of rounding using triple or dual frequency WL method.

◆   **Impact in shorter baseline from triple frequency WL AR**

According to ionosphere error and measurement noise with dual frequency WL AR derived in table 3.3 and which with triple frequency WL AR derived in table 3.4, figure 3.3 gives the probability of success rounding of L1 signal with triple and dual WL AR with increasing of ionosphere error.

From figure 3.3, using triple frequency WL method, in shorter baseline, when $\dfrac{\nabla\Delta I_{L1}}{\lambda_{L1}} < 0.15$ (cycle), because ionosphere error was not greater, the probabilities of L1 signal success rounding were much more higher than which using dual frequency WL method, efficiency and reliability were improved. The impact from triple frequency could be concluded. However, with limitation in WL AR in longer baseline, which was introduced in the last part, ionosphere error became mainly error to influent the AR performance in the last step of WL AR, probability of L1 signal success rounding could not be improved obviously from using triple frequency WL method.

In present dual frequency system, it is very difficult to resolve ambiguity problem completely in longer baseline without the assistance from external sources. However, in triple frequency system, it makes possible to determine ambiguity with LC signals. In this research, geometry-free (GF) method and ionosphere-free (IF) method were proposed for longer baseline AR.

3.3 GEOMETRY-FREE (GF) AR MEHTOD

The geometry-free (GF) method in triple frequency system was introduced in this section. In this method, two linear independent GF signal could be formed with primary and estimated WL signals, and then using an ionosphere-free (IF) combination measurement with two GF signals. The similar GF AR method was developed by Mr. Isshiki at 2003 early. [H.Isshiki (2003)]

3.3.1 GF Combination Signal

Geometry-Free (GF) combination signal can be shown as following:

$$\Phi_{G\kappa\lambda} = \Phi_{\kappa} - \Phi_{\lambda} = \left(-\frac{f_{L1}{}^2}{f_{\kappa}{}^2} + \frac{f_{L1}{}^2}{f_{\lambda}{}^2}\right)I_{L1} + (\lambda_{\kappa}N_{\kappa} - \lambda_{\lambda}N_{\lambda}) + \varepsilon_{G\kappa\lambda} \quad \text{(m)} \tag{3.25.1}$$

where

wavelength of GF signal is: $\lambda_{G\kappa\lambda} = \lambda_{\kappa} - \lambda_{\lambda}$ (m);

when $\lambda_{\kappa} - \lambda_{\lambda} > 0$.

frequency of GF signal is: $f_{G\kappa\lambda} = \dfrac{c}{\lambda_{G\kappa\lambda}}$

c means light velocity;

$\varepsilon_{G\kappa\lambda}$ is the measurement noise in GF signal.

GF signal could also be expressed in unit cycles:

$$\phi_{G\kappa\lambda} = \lambda_{\kappa}\phi_{\kappa} - \lambda_{\lambda}\phi_{\lambda} \quad \text{(cycles)} \tag{3.25.2}$$

In three frequencies system, there are two different GF combinations in the carrier phase measurements. It is the most difference to the dual frequencies because there is only one GF combination in the carrier phase measurements in dual frequency system. Two GF combination signals $\Phi_{GL2L5-L5}$ and $\Phi_{GL1L5-L5}$ which were interested in GF method were derived from primary signal L5 and EWL signal or primary signal L5 and MWL signal.

$$\Phi_{GL2L5-L5} = \Phi_{wL25} - \Phi_{L5} \quad \text{(m)} \tag{3.26.1}$$

$$\Phi_{GL2L5-L5} = \left(\frac{f_{L1}{}^2}{f_{L5}{}^2} + \frac{f_{L1}{}^2}{f_{L2}f_{L5}}\right)I_{L1} + (\lambda_{wL2L5}N_{wL2L5} - \lambda_{L5}N_{L5}) + \varepsilon_{GL2L5-L5} \text{(m)} \tag{3.26.2}$$

$$\Phi_{GL2L5-L5} = \frac{f_{L1}}{f_{L5}}\left(\frac{f_{L1}}{f_{L5}} + \frac{f_{L1}}{f_{L2}}\right)I_{L1} - \lambda_{L5}N_{L5} + \lambda_{wL2L5}N_{wL2L5} + \varepsilon_{GL2L5-L5} \text{ (m)} \qquad (3.26.3)$$

$$\Phi_{GL1L5-L5} = \Phi_{wL15} - \Phi_{L5} \text{ (m)} \qquad (3.27.1)$$

$$\Phi_{GL1L5-L5} = \left(\frac{f_{L1}^2}{f_{L5}^2} + \frac{f_{L1}^2}{f_{L1}f_{L5}}\right)I_{L1} + (\lambda_{wL1L5}N_{wL1L5} - \lambda_{L5}N_{L5}) + \varepsilon_{GL1L5-L5} \text{ (m)} \qquad (3.27.2)$$

$$\Phi_{GL1L5-L5} = \frac{f_{L1}}{f_{L5}}\left(\frac{f_{L1}}{f_{L5}} + 1\right)I_{L1} - \lambda_{L5}N_{L5} + \lambda_{wL1L5}N_{wL1L5} + \varepsilon_{GL1L5-L5} \text{ (m)} \qquad (3.27.3)$$

where,

noise in each GF combination signal: $\varepsilon_{GL2L5-L5} = \varepsilon_{L2L5} - \varepsilon_{L5}$ $\varepsilon_{GL1L5-L5} = \varepsilon_{L1L5} - \varepsilon_{L5}$

Φ_{L5} is L5 carrier signal, Φ_{L25} is L2-L5 WL signal, Φ_{L15} is L1-L5 WL signal

$f_{L1}\ f_{L2}\ f_{L5}$ is frequency of each primary frequency

λ_{L5} is wavelength of L5 signal

λ_{wL2L5} is wavelength of L2-L5 WL signal

λ_{wL1L5} is wavelength of L1-L5 WL signal

I_{L1} is ionosphere error on L1 signal

Ionosphere error in GF signal $\Phi_{GL2L5-L5}$ is:

$$I_{GL2L5-L5} = \left(\frac{f_{L1}^2}{f_{L5}^2} + \frac{f_{L1}^2}{f_{L2}f_{L5}}\right)I_{L1} \text{ (m)} \qquad (3.28.1)$$

$$I_{GL2L5-L5} = \frac{\left(\frac{f_{L1}^2}{f_{L5}^2} + \frac{f_{L1}^2}{f_{L2}f_{L5}}\right)\lambda_{L1}}{\lambda_{GL2L5-L5}} \times \frac{I_{L1}}{\lambda_{L1}} \text{ (cycle)} \qquad (3.28.2)$$

Standard deviation of measurement noise in GF signal $\Phi_{GL5-L2L5}$ in unit m was given in equation (3.29.1) and that in unit cycle was given in equation (3.29.2).

$$\sigma_{GL2L5-L5} = \sqrt{\sigma_{\varepsilon L5}^2 + \sigma_{\varepsilon L2L5}^2} \text{ (m)} \qquad (3.29.1)$$

$$\sigma_{GL2L5-L5} = \frac{\sqrt{\sigma_{\varepsilon L5}^2 + \sigma_{\varepsilon L2L5}^2}}{\lambda_{GL2L5-L5}} \text{ (cycle)} \qquad (3.29.2)$$

where, $\sigma_{\varepsilon L2L5}$ shows the standard deviation of EWL signal noise in unit m, and $\sigma_{\varepsilon L5}$ shows the standard deviation of L5 carrier phase signal noise in unit m.

Ionosphere error in GF signal $\Phi_{GL1L5-L5}$ is:

$$I_{GL1L5-L5} = \left(\frac{f_{L1}^2}{f_{L5}^2} + \frac{f_{L1}^2}{f_{L1}f_{L5}} \right) I_{L1} \quad (m)$$ (3.29.3)

$$I_{GL1L5-L5} = \frac{\left(\dfrac{f_{L1}^2}{f_{L5}^2} + \dfrac{f_{L1}^2}{f_{L1}f_{L5}} \right) \lambda_{L1}}{\lambda_{GL1L5-L5}} \times \frac{I_{L1}}{\lambda_{L1}} \quad (cycle)$$ (3.29.4)

Standard deviation of measurement noise in GF signal $\Phi_{GL5-L2L5}$ in unit m was given in equation (3.29.5) and that in unit cycle was given in equation (3.29.6).

$$\sigma_{GL1L5-L5} = \sqrt{\sigma_{\varepsilon L5}^2 + \sigma_{\varepsilon L1L5}^2} \quad (m)$$ (3.29.5)

$$\sigma_{GL1L5-L5} = \frac{\sqrt{\sigma_{\varepsilon L5}^2 + \sigma_{\varepsilon L1L5}^2}}{\lambda_{GL1L5-L5}} \quad (cycle)$$ (3.29.6)

where, $\sigma_{\varepsilon L1L5}$ shows the standard deviation of MWL signal noise in unit m, and $\sigma_{\varepsilon L5}$ shows the standard deviation of L5 carrier phase signal noise in unit m. Basing on measurement noise in primary signal given in table 3.1 and which in WL signal given in table 3.2, table 3.5 summarized the influence of ionosphere errors and measurement noise in two GF signals.

GF signal	$\Phi_{GL2L5-L5}$	$\Phi_{GL1L5-L5}$
Frequency (MHz)	53.3564	598.6596
Wavelength	5.605	0.495
Ionosphere error (m)	$3.513 I_{L1}$	$3.133 I_{L1}$
Measurement noise (m)	0.1184	0.013
Ionosphere error (cycles)	$0.119 \dfrac{I_{L1}}{\lambda_{L1}}$	$1.19 \dfrac{I_{L1}}{\lambda_{L1}}$
Measurement noise (cycles)	0.021	0.026

Table 3.5 Influence of ionosphere errors and measurement noise in two GF signals

3.3.2 AR with GF Signals

There are three steps in the proposed GF method. Figure 3.4 shows the flow chat of GF method.In figure 3.4, the first step in approach for AR was estimating ambiguity N_{wL2L5} of EWL Φ_{w25} signal. With the result from the first step, N_{wL1L5} of MWL Φ_{w15} signal is resolved in the second step. In the third step, one GF signal was from L5 signal and estimated EWL signal, the other GF signal was from L5 signal and estimated MWL signal. Using IF combination with these two GF signals, N_{L5} of primary L5 signal could be estimated through time average.
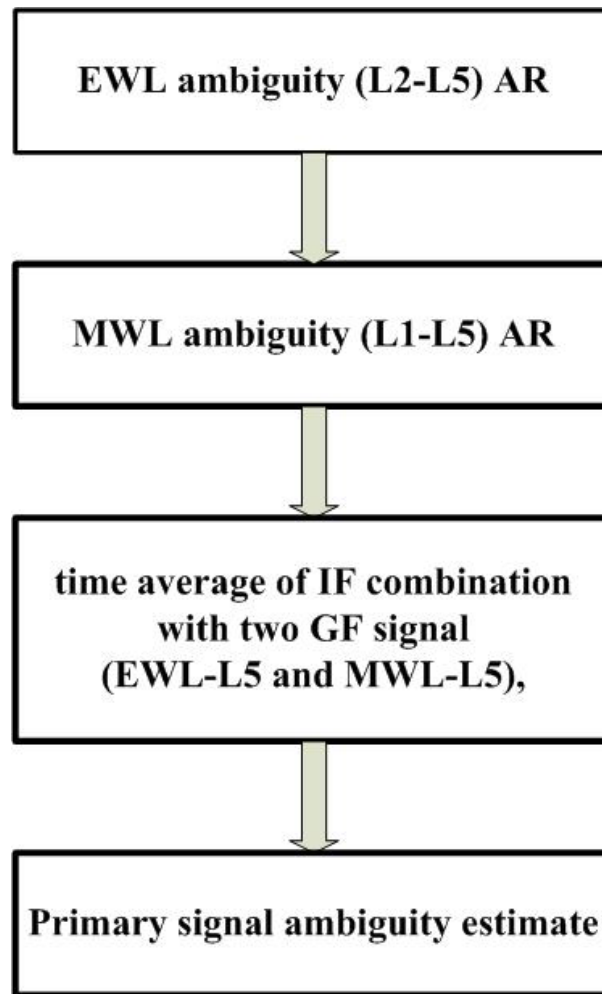
Figure 3.4 Flowchart of GF method

◆ **First Step**

The same as the first step in WL method, EWL ambiguities N_{wL2L5} could be resolved using L1 pseudorange.

◆ **Second Step**

The same as the second step in WL method, MWL ambiguities N_{wL1L5} could be resolved using EWL range.

◆ **Third Step**

Two GF signals could be derived from EWL, MWL and L5 signals. IF combination with two GF signals, ambiguity of primary could be estimated. From equation (3.26.3) and equation (3.27.3), IF combination algorithm between two GF signals is given as following:

$$\Phi_{IF} = \alpha\Phi_{GL1L5-L5} - \beta\Phi_{GL2L5-L5} \qquad\qquad (3.30.1)$$

Where $\alpha = \dfrac{\left(\dfrac{f_{L1}}{f_{L5}} + \dfrac{f_{L1}}{f_{L2}}\right)}{\left(1 - \dfrac{f_{L1}}{f_{L2}}\right)} = -9.2541, \quad \beta = \dfrac{\left(\dfrac{f_{L1}}{f_{L5}} + 1\right)}{\left(1 - \dfrac{f_{L1}}{f_{L2}}\right)} = -8.2553$

$$\tilde{N}_{L5} = \frac{\alpha\left(\Phi_{GL1L5-L5} - \lambda_{wL1L5}N_{wL1L5}\right) - \beta\left(\Phi_{GL2L5-L5} - \lambda_{wL2L5}N_{wL2L5}\right) + \varepsilon_{\tilde{N}_{L5}}}{\lambda_{L5}} \qquad (3.30.2$$

where, noise in equation (3.30.2) is: $\varepsilon_{\tilde{N}_{L5}} = -\alpha\varepsilon_{GL1L5-L5} + \beta\varepsilon_{GL2L5-L5}$

In the equation (3.30), both residual ionosphere errors and geometrical errors are cancelled. However, the measurement noise $\varepsilon_{\tilde{N}_{L5}}$ in equation (3.30) is too **large** to be practical. According to measurement noise in two GF signals given in table 3.5, standard deviation of measurement noise $\sigma_{\tilde{N}_{L5}}$ in equation (3.30) in unit m could be calculated in equation (3.31.1) and noise in unit cycles was given in equation (3.31.2):

$$\sigma_{\tilde{N}_{L5}} = \sqrt{\left(\beta * \sigma_{GL2L5-L5}\right)^2 + \left(\alpha * \sigma_{GL1L5-L5}\right)^2} = 1.1009 \quad (m) \qquad (3.31.1)$$

$$\sigma_{\tilde{N}_{L5}} = \frac{1}{\lambda_{L5}}\sqrt{\left(\beta * \sigma_{GL2L5-L5}\right)^2 + \left(\alpha * \sigma_{GL1L5-L5}\right)^2} = 4.3208 \quad (cycle) \qquad (3.31.2)$$

where, $\sigma_{GL2L5-L5}$ shows the standard deviation of GF signal $\Phi_{GL2L5-L5}$ noise in unit m, and $\sigma_{GL1L5-L5}$ shows the standard deviation of GF signal $\Phi_{GL1L5-L5}$ noise in unit m.

Advantage of GF method is that AR will not be affected by the distance influence. In this method, the troposphere and satellite ephemeris error can be canceled in each GF combinations; the ionosphere error will be canceled in IF combination between equations (3.26) and (3.27), however, the problem is the amplified measurement noise in equation (3.31), the amplified noise is more than 4.0 times of wavelength of L5 signal, it was difficult to estimate ambiguity directly. Assuming measurement noise is near to white noise, by simple time average processing of continuous signal for long sessions, ambiguity could be estimated. Time average was expressed as:

$$N_{L5} = \left(\frac{\displaystyle\sum_{n=0}^{n} \tilde{N}_{L5}(n)}{n}\right)_{round} \qquad\qquad (3.32)$$

where, n is average epoch.

In this research, **GF method was used in long and extra-long baseline AR**, and **120 seconds** was used in time average of continuous signal estimation in GF method.

3.4 IONOSPHERE-FREE (IF) AR METHOD

In the last section, GF method was developed using IF combination with two GF signals. In this section, that using GF combination with two IF signals was proposed, so the method was called ionosphere-free (IF) AR method. The theory of IF method was developed by Mr. Hatch at 2006 [Ronald R. Hatch, (2006)] early.

3.4.1 IF Combination Signal

Carrier phase observation on primary signal in unit m was rewritten as:

$$X_\kappa = (\phi_\kappa - N_\kappa)\lambda_\kappa = \rho + T + \frac{I}{f_\kappa^2} + \varepsilon_\kappa \quad (m) \tag{3.33}$$

where, ϕ means carrier phase observation in unit cycle,

N means ambiguity of signal

λ means wavelength of signal

I means ionosphere error

WL signal in unit m was also rewritten as:

$$X_{w\kappa\lambda} = (\phi_\kappa - \phi_\lambda - N_{w\kappa\lambda})\lambda_{w\kappa\lambda} = \rho + T + \frac{I}{f_\kappa f_\lambda} + \varepsilon_{w\kappa\lambda} \quad (m) \tag{3.34}$$

Where, f means frequency of signal.

◆ **IF with two WL signals**

IF combination signal X_{WIF} in unit m with EWL and WL signals was given as:

$$X_{WIF} = \frac{f_{L1}}{f_{L1} - f_{L5}} X_{WL1L2} - \frac{f_{L5}}{f_{L1} - f_{L5}} X_{WL2L5} = \rho + T + \varepsilon_{WIF} \quad (m) \tag{3.34}$$

where,

measurement noise in unit m in equation (3.34) is

$$\sigma_{WIF} = \sqrt{\left(\frac{f_{L1}}{f_{L1} - f_{L5}} * \sigma_{WL1L2}\right)^2 + \left(\frac{f_{L5}}{f_{L1} - f_{L5}} * \sigma_{WL2L5}\right)^2} \quad (m)$$

Equation (3.34) gives us a carrier phase measurement with no ionosphere range error corruption.

◆ **IF with three frequencies signals**

LC combination signal with three signals was rewritten in unit m as:

$$X_{LC} = aX_a + bX_b + cX_c + \varepsilon \quad (m) \tag{3.36.1}$$

From equation (3.33), LC in unit m was derived as:

$$X_{LC} = (a+b+c)(\rho+T) - \left(\frac{a}{f_{L1}^2} + \frac{b}{f_{L2}^2} + \frac{c}{f_{L5}^2}\right)I + \varepsilon_{LC} \quad (m) \qquad (3.36.2)$$

where: ε_{LC} means noise in LC signal: $\varepsilon_{LC} = a\varepsilon_{L1} + +b\varepsilon_{L2} + +c\varepsilon_{L5}$

Using acknowledges introduced in section (3.1.3), in order to convert LC signal, expressed as equation (3.36.2), into IF combination signal and to minimize the amplified noise in IF signal, the value of coefficients, a b and c should be satisfied :

$$a+b+c=1 \qquad\qquad (3.37.1)$$

$$\frac{a}{f_{L1}^2} + \frac{b}{f_{L2}^2} + \frac{c}{f_{L5}^2} = 0 \qquad (3.37.2)$$

$$a^2 + b^2 + c^2 = \min \qquad\qquad (3.37.3)$$

Equation (3.37.1) ensures the range measurement is not scaled. Equation (3.37.2) ensures that the ionosphere range error is canceled, and equation (3.37.3) ensures that minimum amplified measurement noise.

In this research, equation (3.37.3) was set to zero, the minimum noise IF signal X_{MIF} was shown as:

$$X_{MIF} = a_{MIF}X_{L1} + b_{MIF}X_{L2} + c_{MIF}X_{L5} = \rho + T + \varepsilon_{MIF} \; (m) \qquad (3.38)$$

where,

$$c_{MIF} = 1 - a_{MIF} - b_{MIF} \; ;$$

$$b_{MIF} = \frac{f_{L1}^2}{f_{L1}^2 - f_{L5}^2} - a_{MIF}\frac{f_{L1}^2(f_{L2}^2 - f_{L5}^2)}{f_{L2}^2(f_{L1}^2 - f_{L5}^2)} = \alpha - a_{MIF}\beta$$

$$a_{MIF} = \frac{(1 - \alpha - \beta + 2\alpha\beta)}{2(1 - \beta + \beta^2)}$$

ε_{MIF} means measurement noise in IF signal X_{MIF}, standard deviation of noise in unit m could be estimated from equation (3.5.7).

Basing on measurement signal noise of primary signal given in table 3.1 and which of WL signal given in table 3.2, measurement noises in two IF signals could be estimated. Table 3.6 gives the coefficients and measurement noise for two IF signals. From table 3.6, IF signal Φ_{MIF} from three primary signals has much lower noise than that in Φ_{WIF} signal form two WL signals. It shows that, if the primary ambiguities could be resolved, Φ_{MIF} signal would be in a slightly lower measurement noise.

IF signal	a	b	c	noise (m)
Φ_{WIF}	3.949	2.949	0	0.3568
Φ_{MIF}	-0.3596	2.3269	-0.9673	0.0105

Table 3.6 Coefficients and measurement noise in IF signals

3.4.2 AR with IF Signal

There are three steps in the proposed IF method. Figure 3.5 shows the flow chat of IF method. In figure 3.5, the first step in approach for AR was estimating ambiguity N_{wL2L5} of EWL Φ_{w25} signal. With the result from the first step, N_{wL1L5} of MWL Φ_{w15} signal is resolved in the second step. In the third step, one IF signal was derived from estimated EWL signal and WL signal, which was estimated but noisy. The other IF signal was derived from three primary signals, which was with small measurement but ambiguity was unknown. Using time average method, primary ambiguity could be estimated through GF combination.
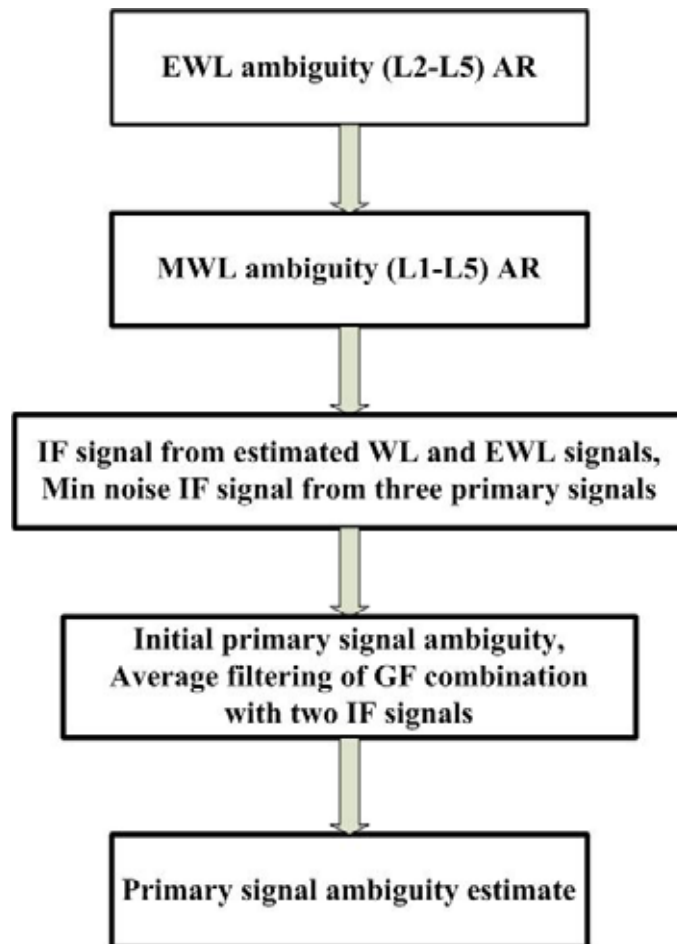
Figure 3.5 Flow chat of IF method

◆ **First Step**

The same as the first step in WL method, EWL ambiguities N_{wL2L5} could be resolved using L1 pseudorange.

◆ **Second Step**

The same as the second step in WL method, MWL ambiguities N_{WL1L5} could be resolved using EWL range.

◆ **Third Step**

Because two WL signal ambiguities were determined, the third WL signal ambiguity could also be estimated, so all three of the wide lane ambiguities N_{wL1L5}, N_{wL2L5} and N_{wL1L2} were known. Measuring IF signal X_{WIF} from equation (3.34) from estimated EWL signal and WL signal.

Now assuming the initial ambiguity of one primary signal, for example: N_{L1}. Estimating error k cycle was included, so

$$\hat{N}_{L1} = N_{L1} + k \qquad (3.39)$$

Because three true WL signal ambiguities were estimated in the first step, we also can get:

$$\hat{N}_{L2} = \hat{N}_{L1} - N_{wL1L2} = N_{L2} + (\hat{N}_{L1} - N_{L1}) = N_{L2} + k \qquad (3.40)$$
$$\hat{N}_{L3} = N_{L3} + k \qquad (3.41)$$

Defining the minimum-noise IF signal with three primary signals could be shown as X_{MIF}, using equation (3.38), X_{MIF} signal with initial ambiguities could be given as:

$$X_{MIF} = a_{MIF}\lambda_{L1}(\phi_{L1} - (N_{L1} + k)) + b_{MIF}\lambda_{L2}(\phi_{L2} - (N_{L2} + k)) + c_{MIF}\lambda_{L5}(\phi_{L5} - (N_{L5} + k)) \text{ (m)} (3.42)$$

Because in equation (3.37.1), $a + b + c = 1$, IF signal could be derived as:

$$X_{MIF} = a_{MIF}X_{L1} + b_{MIF}X_{L2} + c_{MIF}X_{L5} = \rho + T + \varepsilon_{MIF} + +k\lambda_{MIF} \text{ (m)} \qquad (3.43)$$

where, λ_{MIF} was wavelength of minimum noise IF signal : $a_{MIF}\lambda_{L1} + b_{MIF}\lambda_{L2} + c_{MIF}\lambda_{L5}$

The offset difference value at epoch i between two IF signals X_{WIF} (3.34) and X_{MIF} from equation (3.43) was:

$$O_i = X_{WIF,i} - X_{MIF,i} = (\rho + T + \varepsilon_{WIF}) - (\rho + T + \varepsilon_{MIF} + k\lambda_{MIF}) = (\varepsilon_{WIF} - \varepsilon_{MIF}) - k\lambda_{MIF}$$
$$= \varepsilon_i - k\lambda_{MIF} \tag{3.44}$$

Equation (3.44) was also called GF combination, because geometry "$\rho+T$"could be deleted here. From equation (3.44), at a specific epoch, the offset O_i consist of a noise component ε_i which will arise primarily mainly from the noise amplification in the IF signal X_{WIF} and a constant bias $k\lambda_{MIF}$ which arises from the initial error estimate in the whole cycle ambiguity value at primary frequency signal.

According to two IF signals' measurement noises given in table 3.6, standard deviation of noise in unit m in equation (3.44) was given in equation (3.45.1), and noise in unit cycles was also given is equation (3.45.2).

$$\sigma_i = \sqrt{\sigma_{WIF}^2 + \sigma_{MIF}^2} = 0.3570 \,(\text{m}) \tag{3.45.1}$$

$$\sigma_i = \frac{1}{\lambda_{L1}} \sqrt{\sigma_{WIF}^2 + \sigma_{MIF}^2} = 1.88 \,(\text{cycle}) \tag{3.45.2}$$

Because noise in equation (3.44) was too large, it was about 1.88 times of L1 signal wavelength in unit cycles, it was no possible to estimate L1 ambiguity directly. **Assuming the ambiguity was constant and noise of IF signal was white**, using the average filtering, after sufficient smoothing time, noise will average toward zero, and the value $k\lambda_{RC}$ can be estimated. The smoothed offset was defined as S_n. True ambiguity of primary signal could be estimated from equation (3.46).

$$N_{L1} = \hat{N}_{L1} +_{round}\left(S_n / \lambda_{MIF}\right) = \hat{N}_{L1} - k \tag{3.46}$$

IF method was also proposed for long and extra long baseline AR. In the research, the smoothing time was set to **120 seconds**.

3.5 SUMMARY

In this chapter, various linear combination signals with triple frequency signal were developed. WL method, GF method and IF method with triple frequency signals were discussed. Impact from triple frequency was also studied. Table 3.7 summarized three proposed triple frequency LC AR methods.

From table 3.7, the same AR, EWL AR and MWL AR, was performed at the first and second step among three triple frequency AR methods. At the third step, primary ambiguity was estimated using range of MWL signal directly in WL method, performance was affected easily with increasing residual ionosphere error. In GF and IF methods, primary ambiguity was estimate using various LC signals, ionosphere and geometry error could be canceled, however, amplified measurement noise in LC signal became the mainly error.

Ambiguity could not be estimated without extra suitable method.

Because differential ionosphere delay could be canceled in DD method in short or medium baseline, WL method was offered. From analysis, in shorter baseline, with extra frequency signal, probability of success rounding was improved, primary signal ambiguity could be expected to estimate more accurate and fast.

In long or extra-long baseline, differential ionosphere delay was not neglected. Triple frequency signals could also supply the chance to resolve the ambiguity problem using proposed GF method and IF method.

In GF method, measurement noise was about 4.3208 cycle of L5 signal wavelength in L5 signal AR. In IF method, measurement noise was only about 1.88 cycle of L1 signal wavelength in L1 signal AR. AR performance in IF method was expected better than which in GF method.

	WL method	GF method	IF method
First step	EWL AR using L1 pseudorange	EWL AR using L1 pseudorange	EWL AR using L1 pseudorange
Second step	MWL AR using EWL single	MWL AR using EWL single	MWL AR using EWL single
Third step	Primary signal AR using MWL signal	two GF signals ($\Phi_{GL1L5-L5}$: L5 and MWL) ($\Phi_{GL2L5-L5}$: L5 and EWL)	two IF signals (X_{WIF}: WL and EWL) (X_{MIF}: L1, L2 and L5)
		IF combination with two GF signals	GF combination with two IF signals
		Primary signal AR using time average	Primary signal AR using average filter from initial primary ambiguity
Mainly error	Residual ionosphere range error	Amplified measurement noise	Amplified measurement noise
Error in primary signal AR (cycle)	$-2.34\dfrac{I_{L1}}{\lambda_{L1}}+0.07$	4.3208	1.88
Baseline	Short and Medium	Long and Extra-long	Long and Extra-long

Table 3.7 Three proposed triple frequency LC AR methods

In this chapter, expected performance of GPS augmentation with QZSS was studied using estimating NVS, DOP, DGPS positioning results and L1 signal ASR in short baseline. Numerical estimation was used the triple frequency simulator. In this Chapter, flow chart of triple frequency simulator was introduced. QZSS performance in near to Japan area or in East Asia region was discussed. The feature of QZSS orbit was also studied.

4.1 PERFORMANCE EVALUATION PARAMETERS

Performance of QZSS would be evaluated using data from triple frequency simulator as following:

Availability of system was proved using measurement of NVS (Number of Visible Satellites). Higher numbers of NVS are better.

Accuracy of system was assessed using estimation of PDOP (Position Dilution of Precision). Lower numbers of PDOP are better.

Efficiency and **reliability** of system was evaluated using GPS L1 carrier phase ambiguity resolution success rate (ASR). Higher numbers of ASR are better.

4.2 TRIPLE FREQUENCIES SIMULATOR

Because there is no third frequency signal in fact, and QZSS is not in operating, the triple-frequency simulator was developed to evaluate QZSS performance in this research. Range error and noise models used in the simulator were introduced in this section. The details of triple-frequency simulator can also be found in [Yun Zhang, (2005)].

4.2.1 Error Model

The triple-frequency simulator was created to perform numerical estimations of the GPS constellation and measurement [Yun Zhang, Nobuaki Kubo, Akio Yasuda. (2005)]. Figure 4.1 shows the flow chart of the GPS triple-frequency simulator, and Table 4.1 summarizes the model error parameters used in the triple-frequency simulator.
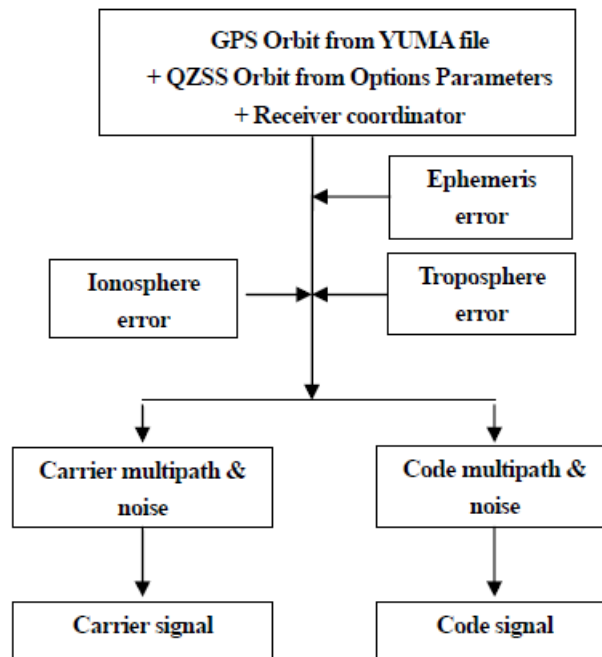
Figure 4.1 Triple-frequency simulator flow chart.

Error Parameters	Error Model
Ionosphere error model	Klobuchar's model
Troposphere error model	Saastamoinen's model
Ephemeris error	RMS 2.1 m white noise
Code noise	DLL thermal noise
Carrier noise	PLL thermal noise
Multipath error	Reflected from ground
Antenna carrier offset	Download from National Geodetic Survey (NGS)

Table 4.1 Model error parameters in GPS triple frequencies simulation

◆ **Ionosphere error**

The ionosphere is a region of ionized plasma that extends from roughly 50km to 2000km surrounding the surface of the earth. The ionosphere can be usually divided into D, E, F1, F2 and H+ regions according to the electron density, thus the F2 regions (210-1000km) is the most dense and also the highest variability, causing most of the potential effects on GPS receiver system. The ionosphere causes GPS signal delays due to the Total Electron Content (TEC) along the path from the GPS satellite to receiver. [Yun Zhang, Falin Wu, Nobuaki Kubo, Akio Yasuda, (2003)] Vertical TEC (VTEC) could be converted from the slang TEC (STEC) using mapping function in the single layer model (SLM). Figure 4.2 shows VTECs measured by single dual-frequency GPS receiver and from International Reference Ionosphere (IRI-95) model (http://modelweb.gsfc.nasa.gov/ionos/iri.html) from 00:00 to 24:00 (LT) July 7, 2003 for 24 hours at (E 35º 39', N 139º47').
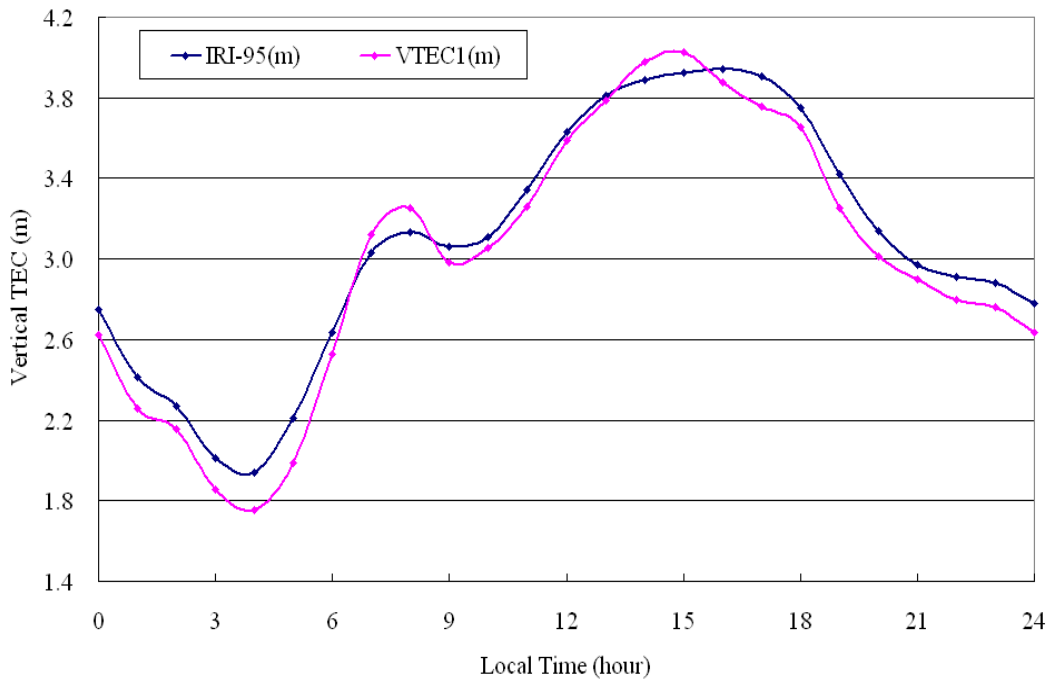
Figure 4.2 Local time variations of the one-hour-average VTEC measured by single dual-frequency receiver and from IRI-95 model for 24 hours

In the simulator, ionosphere range error was modeled as Klobuchar's model.[Klobuchar, 1996] In the model, the ionosphere delay time T_{iono} estimate at local time t is given as following (Here Φ_u is approximate geodetic latitude, λ_u is geodetic longitude, E is elevation angle and A is azimuth for every satellites):

1) Calculate the Earth-centered angle, ψ

$$\psi = 0.0137 /(E + 0.11) - 0.022 \quad \text{(semicircles)} \tag{4.1.1}$$

2) Compute the subionospheric latitude, Φ_I

$$\Phi_I = \Phi_u + \psi \cos A \quad \text{(semicircles)} \tag{4.1.2}$$

if $\Phi_I > +0.416$, then $\Phi_I = +0.416$. If $\Phi_I < -0.416$, then $\Phi_I = -0.416$

3) Compute the subionospheric longitude, λ_I

$$\lambda_I = \lambda_u + (\psi \sin a / \cos \Phi_I) \quad \text{(semicircles)} \tag{4.1.3}$$

4) Find the geomagnetic latitude, Φ_m, of the subionosphere location looking toward each GPS satellite.

It is found by $\Phi_m = \Phi_I + 0.064 \cos(\lambda_I - 1.617)$ (semicircles) $\tag{4.1.4}$

5) Find the local time, t at the subionosphere point

$$t = 4.32 \times 10^4 \lambda_I + GPS \quad time \quad \text{(seconds)} \tag{4.1.5}$$

if t>86,400, use t=t-86,400; if t<0, add 86,400.

6) To convert to slant time delay, compute the slant factor F

$$F = 1.0 + 16.0 \times (0.53 - E)^3 \tag{4.1.6}$$

7) Then compute the ionosphere time delay T_{iono} by first computing x

$$x = \frac{2\pi(t - 50400)}{\sum_{n=0}^{3} \beta_n \Phi_m^n} \tag{4.1.7}$$

if $|x|>1.57$, $T_{iono} = F \times (5 \times 10^{-9})$ (sec ond) $\tag{4.1.8}$

Otherwise

$$T_{iono} = F \times [5 \times 10^{-9} + \sum_{n=0}^{3} \alpha_n \Phi_m^n \times (1 - \frac{x^2}{2} + \frac{x^4}{24})] \text{ (sec} ond)$$

8) Ionosphere delay can be estimated:

$$Iono\_delay = Cs \times T_{iono} \ (meter) \tag{4.1.9}$$

where, Cs is light velocity

◆ **Troposphere error**

Troposphere is the neutral atmosphere comprising the lower 8km of the atmosphere. Troposphere error on GPS signals is of the non-dispersive variety because it is not frequency-dependent and hence impacts on both the L1 and L2 signals by the same amount (unlike that within the Ionosphere). In the simulator, troposphere range error was modeled as Saastamoinen's model. [Saastamoinen, 1973] The zenith dry and wet delays $\tilde{T}_Z$ are given as following:

$$\tilde{T}_Z = 0.002277(1+D)\sec\psi_0(P_0 + (\frac{1255}{T_0}+0.005)e_0 - B\tan^2\psi_0] + \delta_R \text{ (m)} \tag{4.2}$$

where, $D = 0.0026\cos 2\phi + 0.00028h$,

(ϕ is the local latitude, and h is the station height in km)

$\psi_0 = 90\deg - E$ ($E >= 10$ degree, satellite elevation angles).

P_0 and e_0 are in millibars, and T_0 is in K.

◆ **Antenna phase center offset**

Antenna phase center offset is the difference between the phase center and the geometry center, determined by the producer. Most of antenna phase center variation depends on satellite elevation angle. [Frank Czopek, Gerald Mader, (2002)]

In the simulator, the values of the receiver antenna phase center offset were given from National Geodetic Survey (NGS) (http://www.ngs.noaa.gov/ANTCAL/index.shtml). Antenna NOVATEL 702 was considered here, the values are given in table 4.2.

L1 offset (rms): north: 0.2mm; east: 0.2mm; up: 0.3mm								
L2 offset (rms): north: 0.1mm; east: 0.0mm; up: 0.5mm								
Elevation (degree)	90	85	80	75	70	65	60	55	50
L1 offset RMS (mm)	0.0	0.1	0.2	0.2	0.2	0.2	0.1	0.0	0.0
L2 offset RMS (mm)	0.0	0.0	0.0	0.0	0.1	0.1	0.1	0.1	0.1
Elevation (degree)	45	40	35	30	25	20	15	10	5
L1 offset RMS (mm)	0.0	0.0	0.0	0.0	0.0	0.1	0.3	0.0	0.0
L2 offset RMS (mm)	0.2	0.2	0.2	0.3	0.3	0.2	0.3	0.3	0.0

Table 4.2 Sample values of the GPS antenna phase offset for NOVATEL 702

◆ **Ephemeris error**

Ephemeris error is a difference between the expected and actual orbital position of a GPS satellite. The accuracy of the current GPS broadcast ephemeris is around 2.6m, and it will be further reduced to 1.25m in GPS modernization [IGS, (2005)]. Ephemeris errors are largely mitigated by DGPS positioning or in DD carrier phase based positioning when the receivers are not up to a few tens of kilometers apart.

In this research, RMS ranging error caused by ephemeris was set to about 2.1 m for a forecast period of up to 24 hr. [Parkinson, B. W., Spilker, J. J., Axelrad, P., and Enge, P., (1996)]

◆ **Code noise and carrier noise**

Code noise and carrier noise were estimated by delay locked-loop (DLL) and phase locked-loop (PLL), [Parkinson, B. W., Spilker, J. J., Axelrad, P., and Enge, P., (1996)], and the noise simulation parameters in this research are given in table 4.3. Early-late correlator was considered here.

	L1	L2	L5
λ_C (m)	293.05	293.05	29.305
λ_L (m)	0.1903	0.224	0.2548
d (chip)	0.1	0.1	1.0
T_d (ms)	20	20	10
B_{DLL} (Hz)	0.5	0.5	0.5
B_L (Hz)	10	10	10

Table 4.3 Noise simulation parameters in triple-frequency simulator

In Table 4.3, λ_C means chip width of the pseudo random noise (PRN) code. In this simulator, using the chip width of the C/A code for the L1 and L2 signals and using the chip width of the P code for the L5 signal. λ_L gives wavelength for the L1, L2 and L5 signals. d means chip spacing between early, prompt, and late (dimensionless). 0.1chip correlator was used on L1 and L2 signal and 1.0 chip correlator was used on L5 signal. T_d indicates predetection integration time. 20ms was on L1, L2 signal and 10ms was on L5 signal. B_{DLL} means code loop noise bandwidth and B_L means carrier loop noise bandwidth.
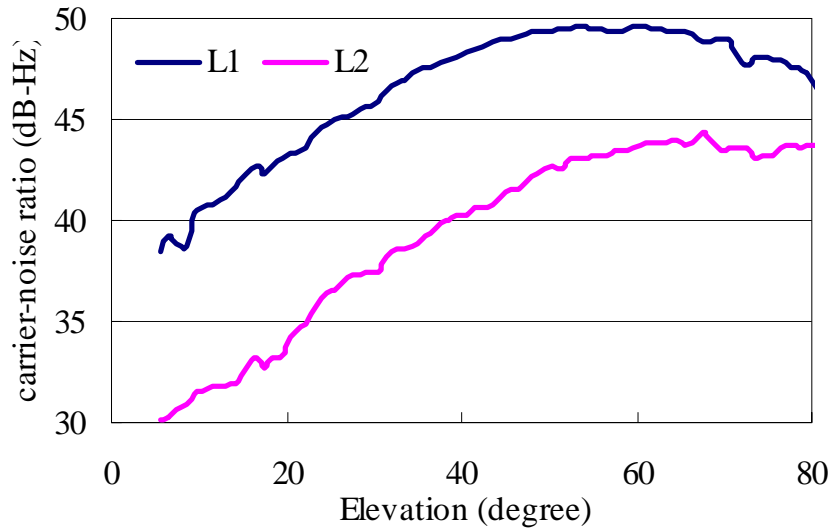
Figure 4.3.1   Results of carrier to noise ratio (c/n_0) estimated using NOVATEL OEM3 receiver and NOVATEL 702 antenna for 12 hours

In order to generate the code and phase noise in the simulation, the signal-noise ratio (c/n_0) with different elevation was determined by the experiment using NOVATEL 702 choke-ring antenna and NOVETAL OEM3 receiver for 24 hours under the clean" environment. [Yun Zhang, Nobuaki Kubo, Akio Yasuda. (2005)] Figure 4.3.1 gives results of carrier to noise ratio (c/n_0) estimated by NOVATEL OEM3 receiver and NOVATEL 702 antenna for 12 hours. Figure 4.3.2 shows simulated code noise generated from PRN31 for 2 hours (multipath error absent), and figure 4.3.23shows simulated carrier phase noise generated from PRN31 for 2 hours (multipath error absent).
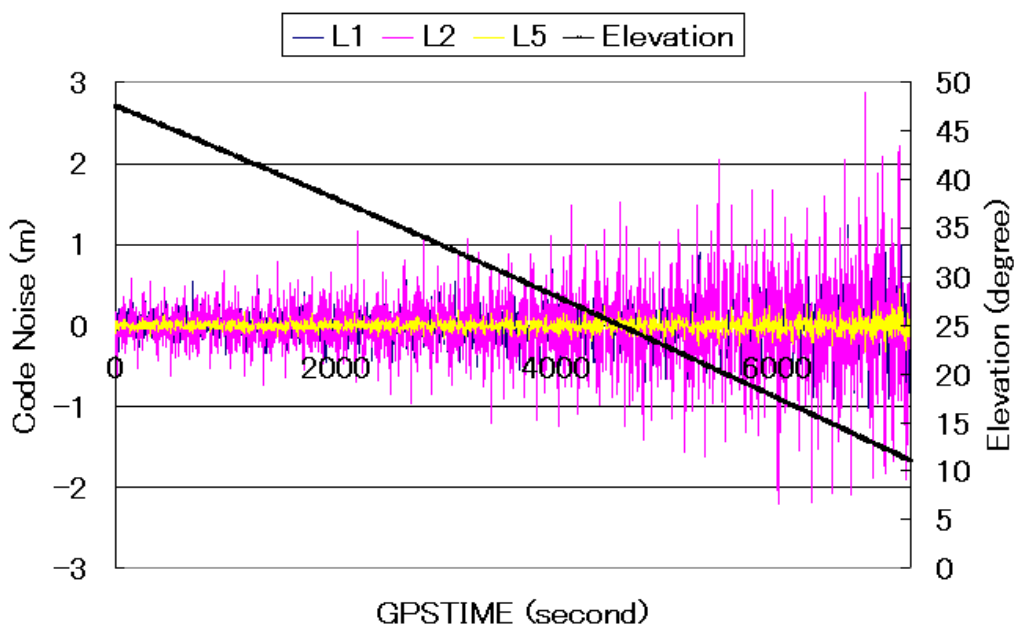
Figure 4.3.2   Simulated code noise generated from PRN31 for 2 hours (multipath error absent)
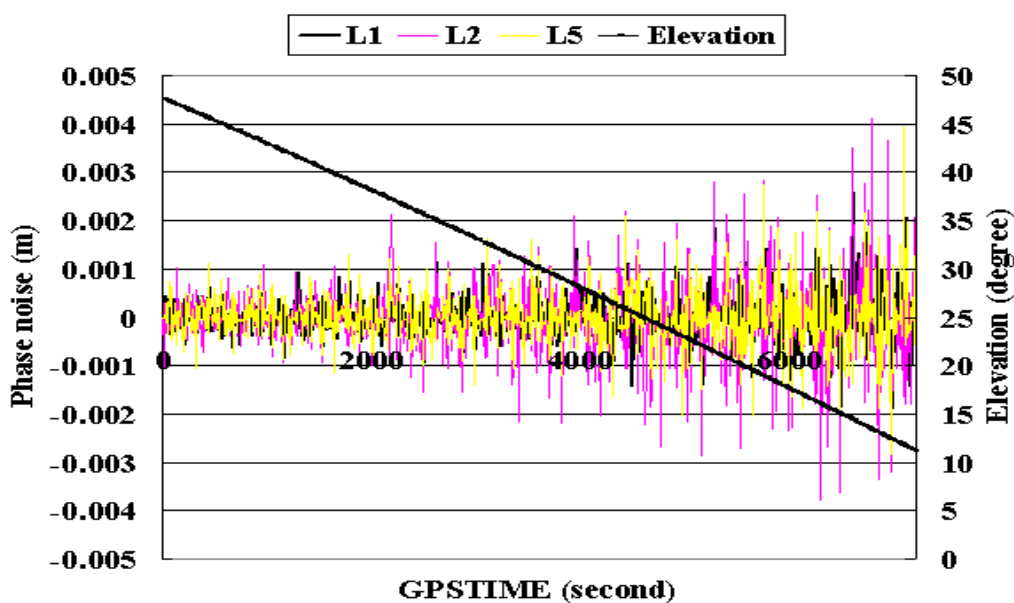
Figure 4.3.3   Simulated carrier noise generated from PRN31 for 2 hours (multipath error absent)

◆ **Multipath error**

In the research, effects of Multipath error on Code Tracking Loop and on Phase Tracking Loop reflected form ground were only considered. The receiver amplitude between the direct and multipath signals was set as 0.25 (about 12dB). Refection material was considered as medium dry ground. Conductivity of reflection coefficient was 0.04 and Relative Permissive was 7. [Jayanta, 1999] Figure 4.3.4 shows simulated multipath code error reflected from ground on PRN31 for 2 hours, and figure 4.3.5 shows simulated multipath carrier error reflected from ground on PRN31 for 2 hours
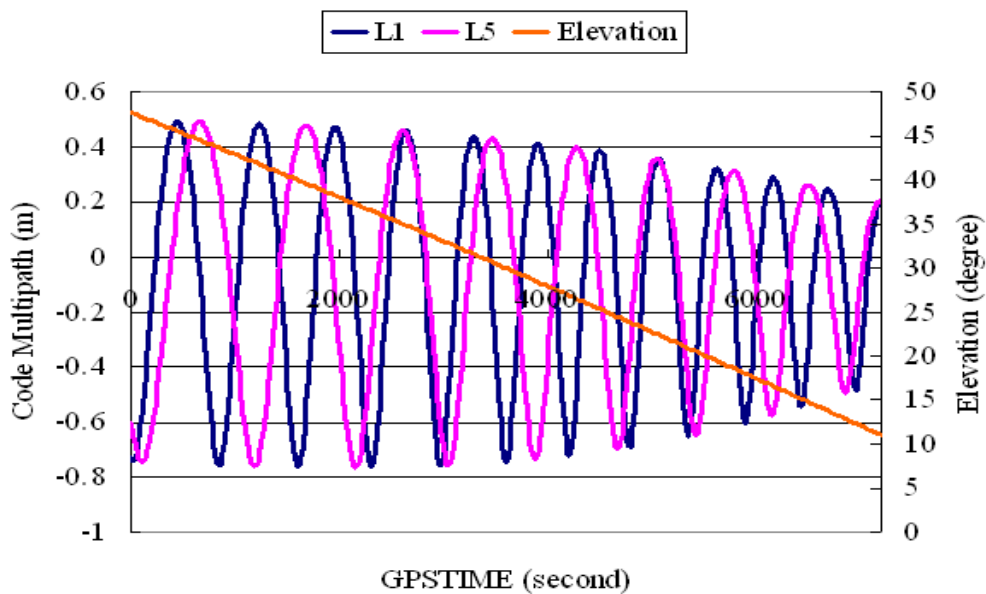
Figure 4.3.4 Simulated multipath code error reflected from ground on PRN31 for 2 hours
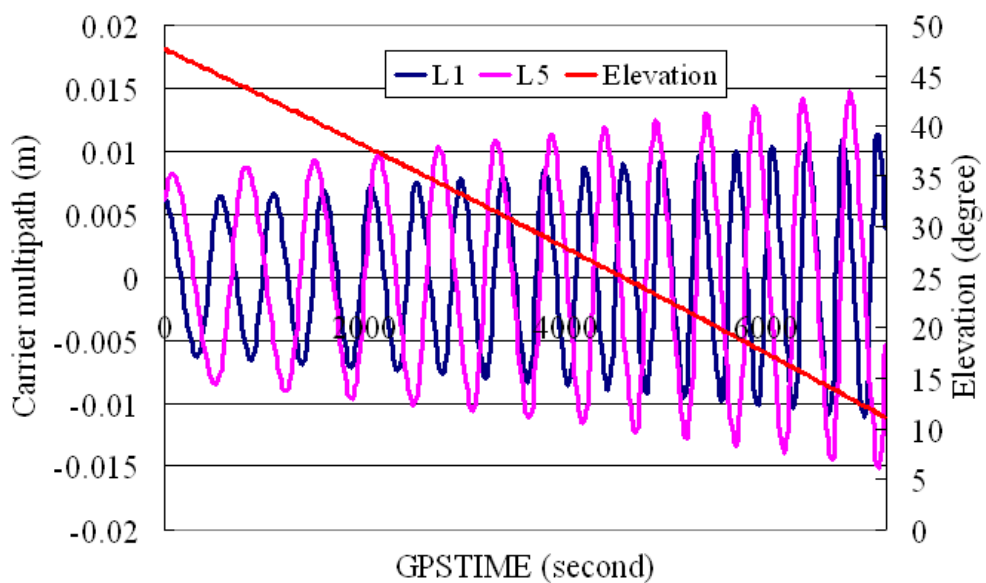
Figure 4.3.5 Simulated multipath carrier error reflected from ground on PRN31 for 2 hours

◆ **Simulator validation**

Validation of the simulator was done using observational data from the Japan Geographical Survey Institute GPS continuousness observation system (GEONET) [GSI, 2004] by [Yun Zhang, Nobuaki Kubo, Akio Yasuda., (2005)]. Further information about the theory of DLL and PLL can be found in reports by [Parkinson, B. W., Spilker, J. J., Axelrad, P., and Enge, P., (1996)] and [Kaplan, E. D., (1996)].

4.2.2 QZSS Orbit Model

In the simulator, four optional QZSS orbit models, (8-shaped, Egg-shaped 1, Asym-8-shaped, Egg-shaped 2, were interested. Table 4.4 summarizes the parameters of the four most favored satellite orbit options for the QZSS in this research. Among them, **Option 3, Asymmetric 8-shaped, was QZSS orbit**. [Japan Aerospace of Exploration Agency, (2007)] Figure 4.4 illustrates the ground tracks of each QZSS constellation options in the simulator. [Wu, F., Kubo, N., and Yasuda, A., (2004)]

In Table 4.4, "*Right ascension*" means right ascension of the ascending node. Because three operating QZSS satellites are considered, regular *right ascensions* were simulated as 0.5° for QZSS1, 120.5° for QZSS2 and 240.5° for QZSS3, and four *mean motions* were simulated as 120.0° for QZSS1, 0.0° for QZSS2 and 240° for QZSS3.

QZSS Option	Option 1 8-shaped	Option 2 Egg-shaped 1	**Option 3 Asym. 8-shaped**	Option 4 Egg-shaped 2
Satellites	3	3	**3**	3
Semi-major axis (km)	42,164.17	42,164.17	**42,164.17**	42,164.17
Eccentricity	0.0	0.21	**0.099**	0.36
Inclination (°)	45.0	42.5	**45.0**	52.6
Argument of perigee (°)	270.0	270.0	**270.0**	270.0
Right ascension (°)	0.5	0.5	**0.5**	0.5
	120.5	120.5	**120.5**	120.5
	240.5	240.5	**240.5**	240.5
Mean motion (°)	120.0	120.0	**120.0**	120.0
	0.0	0.0	**0.0**	0.0
	240.0	240.0	**240.0**	240.0

Table 4.4 Parameters of four satellite orbit options for QZSS

Satellite ground track				
	Option 1	Option 2	Option 3	Option 4
Inclination	45°	42.5°	45°	52.6°
Eccentricity	0	0.21	0.099	0.36
Number of satellites	3	3	3	3
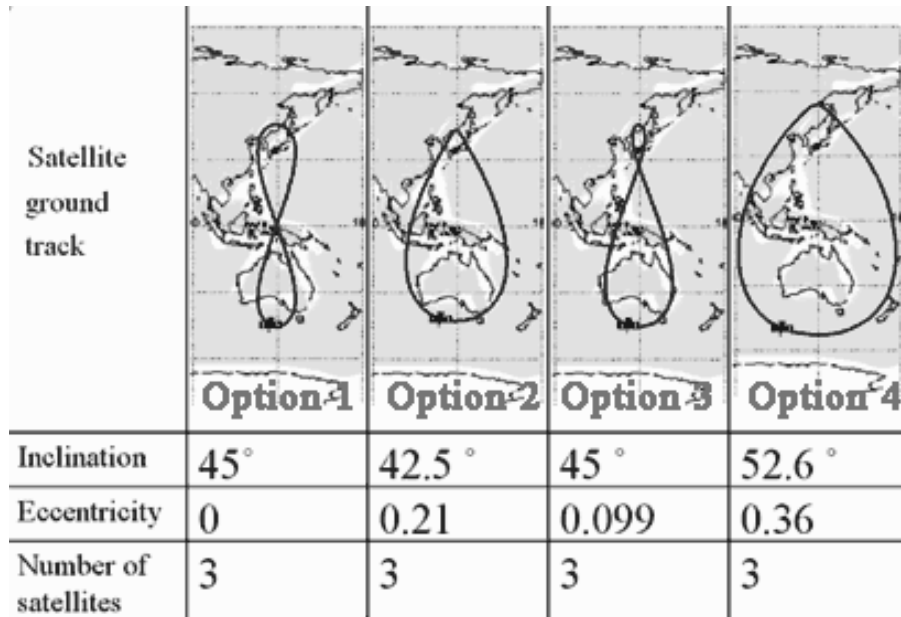
Figure 4.4 Ground tracks of each QZSS option in simulator

4.2.3 Data from Triple Frequency Simulator

In this research, L1, L2 and L5 signal data from the triple-frequency simulator were used in dual- and triple-frequency numerical estimation.

Single GPS (SGPS) positioning results using data from triple simulator on horizontal coordinator at Sapporo for 24 hours was given from figure 4.5.1 to figure 4.5.4. Figure 4.5.1 shows SGPS using range data from simulation only includes code thermal noise with GPS only. Figure 4.5.2 shows SGPS using range data including code noise and multipath error form ground with GPS only. Figure 4.5.3 shows SGPS using range data including code noise, multipath error and other error, i.e. ionosphere and troposphere error, with GPS only. Figure 4.5.4 shows SGPS using range including noise and all range error with GPS integrating QZSS Option 3.

GPS Only SGPS
(only including code noise)
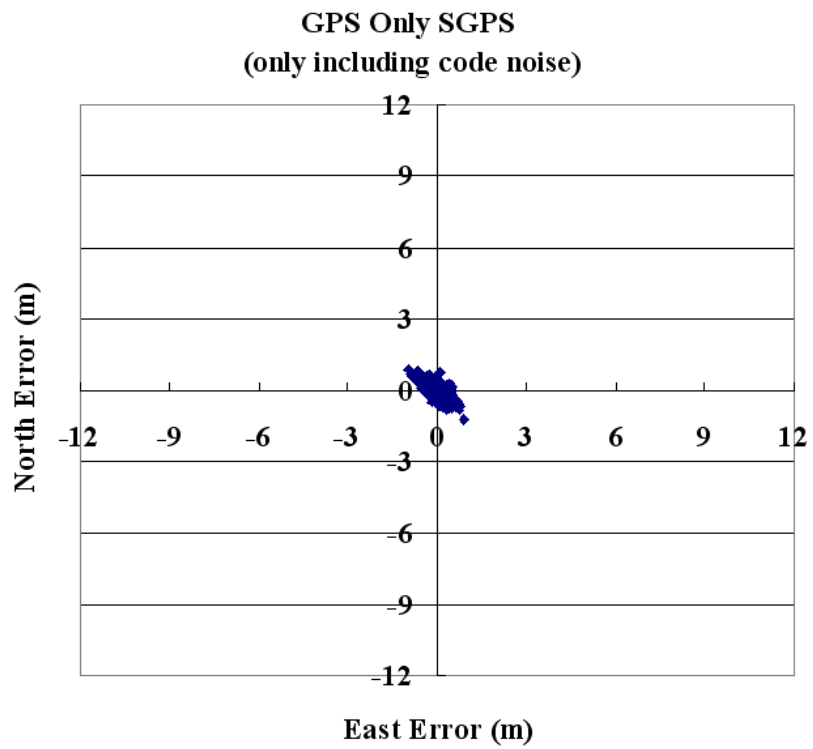
Figure 4.5.1 SGPS positioning using simulated range includes code thermal noise with GPS only

GPS Only SGPS
(including code noise and multipath error)
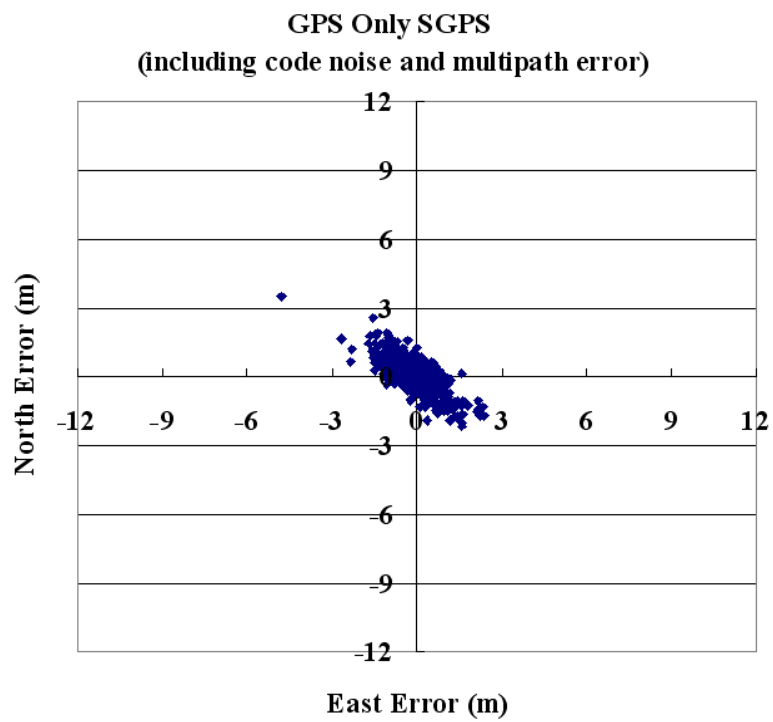
Figure 4.5.2 SGPS positioning using simulated range includes code noise and multipath error

with GPS only

51

GPS Only SGPS (including code noise, multipath
error and other range error)
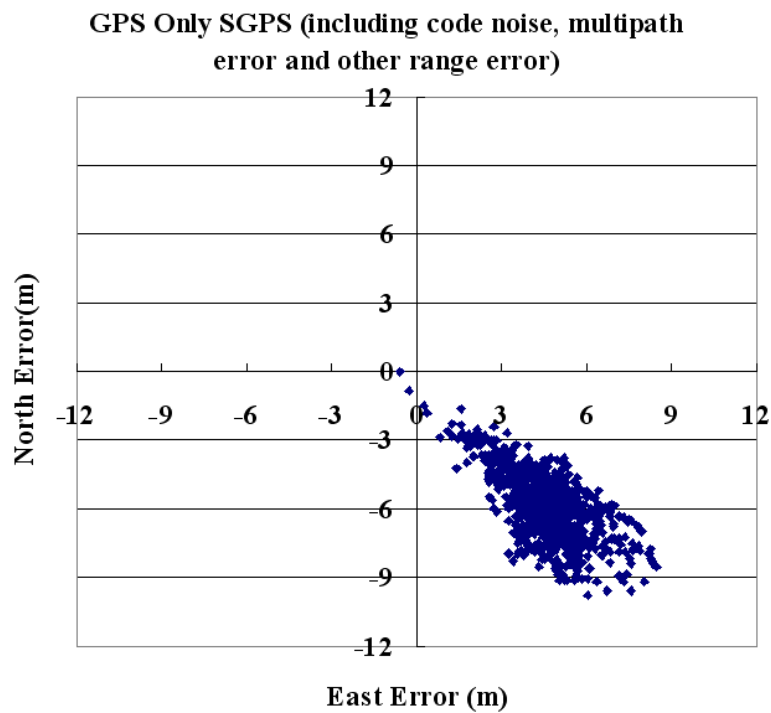
Figure 4.5.3 SGPS using simulated range including noise and various ranger errors with GPS only

GPS with QZSS SGPS (including code noise,
multipath error and other range error)
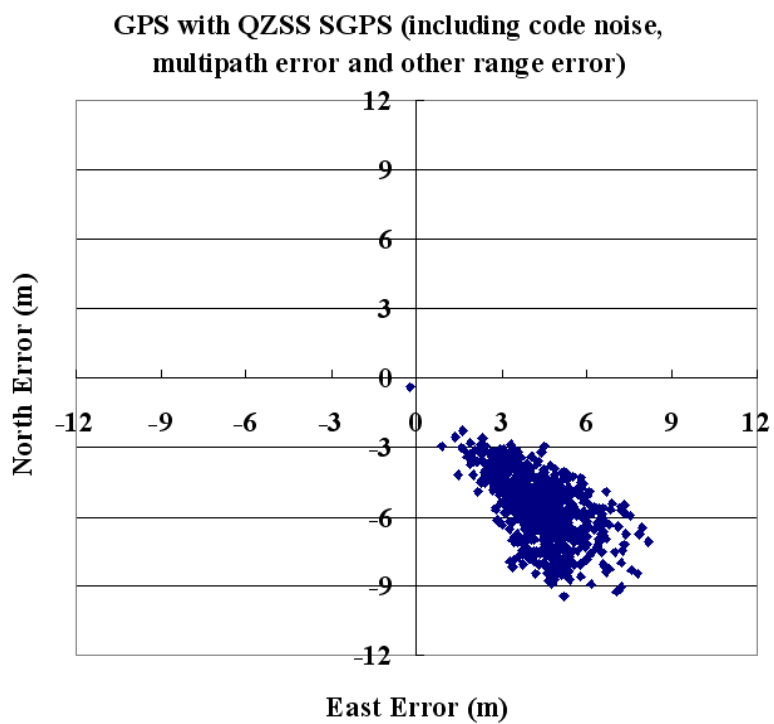
Figure 4.5.4 SGPS using simulated range including noise and various ranger errors

with GPS and QZSS

52

Table 4.5 shows standard deviation and average amount of north error and east error on SGPS positioning. From figure 4.5 and table 4.5, basing on code noise generated form noise parameter in Table 4.2 and various range errors generated from error model in Table 4.1, influence of simulated noise and range error on positioning could be seen. From figure 4.5.4 and table 4.5, impact on positioning with simulated QZSs generated from orbit parameters could also be presented.

Range from triple simulator		SGPS East error (m)	SGPS North error (m)
GPS Only			
Code noise	Std.	0.37	0.38
	Ave.	0.01	0.02
Code noise + multipath error from ground	Std.	0.67	0.69
	Ave.	0.05	0.04
Code noise + multipath error from ground + other range error	Std.	1.50	1.64
	Ave.	4.64	5.91
GPS + QZSS			
Code noise + multipath error from ground + other range error	Std.	1.17	1.42
	Ave.	4.38	5.59

Table 4.5 Accuracy of SGPS positioning at Sapporo for 24 hours without QZSS or with QZSS Option 3 using different range data from triple simulator

4.2.4 Numerical Estimation Parameters

The parameters of estimation in performance analysis are shown in Table 4.6. Yuma 191 downloaded from Navigation Center [Navigation Center, (2006)] was used to estimate the GPS constellation. Four options of QZSS constellation and three QZSs were considered.

East Asia region (Longitude: 60º E - 152º E, Latitude: 10º S - 60º N) and near to Japan area (Longitude: 125º E - 145º E, Latitude: 25º N - 45º N) were interested for spatial estimation. Mesh grid was 0.5 degree. Six East Asian cities, Sapporo (north of Japan), Naha (south of Japan), Tokyo (mid of Japan), Shanghai (East of China), Kashi (west of China) and Jakarta (south of East Asia) were chosen to perform temporal estimating.

Estimation time was 00:00 UTC -- 24:00 UTC April 21, 2003 for 24 hours. Sampling time of output data from simulator is 120 seconds. Multipath error was only simulated as refracting from ground. Only short distance positioning was interested here. No carrier smoothing L1 code DGPS and single L1 Ambiguity were estimated.

System	GPS, GPS + QZSS (four options)
Number of QZS	3
GPS ephemeris	YUMA191 file
Region	East Asian Region (Longitude: 60º E - 152º E, Latitude: 10º S - 60º N)
	Near to Japan area (Longitude: 125º E - 145º E, Latitude: 25º N - 45º N)
Location	Sapporo, Naha, Tokyo, Shanghai, Kashi, Jakarta
Estimation time	24 hours, 00:00 UTC – 24:00 UTC April 21, 2003
Mesh grid	0.5º
Sampling interval	120 seconds
Simulator computer	Dell GX270, Celeron 2.2 GHz
Distance between Base and Rover stations	about 5.56km
Antenna	NOVATEL 702
Multipath error	Reflected from ground on each station
Height	100m at each station
DGPS	No carrier smoothing L1 code
AR	Single epcoh

Table 4.6 Parameters in numerical estimation

Figure 4.6 shows the locations of six cities for temporal estimation. Table 4.7 shows the locations of base and rover stations in DGPS positioning estimation or DD AR. Distance between the base and rover stations is about 5.56 km. Height of every site is 100m.

Area	Base Station	Rover Station
Sapporo	Lat: 43.04º N, Lon: 141.21º E	Lat: 43.09º N. Lon: 141.21º E
Tokyo	Lat: 35.67 º N, Lon: 139.74 E	Lat: 35.72 N, Lon: 139.74E
Naha	Lat: 26.13º N, Lon: 127.41º E	Lat: 26.18º N, Lon: 127.41º E
Shanghai	Lat: 31.06º N, Lon: 121.22º E	Lat: 31.11º N, Lon: 121.22º E
Kashi	Lat: 39.28º N, Lon: 75.59º E	Lat: 39.33º N, Lon: 75.59º E
Jakarta	Lat: 6.08º S, Lon: 106.45º E	Lat: 6.03º S, Lon: 106.45º E

Table 4.7 Locations of base and rover cities in DGPS positioning or DD AR
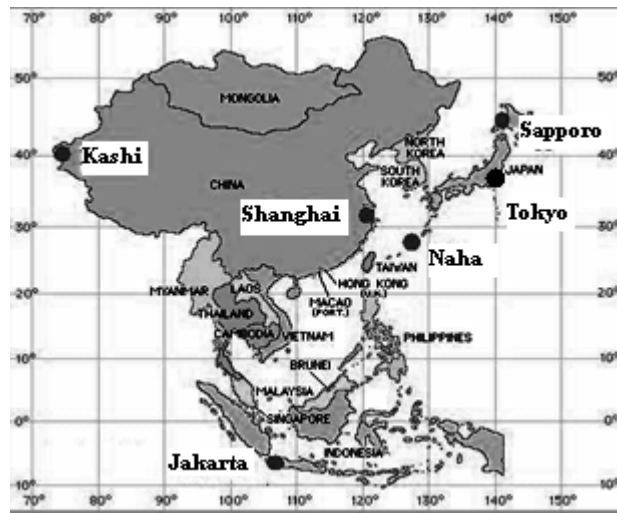
Figure 4.6 Locations of cities for temporal estimation

4.2.5 ASR Estimation

For carrier phase-based positioning, AR is the mathematical process of converting ambiguity ranges (carrier phase measurements) to unambiguous range data. Triple-frequency measurements provided the opportunity to resolve the integer ambiguities for the WL combination between L2 and L5 signals using pseudo-range measurements directly.

Single epoch AR in short distance was investigated in this research. **WL AR method** which has been introduced in the last chapter was used here. In AR, with a sampling interval of 2 min, the total estimation epoch number is 720. After each interval of 2 min, only one epoch of data was taken, processed and analyzed. In AR, the necessary NVS was more than 5.The ASR is given by Equation (4.3).

$$ASR = \frac{Success\,EpochNumber}{Epochs\,(Common\,NSV > 4)} \dots\dots\dots\dots\dots\dots\dots\dots\dots\dots\dots\dots\dots\dots\dots\dots\dots\dots\dots\dots\dots\dots(4.3)$$

4.3 SPATIAL ESTIMATION

In this section, NVS, PDOP with four QZSS options or without QZSS in East Asian region or in near to Japan region were estimated. From spatial estimation, expected impact from QZSS could be concluded, and the feature QZSS orbit was also studied here.

4.3.1 Number of visible satellites (NVS)

The NVS is an important parameter of satellite positioning because three-dimensional GPS position calculation based on horizontal coordinates and elevation requires a minimum of four visible satellites.

◆ **NVS in East Asian region**

In this part, the minimum, maximum and average NVS with or without QZSS in 24 hr at each mesh grid in two regions were calculated when the mask angle was set to 15º, 25º and 30º, respectively.

Mask angle	Opt. 1+ GPS	Opt. 2+ GPS	**Opt. 3+ GPS**	Opt. 4+ GPS	GPS Only
Min. NVS = 4					
15º	100%	100%	**100%**	100%	93.02%
25º	83.38%	91.17%	**86.44%**	91.19%	16.70%
30º	60.16%	67.29%	**67.02%**	64.23%	0.0%
Min. NVS = 5					
15º	94.87%	95.60%	**99.45%**	97.44%	53.79%
25º	54.35%	64.65%	**62.56%**	70.26%	0.0%
30º	31.24%	38.21%	**34.20%**	32.97%	0.0%
Min. NVS = 6					
15º	82.72%	90.72%	**88.36%**	91.05%	17.59%
25º	26.37%	29.95%	**27.97%**	23.20%	0.0%
30º	1.05%	1.20%	**1.09%**	0.29%	0.0%
Min. NVS = 7					
15º	51.78%	53.99%	**51.38%**	55.36%	0.34%
25º	3.66%	3.19%	**3.24%**	0.56%	0.0%
30º	0.0%	0.0%	**0.0%**	0.0%	0.0%

Table 4.8 Percentage of minimum NVS in 24 hr in the East Asian region
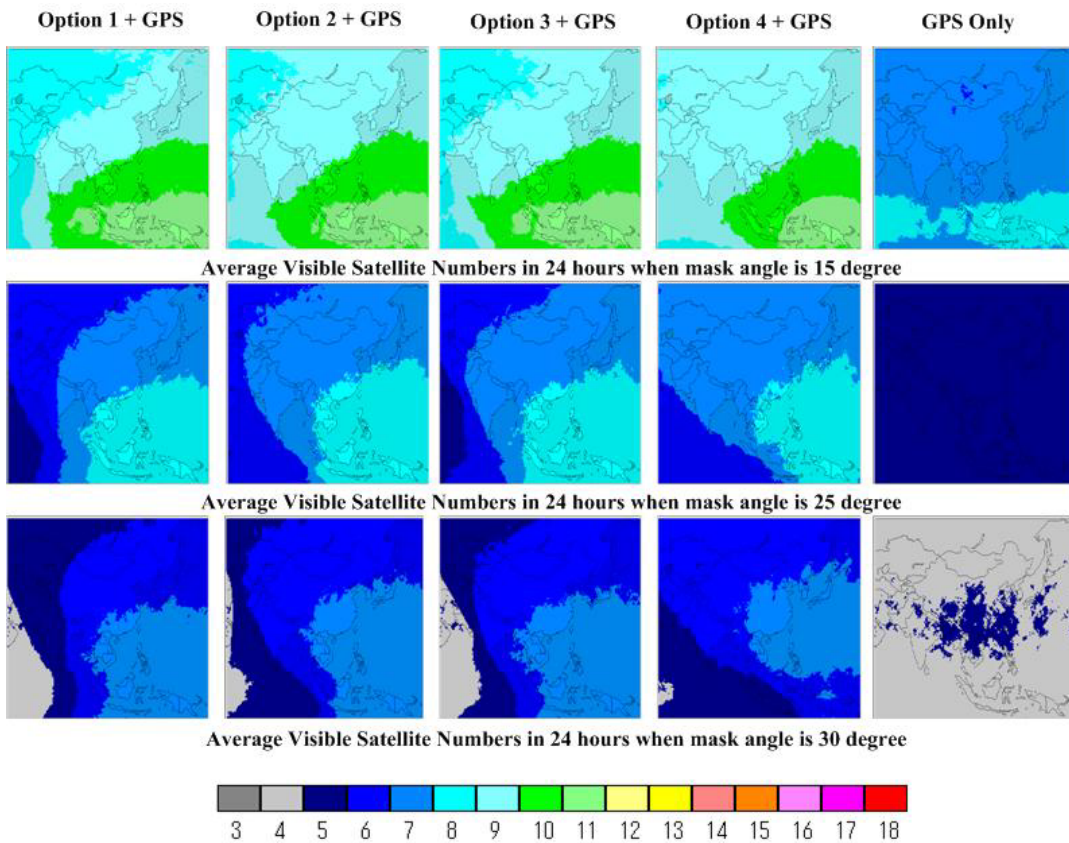
Figure 4.7.1 Average NVS with and without QZSS in 24 hr in the East Asian region.
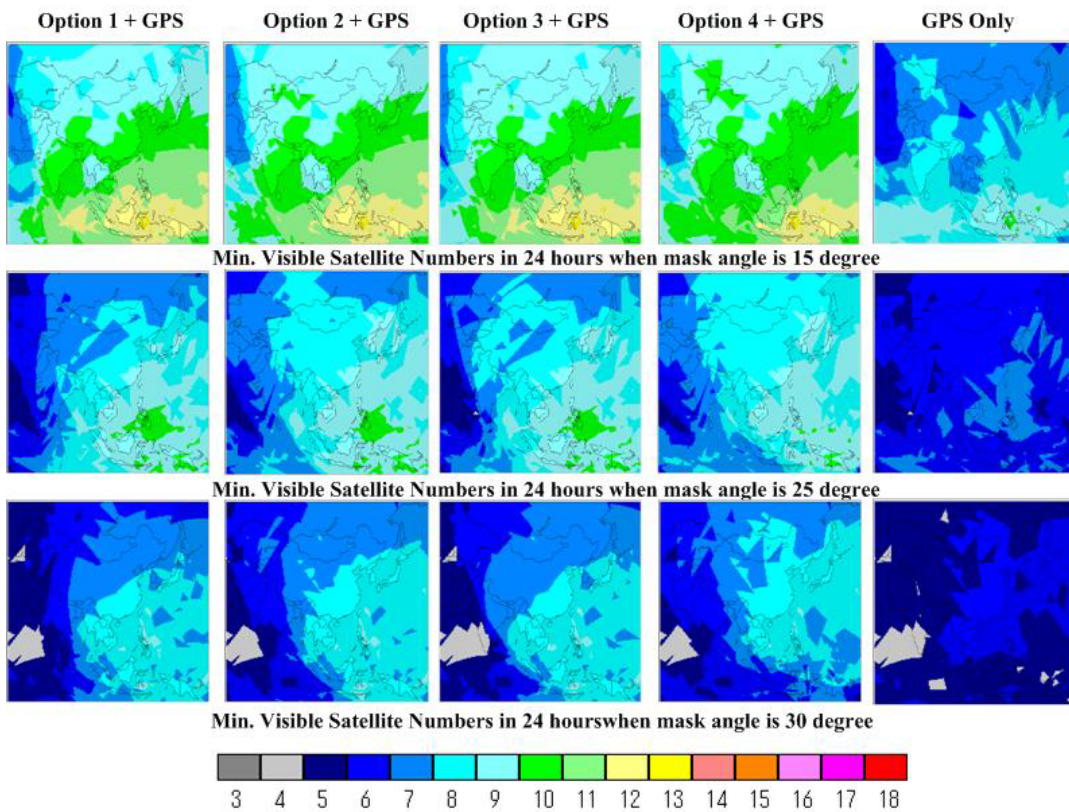
Figure 4.7.2 Min. NVS with and without QZSS in 24 hr in the East Asian region.
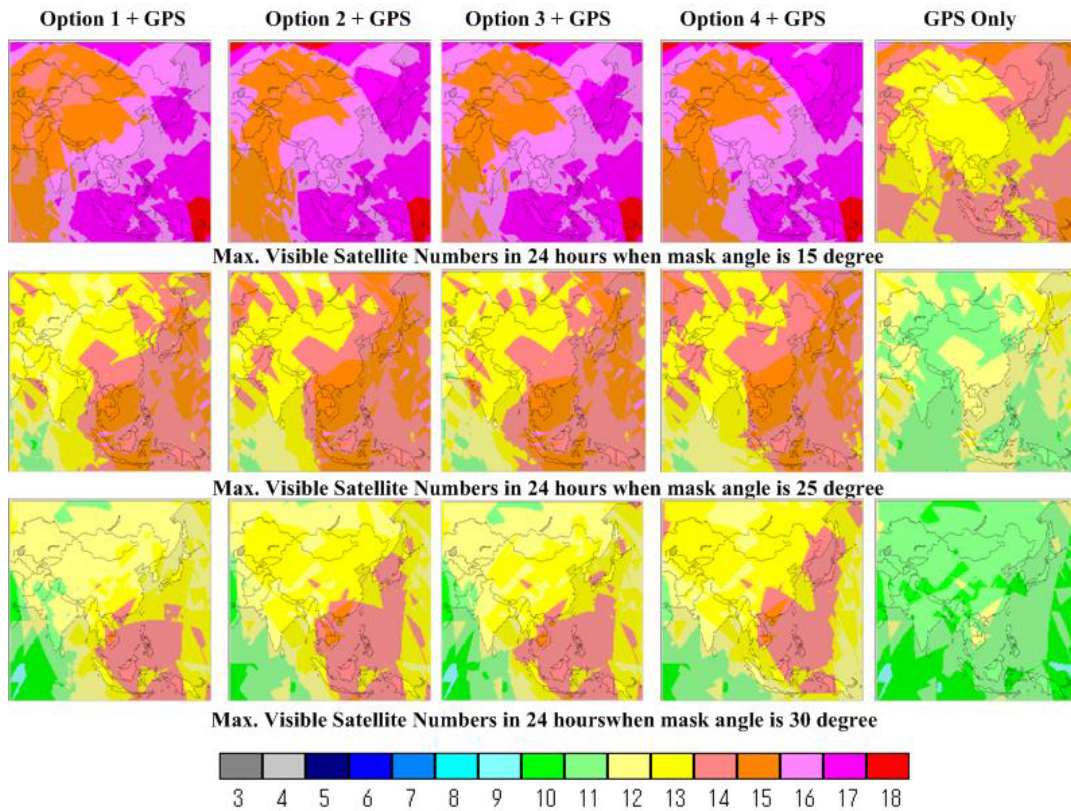
Figure 4.7.3 Max. NVS with and without QZSS in 24 hr in the East Asian region.

Table 4.8 shows the percentages of minimum NVS in 24 hr when the minimum NVS was 4, 5, 6 and 7, respectively, in the East Asian region. Figure 4.7 shows NVS with four options QZSS or without QZSS in 24 hours in the East Asian region. Figure 4.7.1 shows average NVS, figure 4.7.2 shows min. NVS and figure 4.7.3 shows max NVS.

Tables 4.8 and figure 4.7 show that in each QZSS orbit option, NVSs with different orbit options could all be improved when the mask angle was 15º, 25º and 30º, respectively, not only in the Japan region, but also in the East Asian region. Especially, when the mask angle was 15º, by integrating QZSS, the minimum NVS could be at least 5 for more than 95% of the East Asian region.

◆ **NVS Comparison in the East Asian and near the Japan areas**

Table 4.9 shows the percentages of minimum NVS in 24 hr when the minimum NVS was 4, 5, 6 and 7, respectively, in the neat to Japan region. Basing on table 4.8 and table 4.9, figure 4.7.4 indicates the average of all percentage numbers in all cases in two tables with four QZSS options or without QZSS in two regions. Among four QZSS options, Option 2 revealed the best improvement of NVS in the East Asian region, and Option 3 gave the best performance for the near Japan area.

Mask angle	Opt. 1+GPS	Opt. 2+GPS	**Opt. 3+GPS**	Opt. 4+GPS	GPS Only
Min. NVS = 4					
15°	100%	100%	**100%**	100%	100%
25°	100%	100%	**100%**	100%	42.06%
30°	100%	100%	**100%**	100.0%	0.0%
Min. NVS = 5					
15°	100%	100%	**100%**	100%	61.17%
25°	100%	98.0%	**100%**	94.88%	0.0%
30°	91.76%	64.93%	**92.12%**	46.26%	0.0%
Min. NVS = 6					
15°	100%	100%	**100%**	100%	0.0%
25°	55.18%	41.46%	**56.85%**	26.39%	0.0%
30°	0.0%	0.0%	**0.0%**	0.0%	0.0%
Min. NVS = 7					
15°	77.25%	70.17%	**77.77%**	66.45%	0.0%
25°	0.0%	0.0%	**3.24%**	0.0%	0.0%
30°	0.0%	0.0%	**0.0%**	0.0%	0.0%

Table 4.9 Percentage of minimum NVS in 24 hr in near to Japan area

Figure 4.7.4 NVS comparison with four QZSS options or without QZSS in two regions

The NVS results analysis indicates that with extra satellites through using QZSS, the availability of satellites could be improved. Positioning geometry condition was expected to be improved.

4.3.2 Dilution of Precision of Position (PDOP)
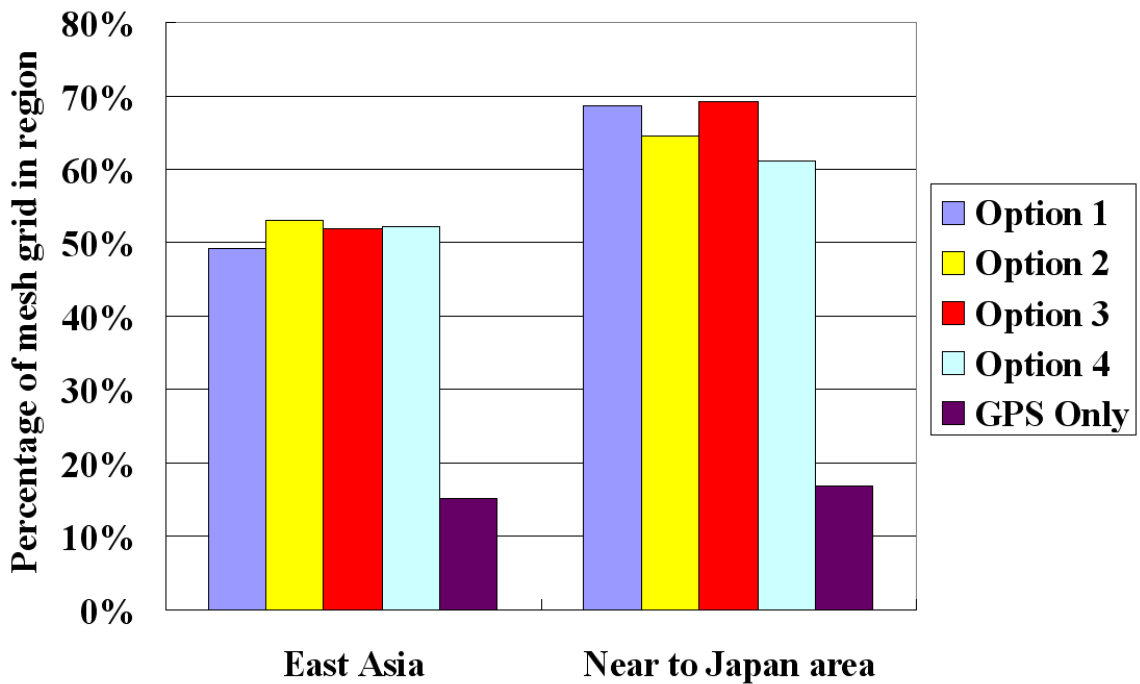
◆ **PDOP definition**

DOP Value	Rating	Description
1	Ideal	This is the highest possible confidence level to be used for applications demanding the highest possible precision at all times
2-3	Excellent	At this confidence level, positional measurements are considered accurate enough to meet all but the most sensitive applications
4-6	Good	Represents a level that marks the minimum appropriate for making business decisions. Positional measurements could be used to make reliable in-route navigation suggestions to the user
7-8	Moderate	Positional measurements could be used for calculations, but the fix quality could still be improved. A more open view of the sky is recommended
9-20	Fair	Represents a low confidence level. Positional measurements should be discarded or used only to indicate a very rough estimate of the current location
21-50	Poor	At this level, measurements are inaccurate by as much as half a football field and should be discarded

Table 4.10 Interpretation of DOP value

DOP is a function expressing the mathematical quality of solutions based on the geometry of the satellites. PDOP (dilution of precision of position), the most common such value, has a best case value of one. Higher numbers of PDOP are worse. Table 4.10 shows the interpretation of DOP value. [Jon Person, (2004)]

Figure 4.8.1 shows solution area created from three satellites. Estimated location could be any point within the gray-colored area. DOP becomes worse when the grey area grows larger. Figure 4.8.2 shows solution area estimated from three more evenly distributed throughout the sky. The solution area in figure 4.8.2 was smaller than in figure 4.8.1, DOP was improved. From figure 4.8, using extra suitable satellite, better positioning environment could be provided.
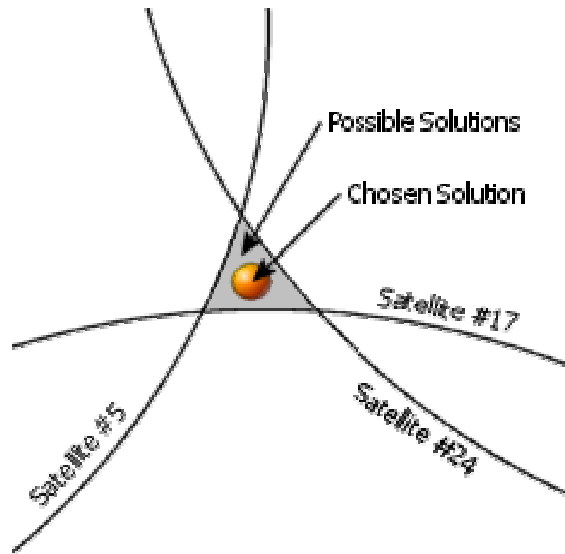
Figure 4.8.1 DOP estimated from three satellites
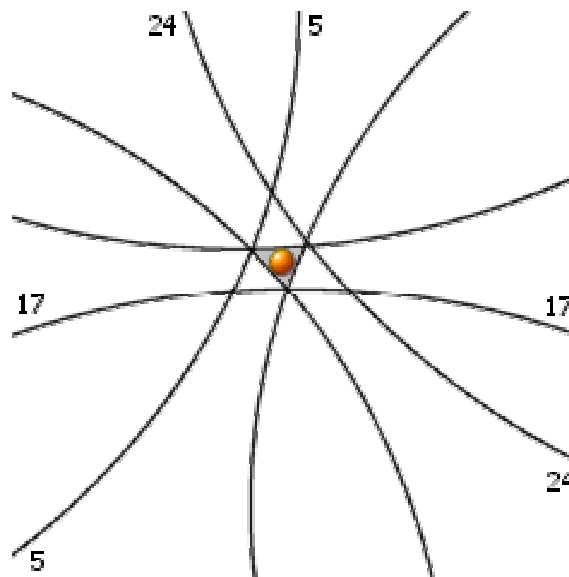
Figure 4.8.2 DOP estimated from three more evenly-distributed satellites

◆ **PDOP in East Asian region**

In this research, min and average PDOP (NVS > 3) for 24 hr at each mesh grid in the East Asian region was measured when the mask angle of the visible satellite was 15°.

Average PDOP in different longitude regions was also estimated using equation (4.4) when NVS > 3.

$$Ave_{PDOP} = \frac{\sum\limits_{Lon1}^{Lon2}\sum\limits_{Lat1}^{Lat2} PDOP_{Avein24hour}(M)(N)}{M * N} \quad \ldots\ldots\ldots\ldots\ldots\ldots\ldots\ldots\ldots\ldots\ldots\ldots\ldots\ldots\ldots\ldots\ldots\ldots\ldots\ldots\ldots..(4.4)$$

$$(if\ NVS(M)(N) > 3)$$

where, M is longitude grid index and N is latitude grid index.
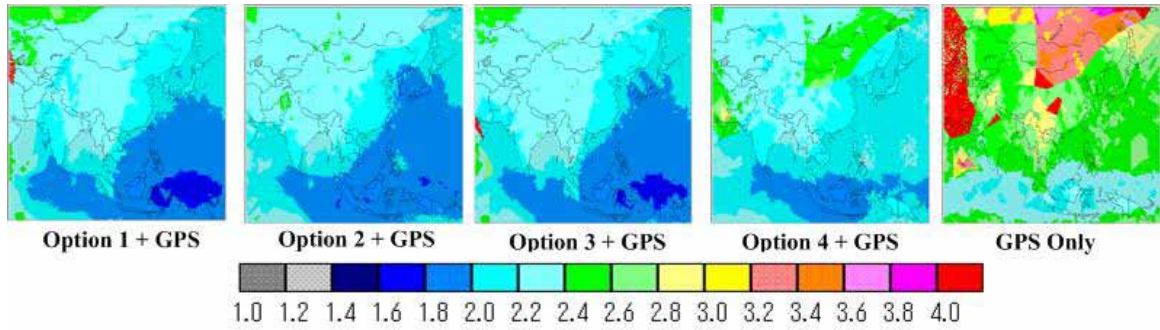
Figure 4.9.1   Average PDOP for 24 hr with and without QZSS when the mask angle is 15º.
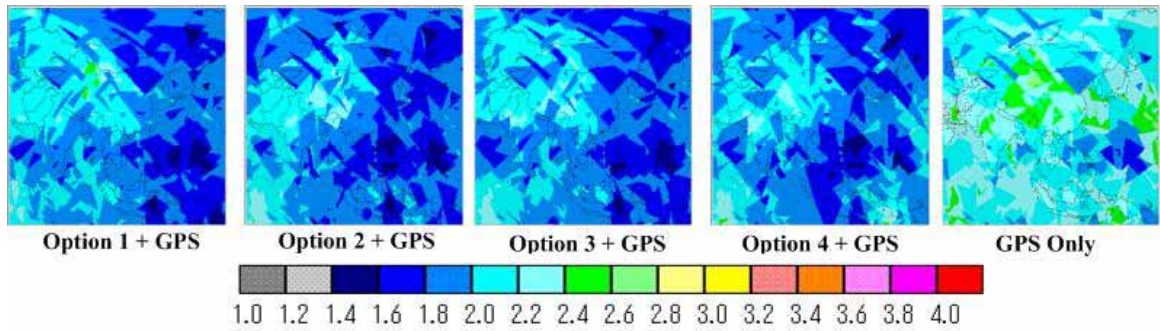
Figure 4.9.2   Min. PDOP for 24 hr with and without QZSS when the mask angle is 15º.

Different longitude regions in East Asian region were shown as follows:

- Region 1: Lon 60º E - 75º E, Lat 10º S - 60º E
- Region 2: Lon 75º E - 90º E, Lat 10º S - 60º E
- Region 3: Lon 90º E - 105º E, Lat: 10º S - 60º E
- Region 4: Lon 105º E - 120º E, Lat: 10º S - 60º E
- Region 5: Lon 120º E - 135º E, Lat: 10º S - 60º E
- Region 6: Lon 135º E - 150º E, Lat: 10º S - 60º E
- Total mesh grid amount in every region was **6330**.

From analysis of different PDOP amounts in different longitude region, the feature of QZS could be indicated.

	Opt.1+GPS	Opt.2+GPS	**Opt.3+GPS**	Opt. 4+GPS	GPS Only
Region 1					
NVS>3	98.37%	100.0%	**100.0%**	100.0%	85.59%
PDOP (NVS>3)	1.70	1.68	**1.69**	1.72	1.76
Region 2					
NVS>3	100.0%	100.0%	**100.0%**	100.0%	100.0%
PDOP (NVS>3)	2.18	2.19	**2.20**	2.16	2.55
Region 3					
NVS>3	100.0%	100.0%	**100.0%**	100.0%	98.88%
PDOP (NVS>3)	2.21	2.17	**2.22**	2.20	2.67
Region 4					
NVS>3	100.0%	100.0%	**100.0%**	100.0%	99.95%
PDOP (NVS>3)	2.09	2.07	**2.08**	2.18	2.73
Region 5					
NVS>3	100.0%	100.0%	**100.0%**	100.0%	100.0%
PDOP (NVS>3)	1.98	2.01	**1.98**	2.14	2.67
Region 6					
NVS>3	100.0%	100.0%	**100.0%**	100.0%	99.15%
PDOP (NVS>3)	1.97	1.99	**1.97**	2.13	2.72

Table 4.11 Average PDOP (NVS>3)in each region in 24 hours

Table 4.11 shows the average PDOP for 24 hr in different longitude regions. Figure 4.9.1 shows average PDOP (NVS > 3) and figure 4.9.2 shows min PDOP for 24 hr at each mesh grid with and without QZSS when the mask angle is 15º.

From Figure 4.9 and Table 4.11, usable grid mesh amount was improved to 6330 in each region except for the case of Region 1 by integrating Option 1. Moreover, PDOP could be improved about 2.3% ~ 4.5% in region 1, 13.7% ~ 15.3% in region 2, 16.9% ~ 18.7% in region 3, 20.1% ~ 24.2% in region 4, 19.9% ~ 25.8% in region 5, and 21.7% ~ 27.6% in region 6. After using QZSS in East Asia region, PDOP could be improved significantly when longitude of location is close to Japan center longitude (135ºEast). .

Table 4.12 shows the average PDOP (NVS > 3) comparison in the East Asian and near the Japan areas. Basing on table 4.12, figure 4.8.3 indicates comparing PDOP with four QZSS options or without QZSS in two regions, among the four QZSS options, augmentation with QZSS Option 2 obtained the best performance of PDOP in the East Asian region, and using Option 3 was the best for the near Japan area. The same result was also derived form NVS analysis in the last section. It indicates that option 3, QZSS orbit, was the best option for improving availability and augmentation in near to Japan area.

◆ **PDOP Comparison in the East Asian and near the Japan areas**

	Average PDOP (NVS > 3)				
	Opt.1+GPS	Opt.2+GPS	**Opt.3+GPS**	Opt.4+GPS	GPS Only
East Asia	2.08	2.00	**2.02**	2.08	2.52
Near to Japan area	2.03	2.00	**1.98**	2.08	2.58

Table 4.12 Average PDOP (NVS > 3) in the East Asian region and near to Japan area
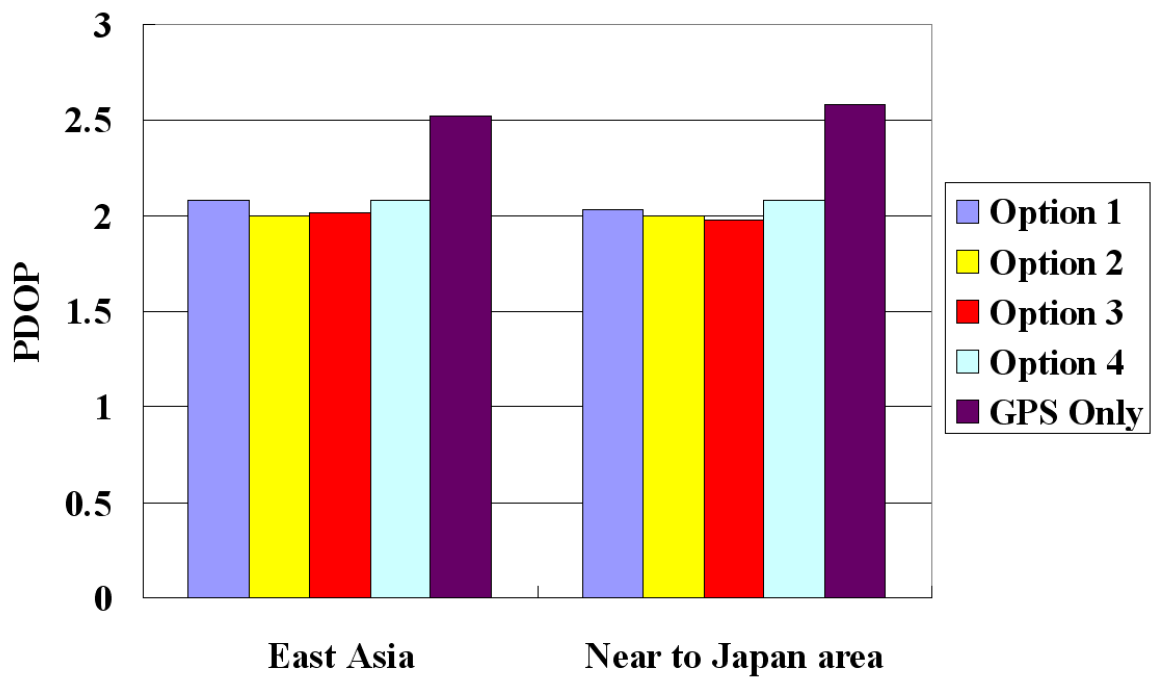
Figure 4.9.3 Comparing average PDOP with four QZSS options or without QZSS in two regions

4.4 TEMPEROAL ANALYSIS

In this section, temporal analysis at six East Asian cities, which was given in table 4.7, for 24 hours was performed. Mask angle was 15 degree. NVS, PDOP, short baseline L1 code DGPS positioning and primary signal short baseline AR were estimated. From results analysis, performance of QZSS could be proved.

4.4.1 QZSS Constellation

◆ **QZSs elevation**
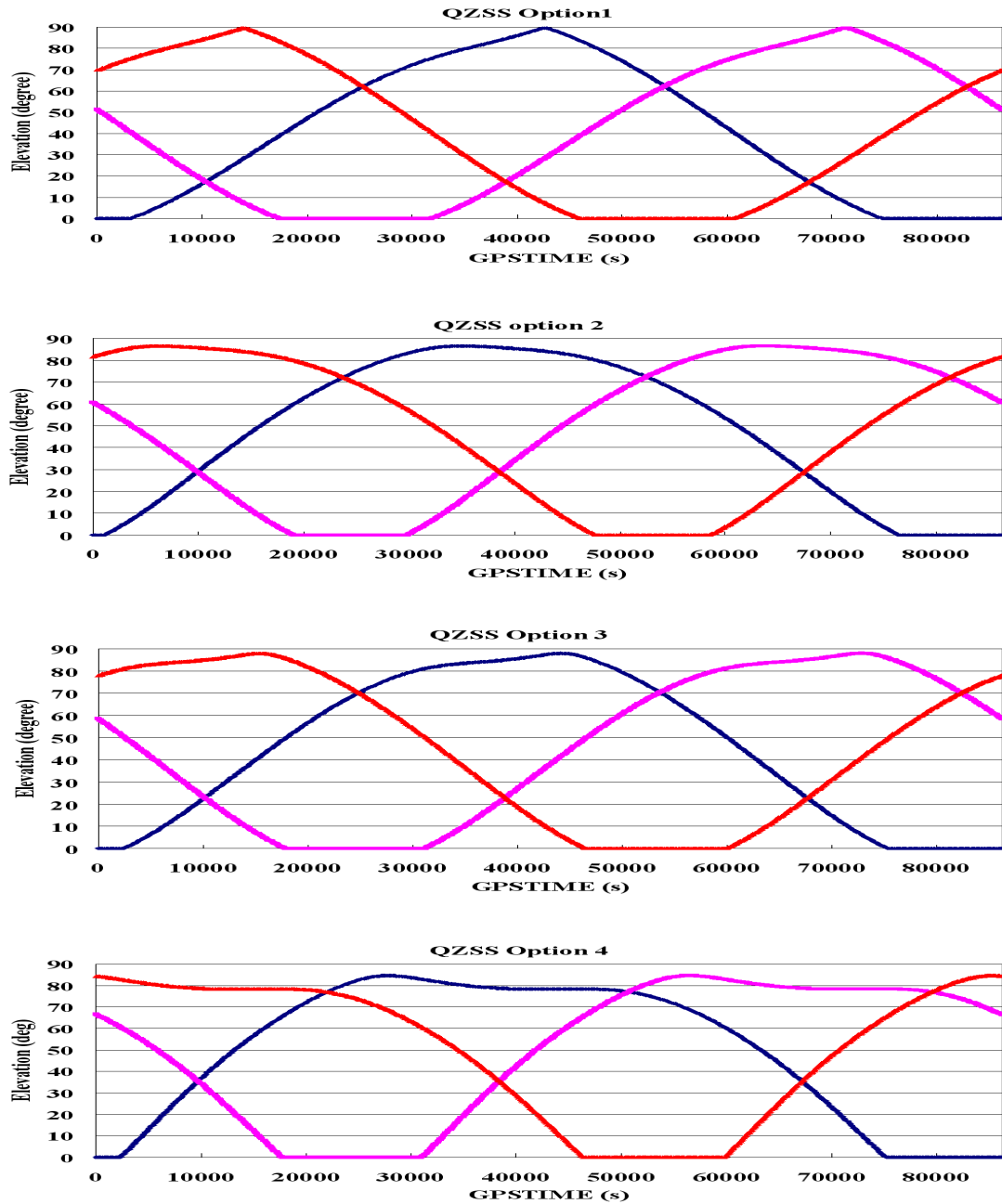
Figure 4.10.1 Elevation of three QZSs with four QZSS options at Japanese Sapporo
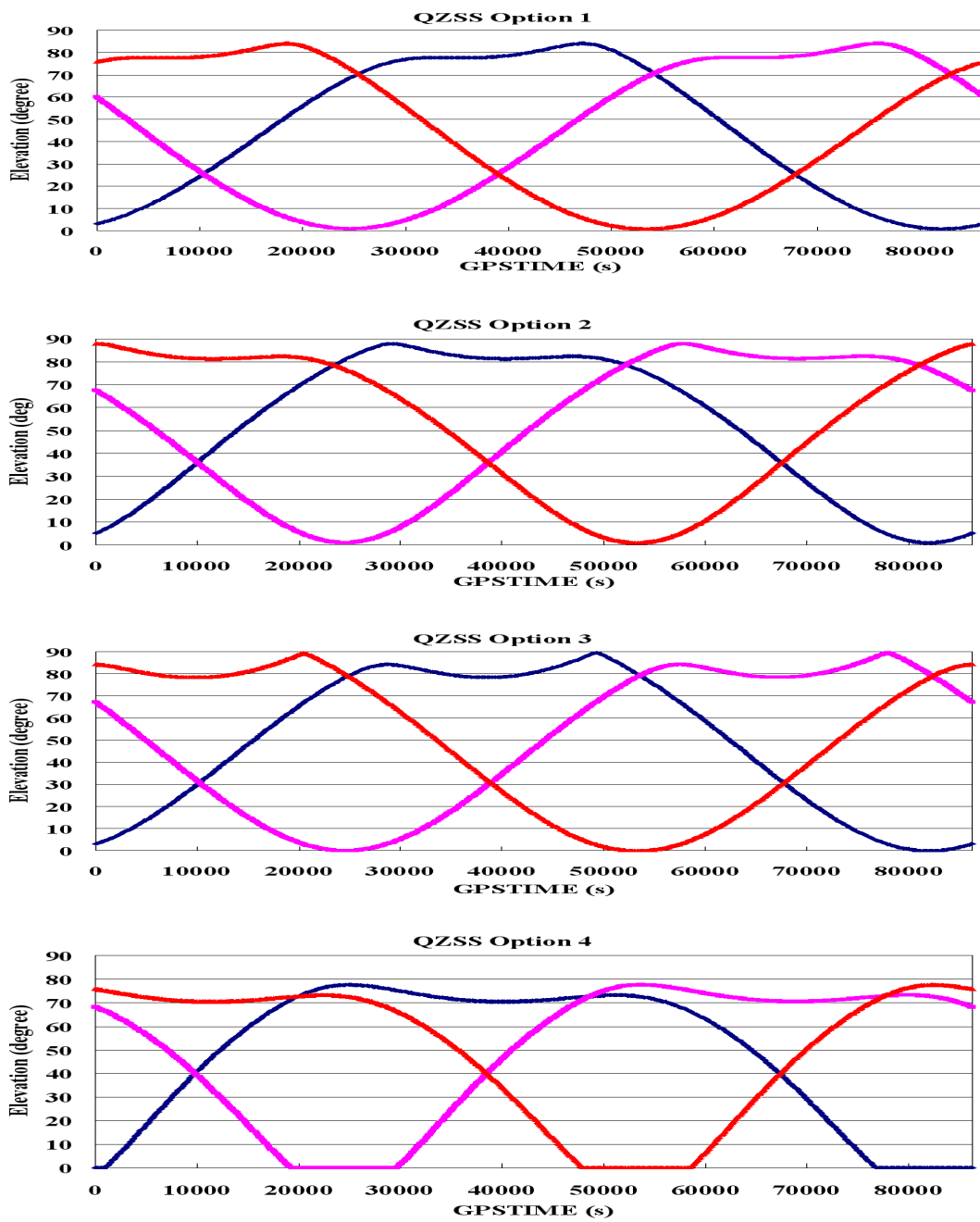
Figure 4.10.2 Elevation of three QZSs with four QZSS options at Japanese Tokyo
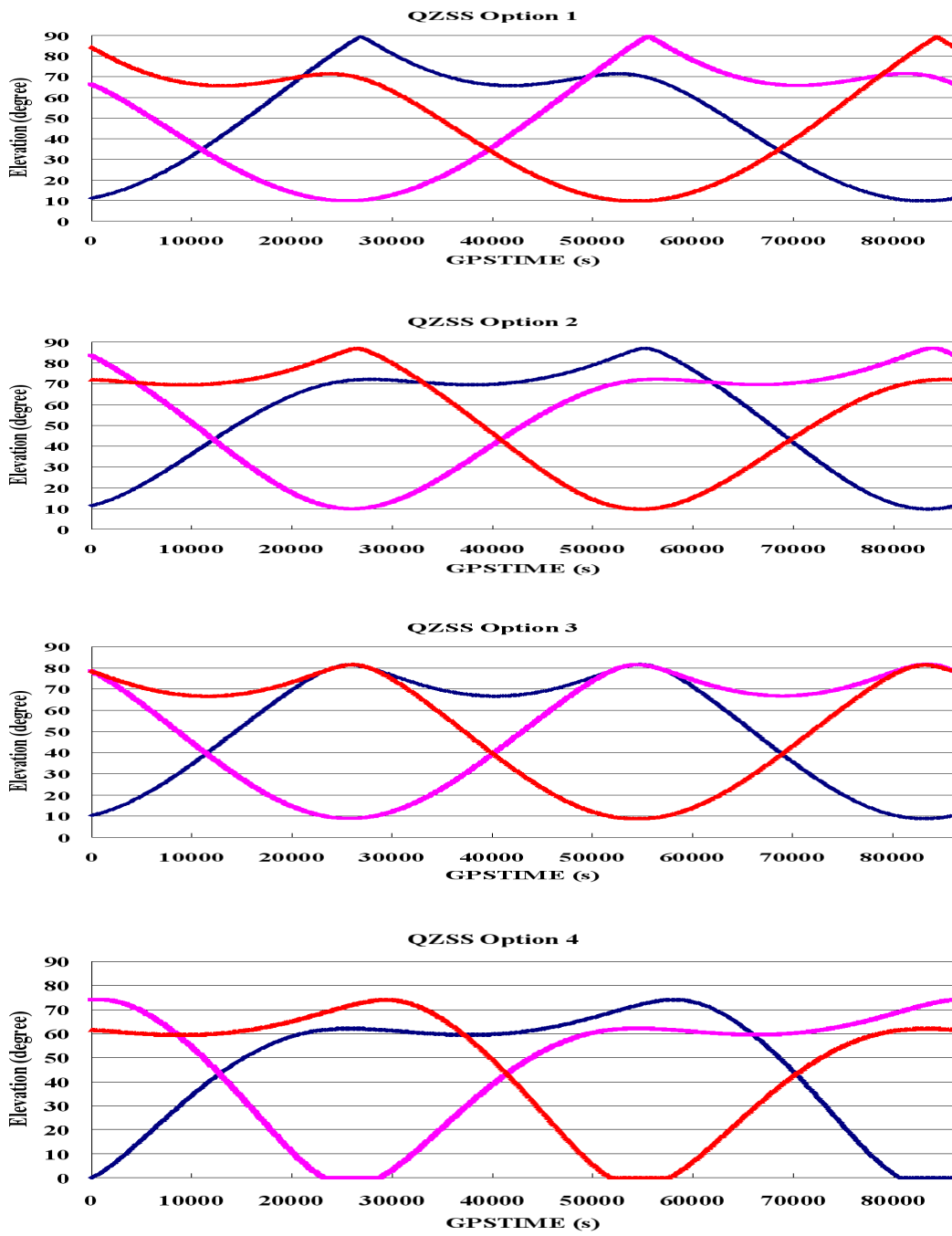
Figure 4.10.3 Elevation of three QZSs with four QZSS options at Japanese Naha

67
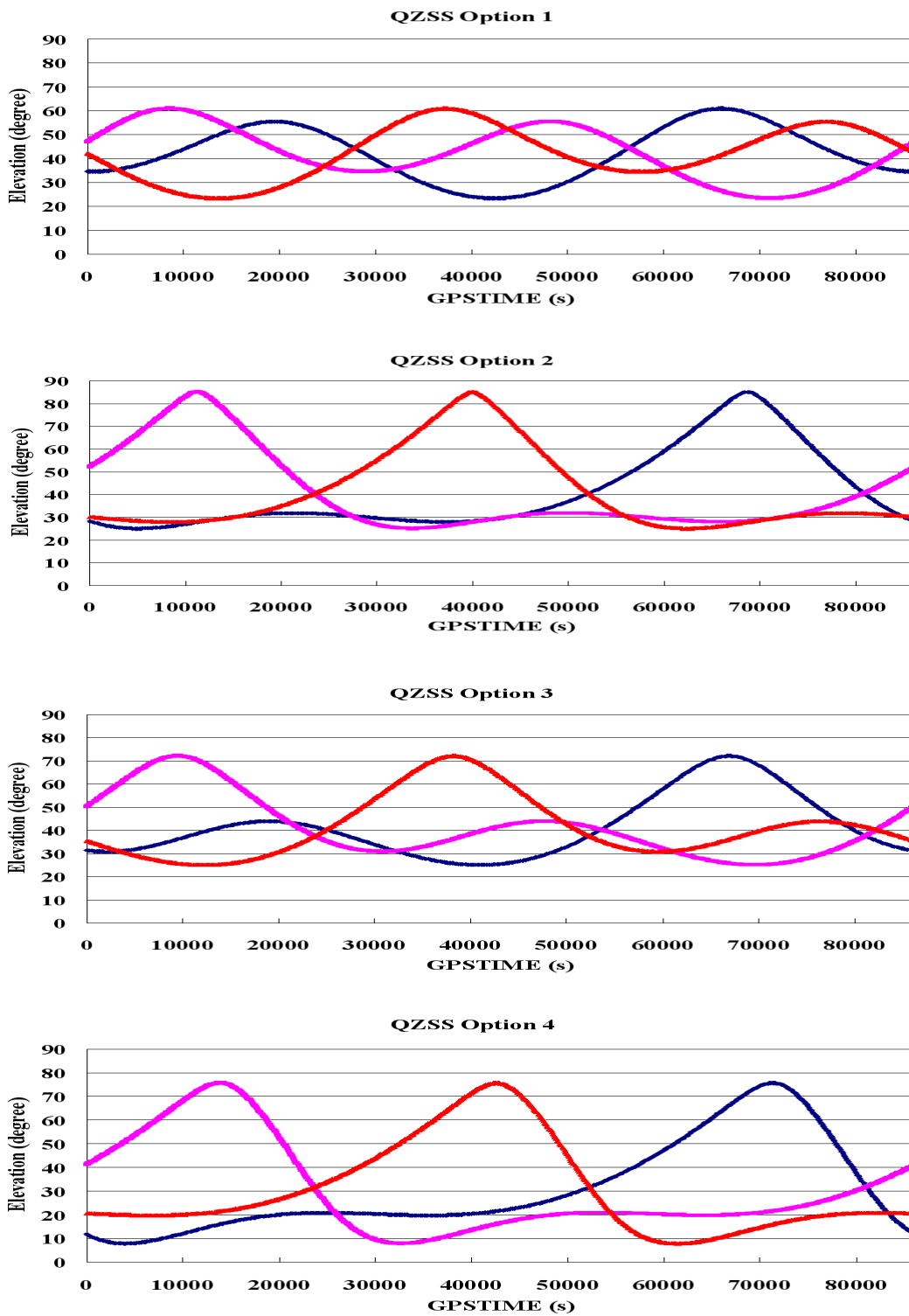
Figure 4.10.4 Elevation of three QZSs with four QZSS options at Indonesia Jakarta
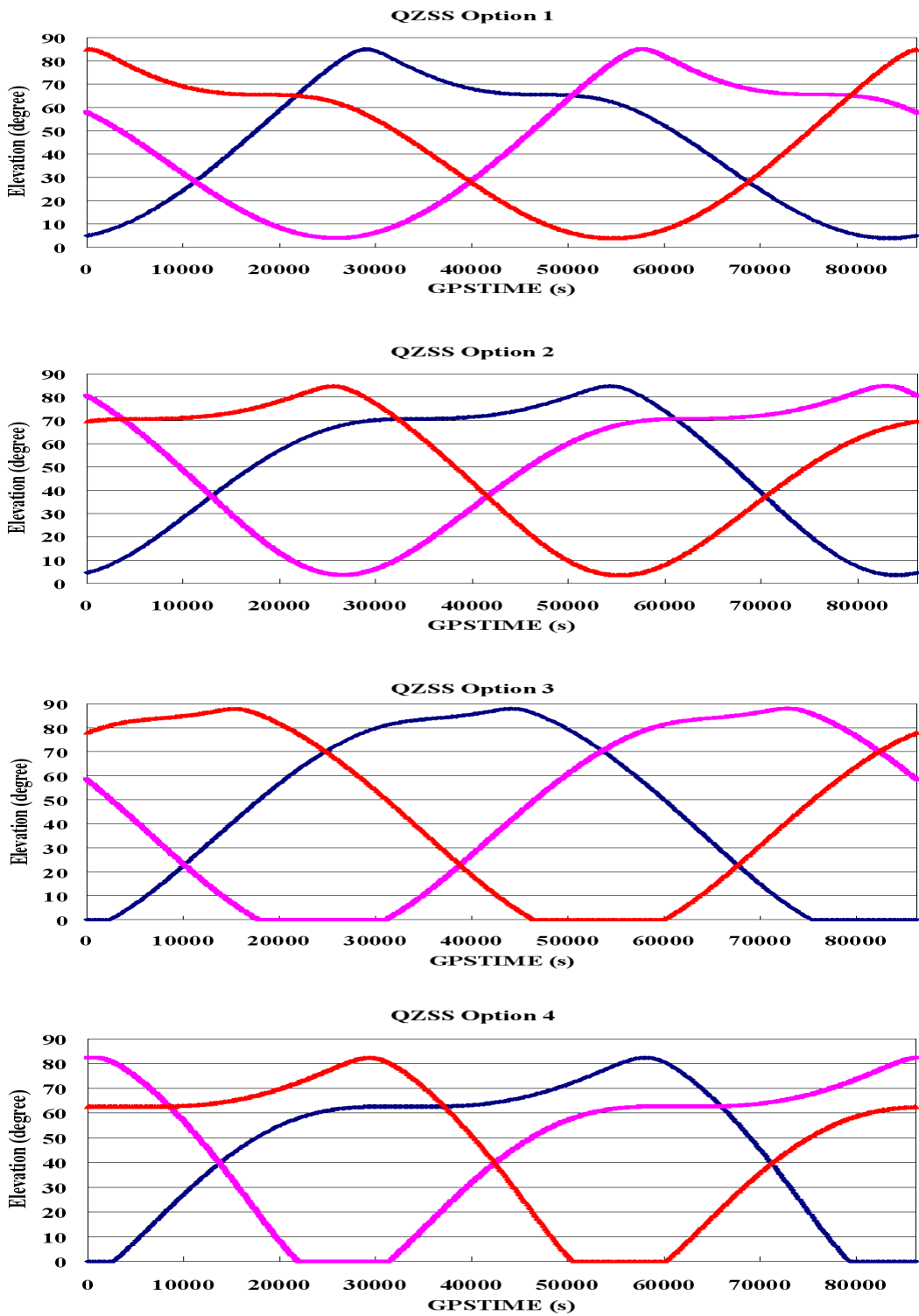
Figure 4.10.5 Elevation of three QZSs with four QZSS options at Chinese Shanghai
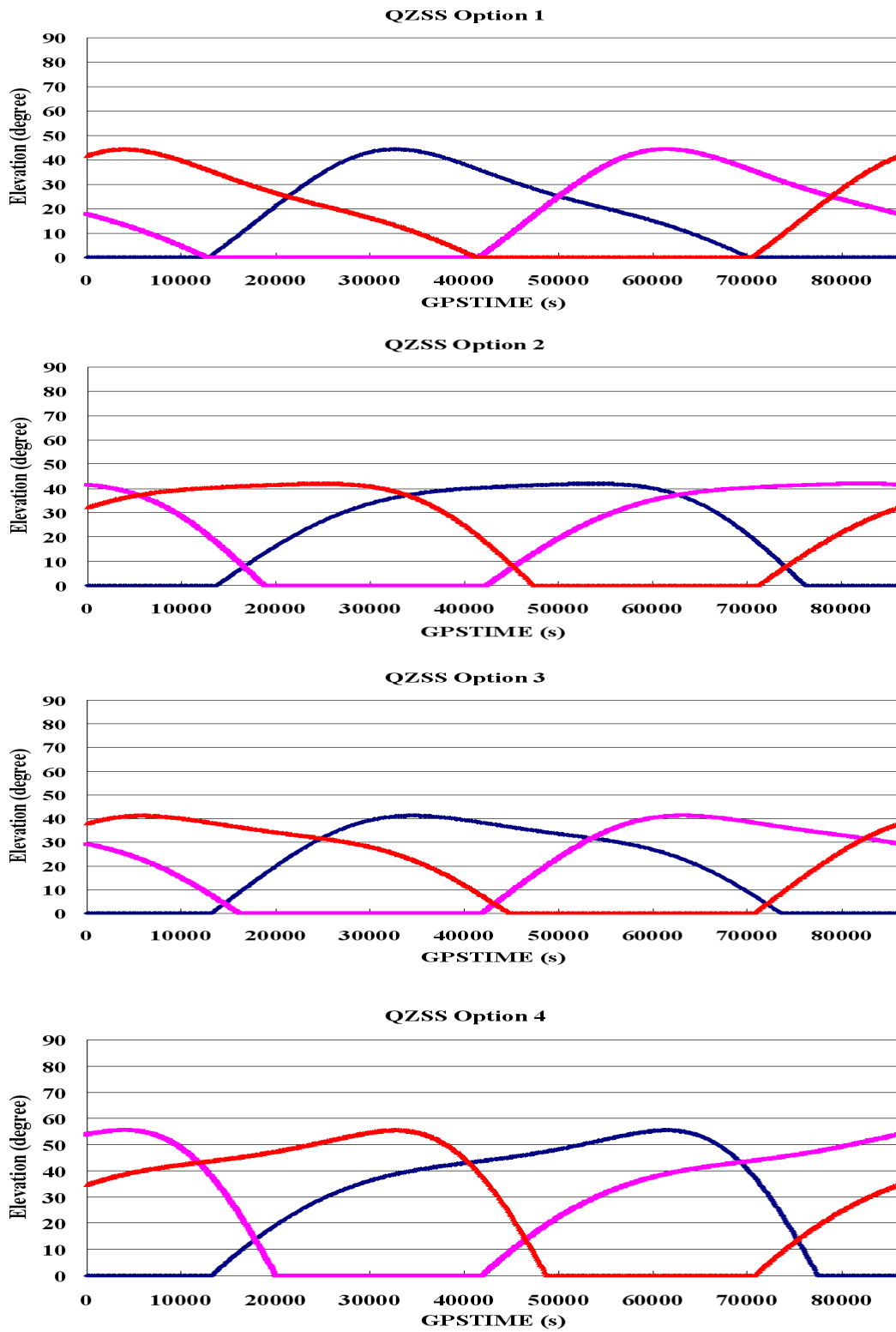
Figure 4.10.6 Elevation of three QZSs with four QZSS options at Chinese Kashi

From figure 4.10.1 to figure 4.10.6, elevations of three QZSs with four QZSS options at each city were given. Figure 4.10.1 shows which at Japanese Sapporo, figure 4.10.2 shows which at Japanese Tokyo, figure 4.10.3 shows which at Japanese Naha, figure 4.10.4 shows which at Indonesia Jakarta, figure 4.10.5 shows which at Chinese Shanghai, and figure 4.10.6 shows which at Chinese Kashi. Elevations and visibility time of three QZSs with four QZSS options were given from figures.

◆ **QZSs sky plot**

From figure 4.10.7 to figure 4.10.10, sky plots of one QZS in 24 hr at six cities were given. Figure 4.10.7 shows which using orbit option 1, figure 4.10.8 shows which using orbit option 2, figure 4.10.9 shows which using QZSS orbit (orbit option 3), and figure 4.10.10 shows which using orbit option 4.Elevation and azimuth of QZS were shown in the figures with four QZSS options.
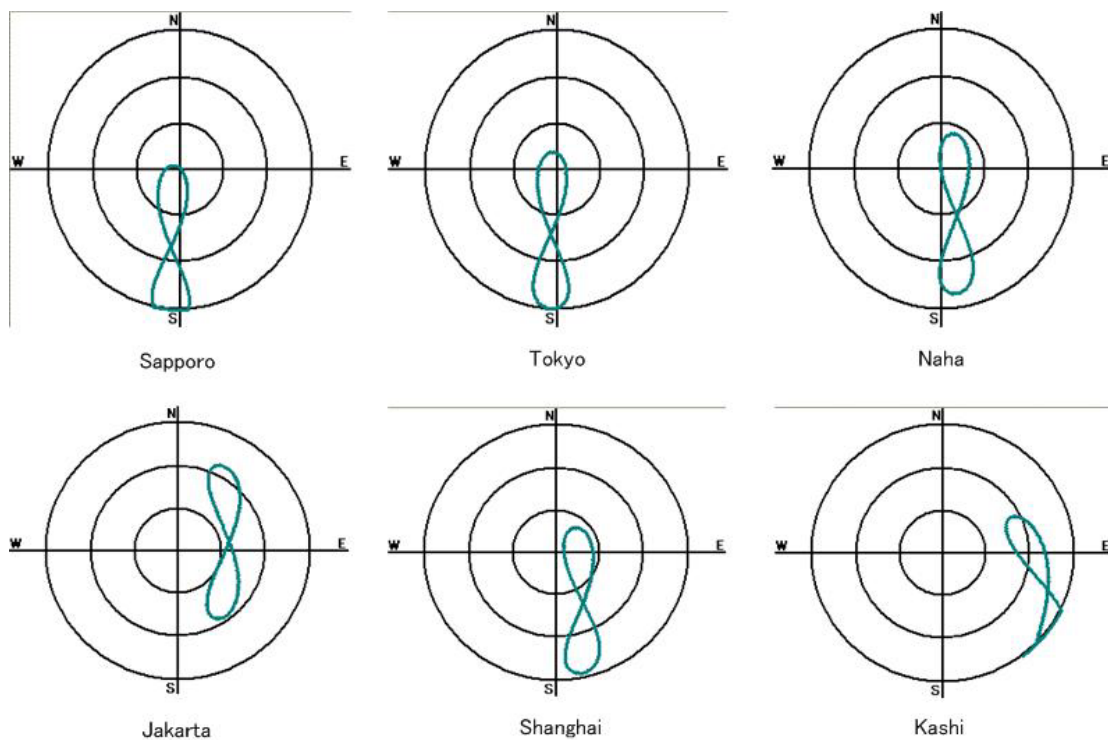
Figure 4.10.7 Sky plot of one QZS in 24 hr at six cities using orbit option 1
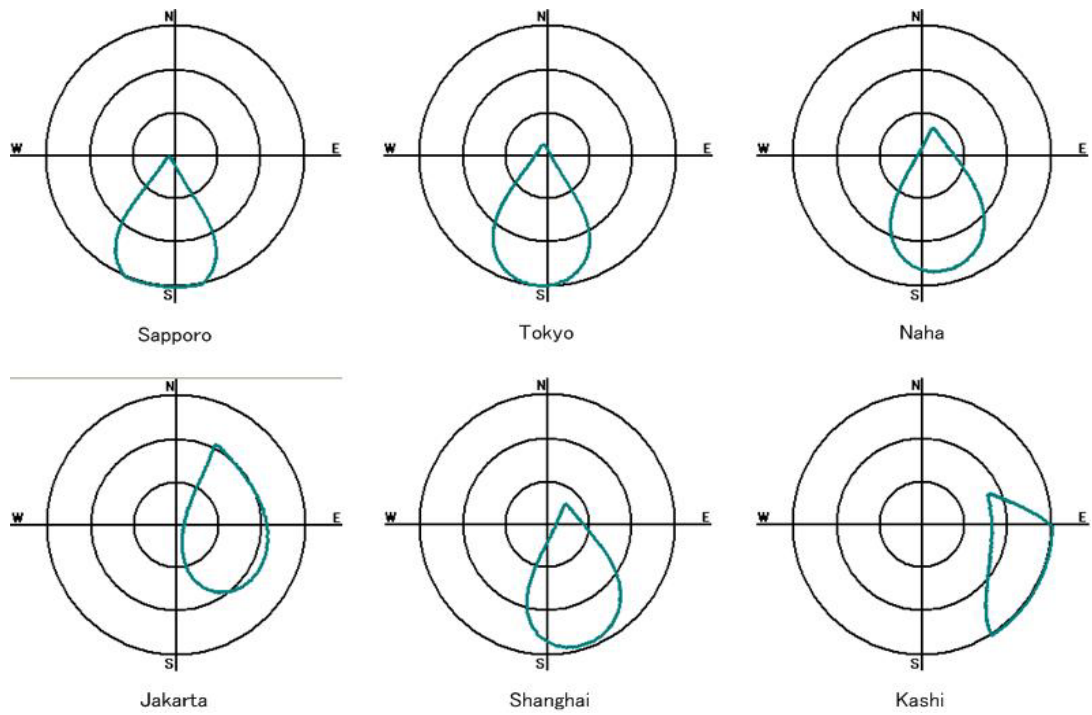
Figure 4.10.8 Sky plot of one QZS in 24 hr at six cities using orbit option 2
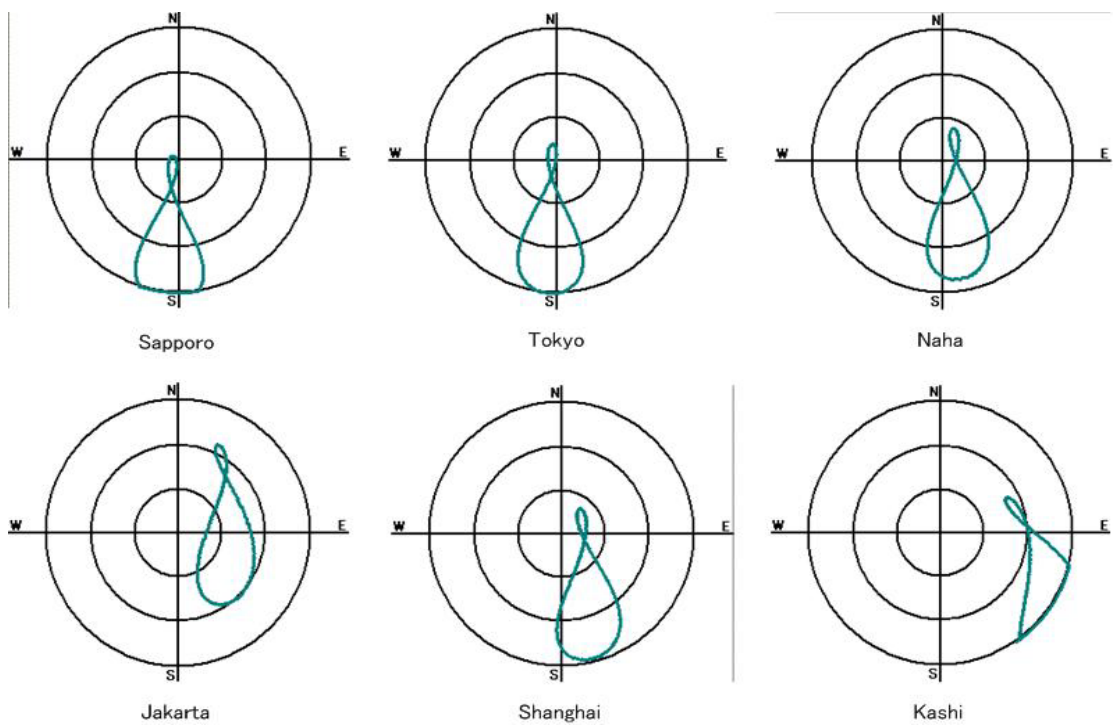
Figure 4.10.9 Sky plot of one QZS in 24 hr at six cities using QZSS orbit (option 3)
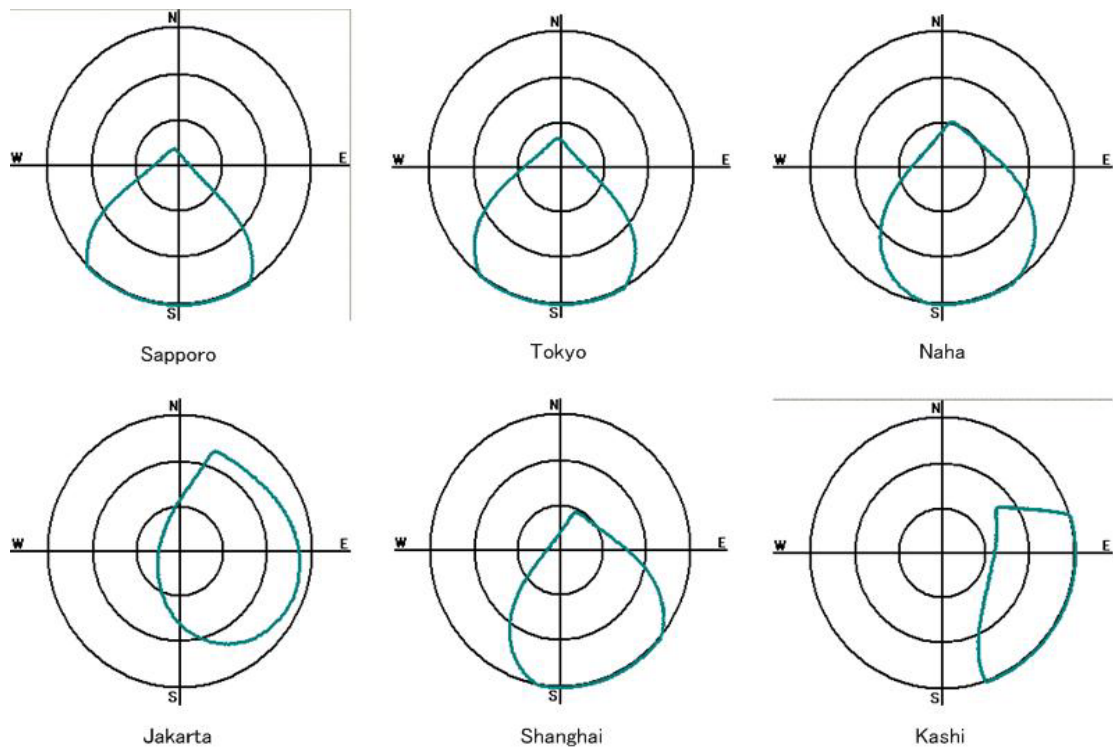
Figure 4.10.10 Sky plot of one QZS in 24 hr at six cities using orbit option 4

Table 4.13 shows min. QZS mask elevation with three QZSs in 24 hours at each city. From figure 4.10 and table 4.13, at each city, QZSs could offer high visibility elevation for user, and a user can track at least one QZSS satellite with 25º mask elevation using QZSS.

After using QZSS orbit (option 3), at three Japanese cities, at least one QZS could be tracked about 70º mask elevation in one day. Highest elevation of QZS in 24 hours was at Tokyo, and lowest elevation was at Kashi, because the longitude of Kashi was far from the centre longitude of Japan (135ºEast.).

City	QZSS Option1	QZSS Option2	**QZSS Option3**	QZSS Option4
Sapporo	62.2º	72.3º	**72.3º**	77.1º
Tokyo	70.5º	78.3º	**78.5º**	70.4º
Naha	65.7º	69.5º	**69.6º**	59.4º
Jakarta	44.6º	40.5º	**40.3º**	31.7º
Shanghai	65.1º	70.6º	**68.6º**	62.6º
Kashi	25.0º	37.2º	**31.7º**	43.2º

Table 4.13 Min. QZS mask elevation with three QZSs in 24 hours at each city

4.4.2 NVS in 24 hr

Figure 4.11.1 NVS at Sapporo with four QZSS options or without QZSS (mask angle is 15º)

Figure 4.11.2 NVS at Tokyo with four QZSS options or without QZSS (mask angle is 15º)

Figure 4.11.3 NVS at Naha with four QZSS options or without QZSS (mask angle is 15º)

Figure 4.11.4 NVS at Jakarta with four QZSS options or without QZSS (mask angle is 15º)

NVS at Shanghai

Figure 4.11.5 NVS at Shanghai with four QZSS options or without QZSS (mask angle is 15º)

NVS at Kashi

Figure 4.11.6 NVS at Kashi with four QZSS options or without QZSS (mask angle is 15º)

Area		NVS in 24 hours				
		Opt. 1 +GPS	Opt. 2 + GPS	**Opt. 3 + GPS**	Opt. 4 + GPS	GPS Only
Sapporo	min	6	6	**6**	6	4
	max	14	14	**14**	14	11
	average	9.33	9.54	**9.58**	9.54	7.27
Tokyo	min	6	7	**7**	7	4
	max	14	14	**14**	14	11
	average	9.66	9.73	**9.82**	9.79	7.39
Naha	min	7	7	**7**	7	5
	max	13	13	**13**	13	10
	average	10.0	10.1	**10.1**	9.95	7.45
Jakarta	min	8	8	**8**	8	5
	max	14	14	**14**	14	11
	average	10.95	10.95	**10.95**	10.46	7.95
Shanghai	min	7	7	**7**	7	4
	max	13	13	**13**	13	10
	average	9.71	9.83	**9.80**	9.76	7.35
Kashi	min	5	6	**6**	6	4
	max	12	12	**12**	12	10
	average	8.63	8.99	**8.88**	9.14	7.17

Table 4.14 NVS analysis in 24 hours at six cities (mask angle is 15º)

NVS in 24 hours with four QZSS options or without QZSS in each city when mask angle is 15º was given from figure 4.11.1 to figure 4.11.6. Figure 4.11.1 shows at Japanese Sapporo, figure 4.11.2 shows at Japanese Tokyo, figure 4.11.3 shows at Japanese Naha, figure 4.11.4 shows at Indonesia Jakarta, figure 4.11.5 shows at Chinese Shanghai, and figure 4.11.6 shows at Chinese Kashi.

Table 4.14 also gives NVS in 24 hours at six cities when mask angle is 15º. According to table 4.14, after using QZSS:

- min NVS was 2 more than in Sapporo, 2~3 more than in Tokyo, 2 more than in Naha, 3 more than in Shanghai, 1~2 more than in Kashi, and 3 more than in Jakarta.
- max NVS was 3 more than in Sapporo, 3 more than in Tokyo, 3 more than in Naha, 3 more than in Shanghai, 2 more than in Kashi, and 3 more than in Jakarta.

- average NVS could be could be improved 28.34%~31.77% in Sapporo, 30.72%~32.88% in Tokyo, 33.56%~34.36% in Naha, 32.11%~33.74% in Shanghai, 20.36%~27.48% in Kashi, and 31.57%~37.74% in Jakarta.

NVS could all be improved with 4 QZSS options in each city. Impact from QZSS could be seen.

Figure 4.11.7 gives visible QZS number at six cities using QZSS orbit (option 3) only when mask angle is 15º. From figure 4.11 and table 4.14, min NVS could all be improved at each six cities, at least six satellites and one QZSS satellite with 15º mask degree can be seen in all day. Using QZSS orbit (option 3), two QZSs can be tracked in all the time of the day except for which at Chinese Kashi.
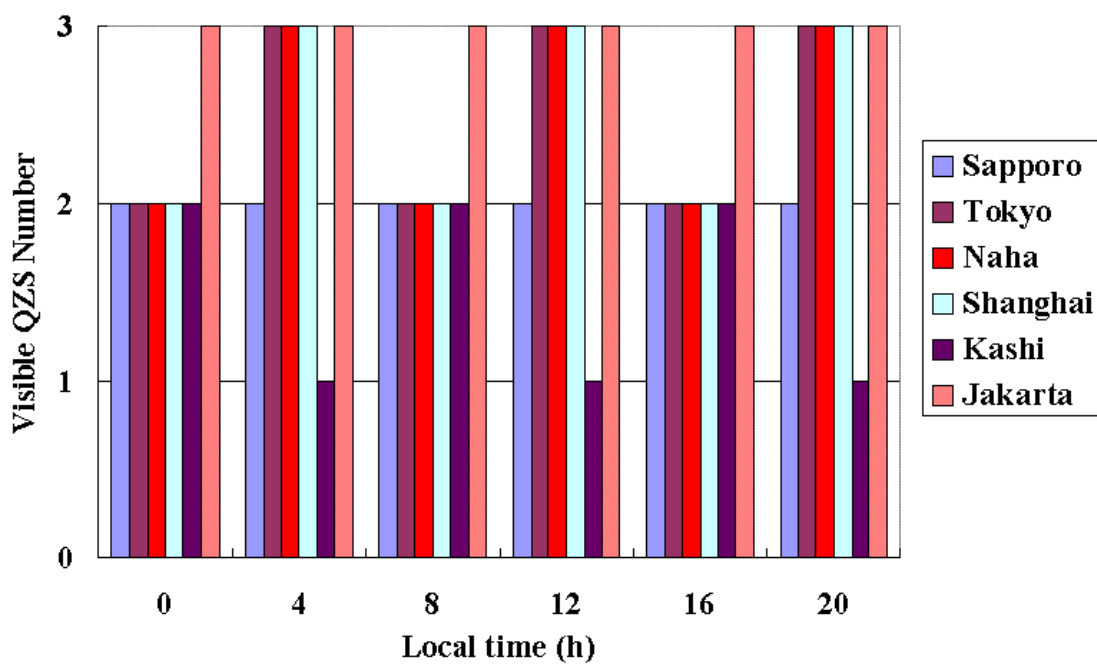
Figure 4.11.7 Visible QZS number at six cities using QZSS orbit (option 3) when mask angle is 15º
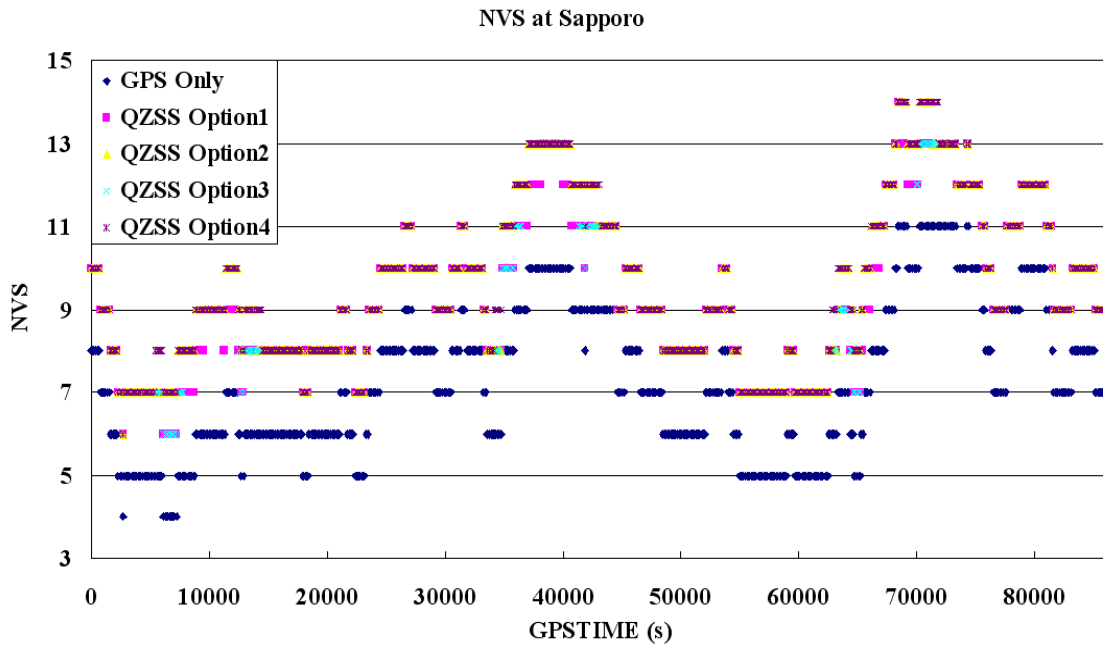
4.4.3 PDOP in 24 hr

Figure 4.12.1 PDOP at Sapporo with four QZSS options or without QZSS (mask angle is 15º)
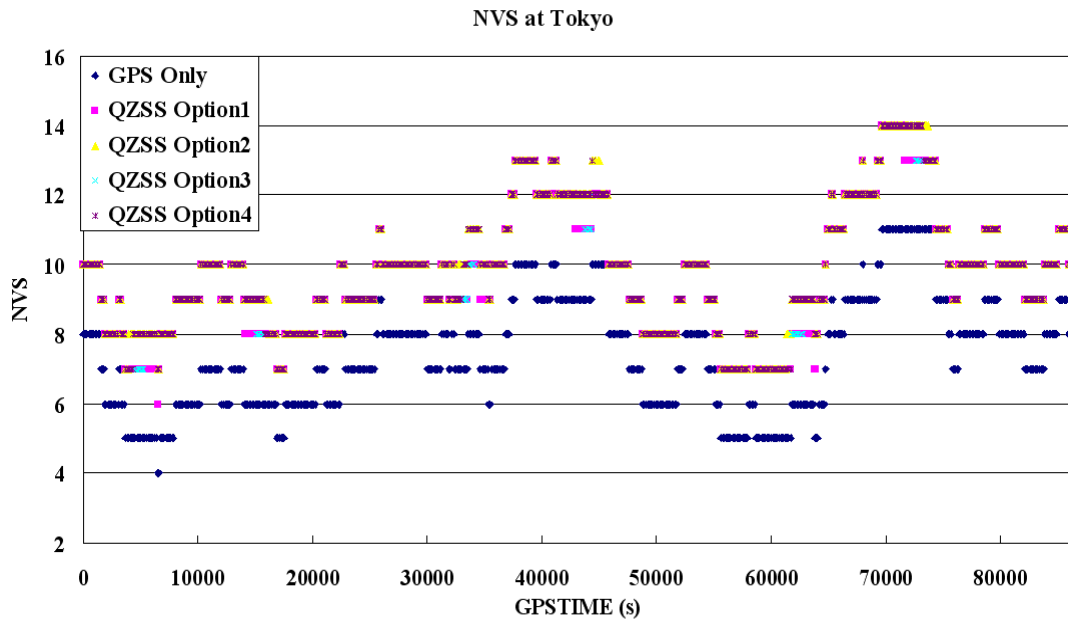

Figure 4.12.2 PDOP at Tokyo with four QZSS options or without QZSS (mask angle is 15º)
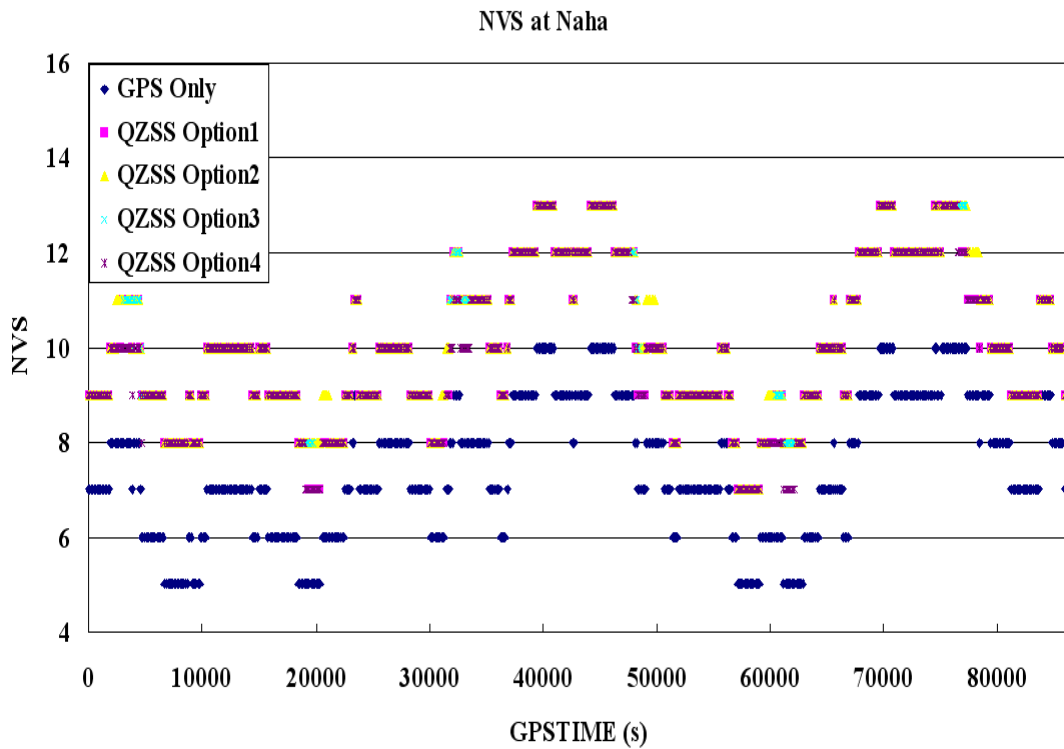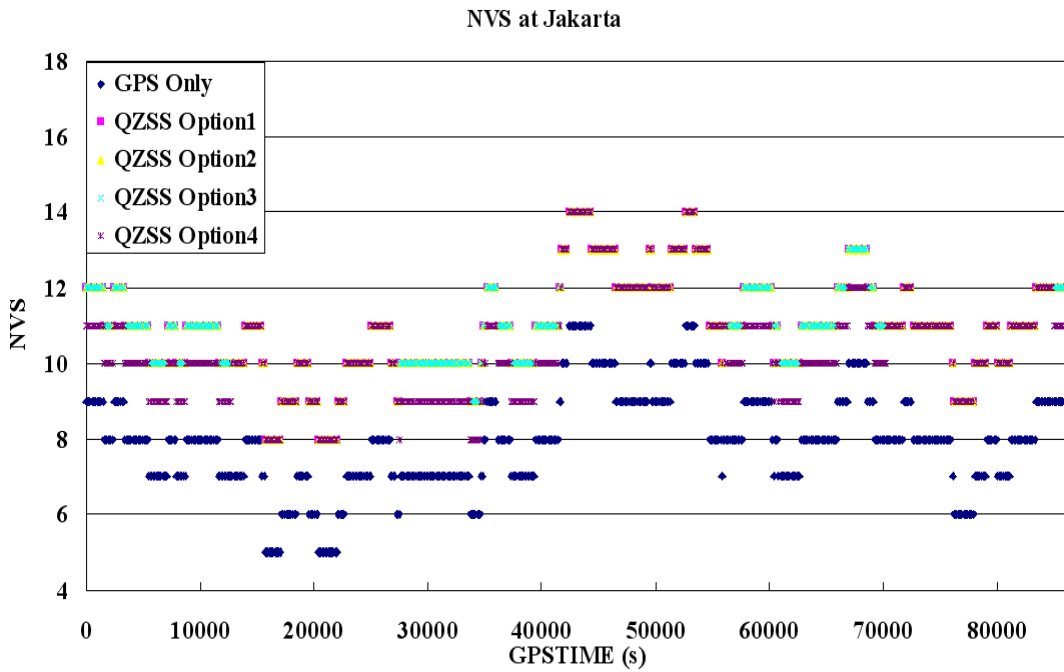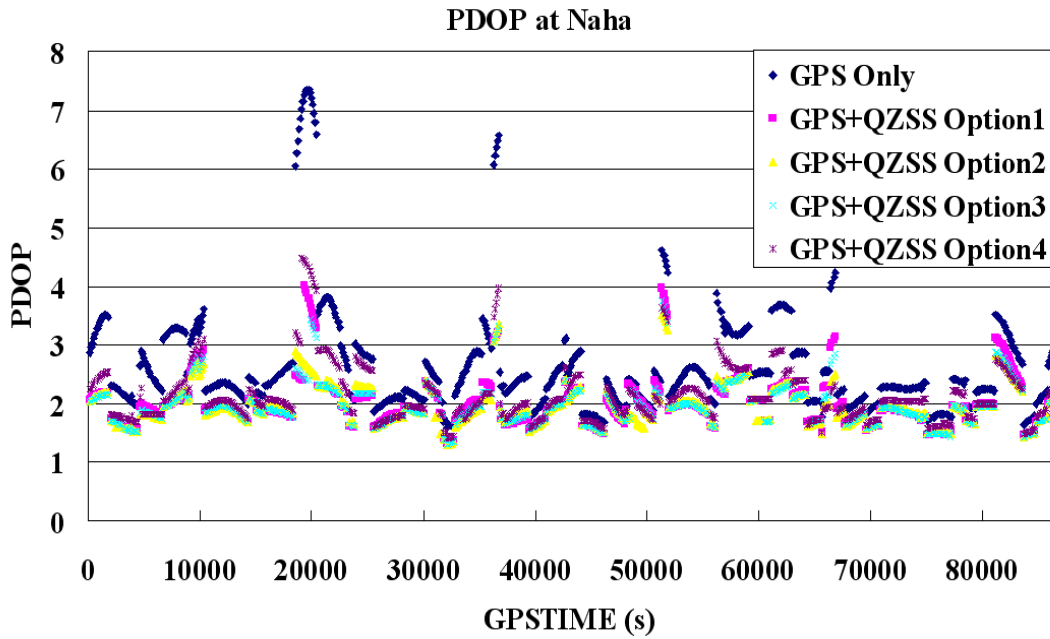
PDOP at Naha

Figure 4.12.3 PDOP at Naha with four QZSS options or without QZSS (mask angle is 15º)
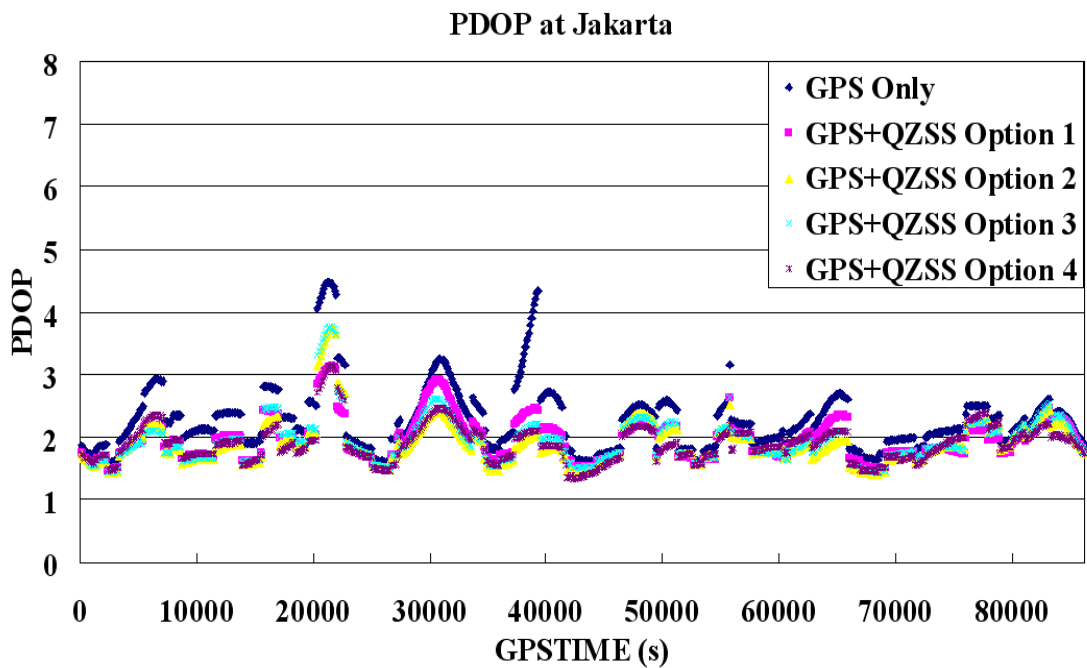
PDOP at Jakarta

Figure 4.12.4 PDOP at Jakarta with four QZSS options or without QZSS (mask angle is 15º)
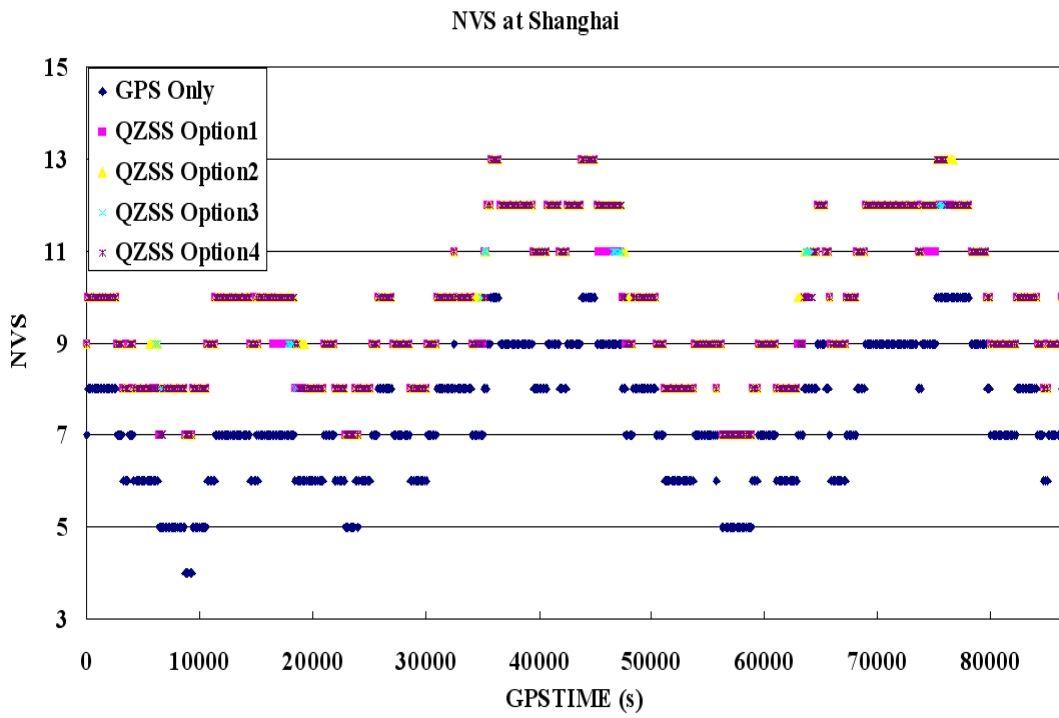
PDOP at Shanghai

Figure 4.12.5 PDOP at Shanghai with four QZSS options or without QZSS (mask angle is 15º)
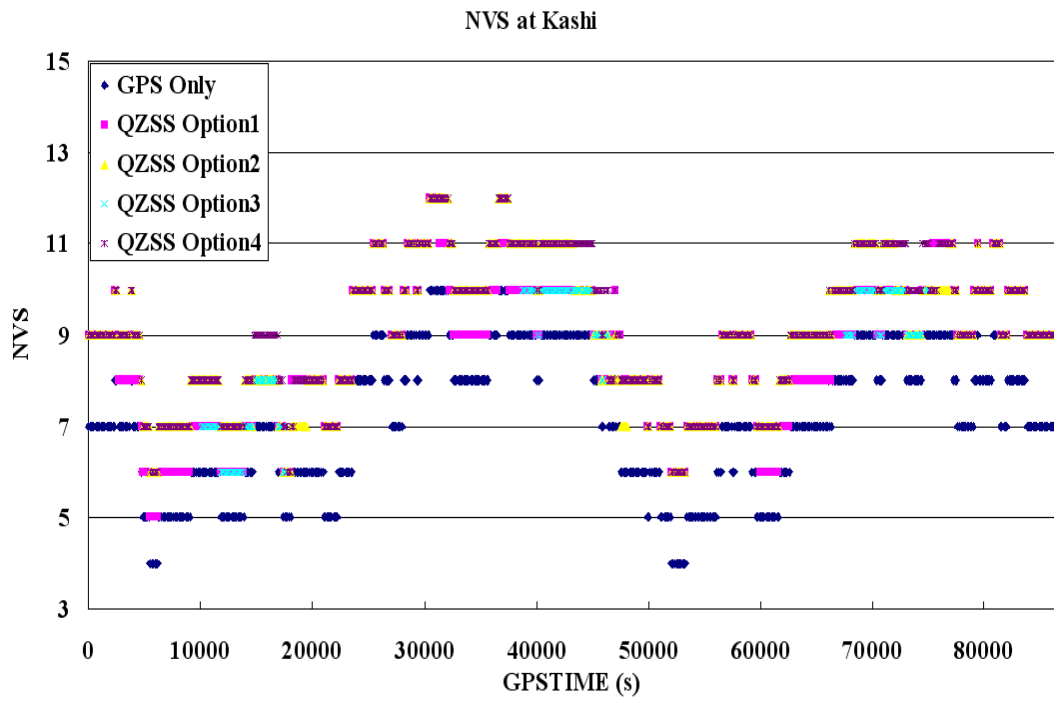

PDOP at Kashi

Figure 4.12.6 PDOP at Kashi with four QZSS options or without QZSS (mask angle is 15º)

Area		Opt. 1 +GPS	Opt. 2 + GPS	**Opt. 3 + GPS**	Opt. 4 + GPS	GPS Only
Sapporo	average	2.09	2.07	**2.06**	2.11	3.12
Tokyo	average	2.02	1.98	**1.97**	2.06	2.81
Naha	average	2.00	1.95	**1.95**	2.13	2.62
Jakarta	average	1.95	1.89	**1.93**	1.89	2.26
Shanghai	average	2.08	2.01	**2.02**	2.04	2.60
Kashi	average	2.29	2.28	**2.27**	2.27	2.60

Table 4.15 Average PDOP (NVS > 3) analysis in 24 hours at six cities (mask angle is 15º)

Figure 4.12 shows PDOP (NVS > 3) in 24 hours with four QZSS options or without QZSS in each city when mask angle is 15 degree. Figure 4.12.1 shows at Japanese Sapporo, figure 4.12.2 shows at Japanese Tokyo, figure 4.12.3 shows at Japanese Naha, figure 4.12.4 shows at Indonesia Jakarta, figure 4.12.5 shows at Chinese Shanghai, and figure 4.12.6 shows at Chinese Kashi.

Table 4.15 shows average PDOP in 24 hours at six cities when mask angle is 15 degree. Form figure 4.12 and table 4.15, average PDOP could be could be improved 32.37%~33.97% in Sapporo, 26.69%~29.89% in Tokyo, 18.70%~25.57% in Naha, 20.0%~22.69% in Shanghai, 11.92%~12.69% in Kashi, and 13.72%~16.37% in Jakarta. With extra QZSs, the satellite geometry could be even better at each cities, accuracy of positioning was expected to be improved.

4.4.4 L1 Code DGPS in 24 hr

L1 code DGPS positioning in short baseline was invested here. Carrier smoothing was not used in positioning. Figure 4.13 shows DGPS results in 24 hours with four QZSS options or without QZSS in each city when mask angle is 15 degree. Figure 4.13.1 shows at Japanese Sapporo, figure 4.13.2 shows at Japanese Tokyo, figure 4.13.3 shows at Japanese Naha, figure 4.13.4 shows at Indonesia Jakarta, figure 4.13.5 shows at Chinese Shanghai, and figure 4.13.6 shows at Chinese Kashi.

Table 4.16 shows the horizontal standard deviation of the L1 code DGPS positioning results. In table 4.16, 2drms (m) of DGPS positioning results could be improved 33.78%~45.27% in Sapporo, 42.0%~45.33% in Tokyo, 11.21%~23.36% in Naha, 8.08%~16.16% in Shanghai, 7.87%~11.24% in Kashi, and 6.86%~12.75% in Jakarta. From 4.16 and figure 4.13, L1 Code DGPS positioning results show that the accuracy of positioning could be improved using QZSS.
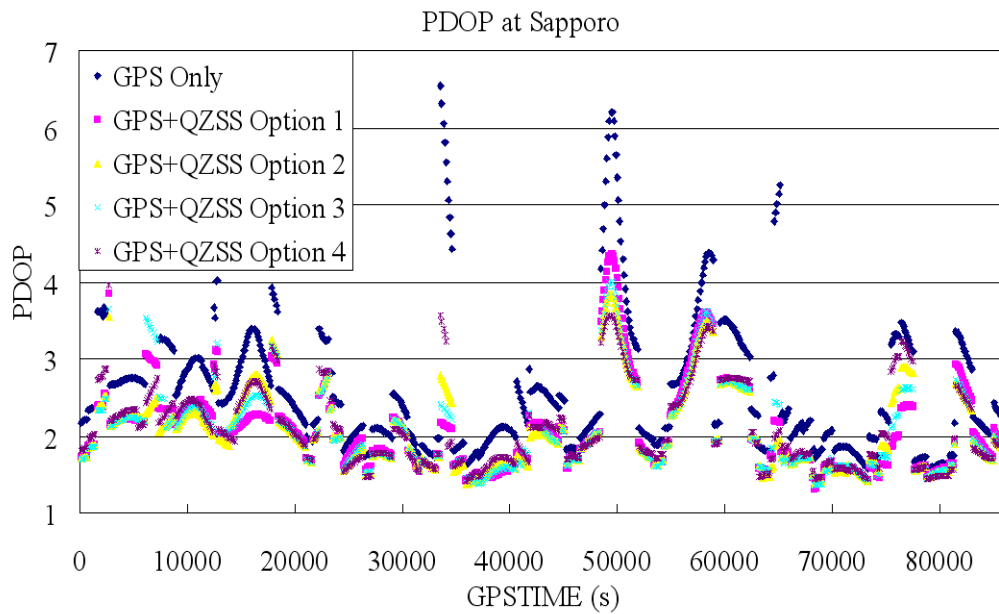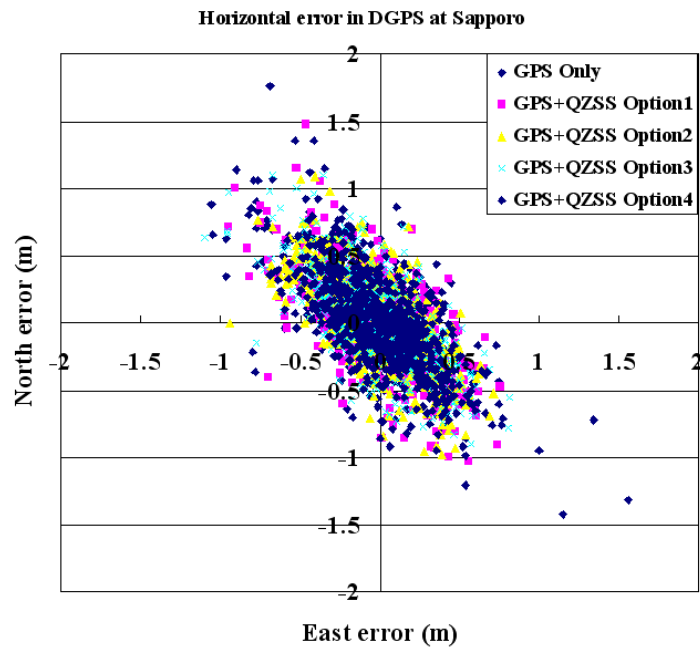
Figure 4.13.1 DGPS results at Sapporo with four QZSS options or without QZSS (mask angle is 15º)
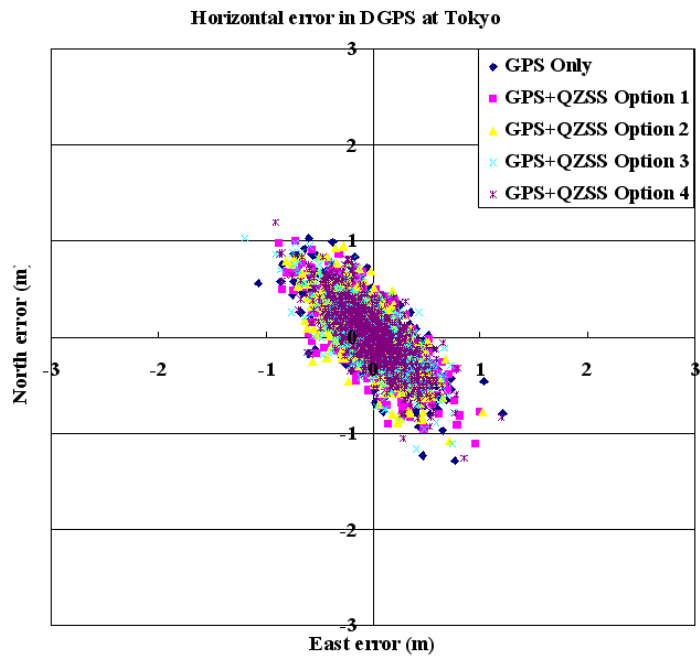
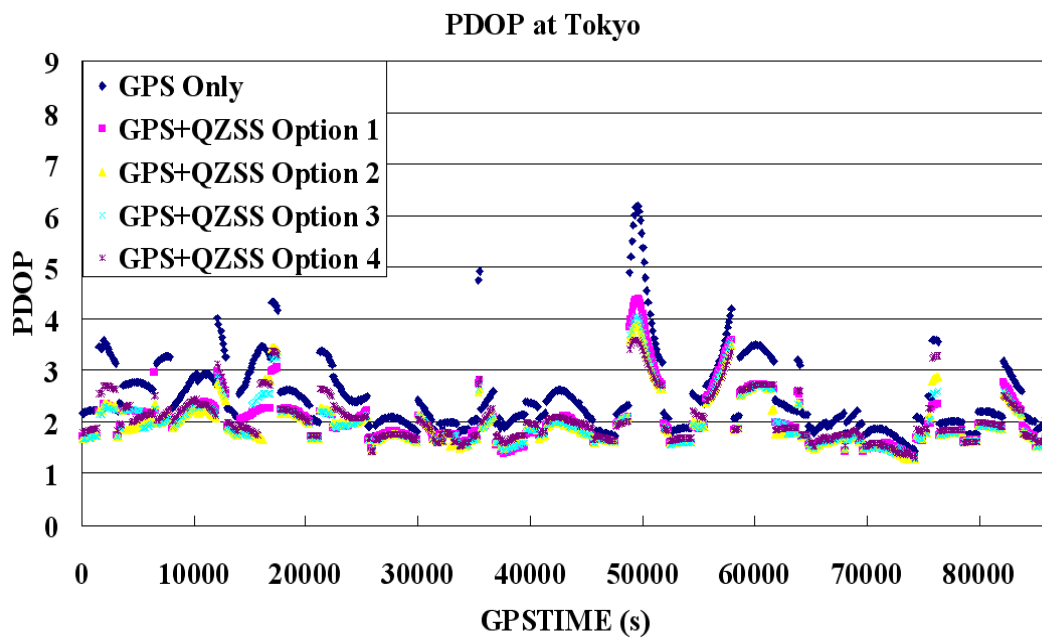**Figure 4.13.2 DGPS results at Tokyo with four QZSS options or without QZSS (mask angle is 15º)**
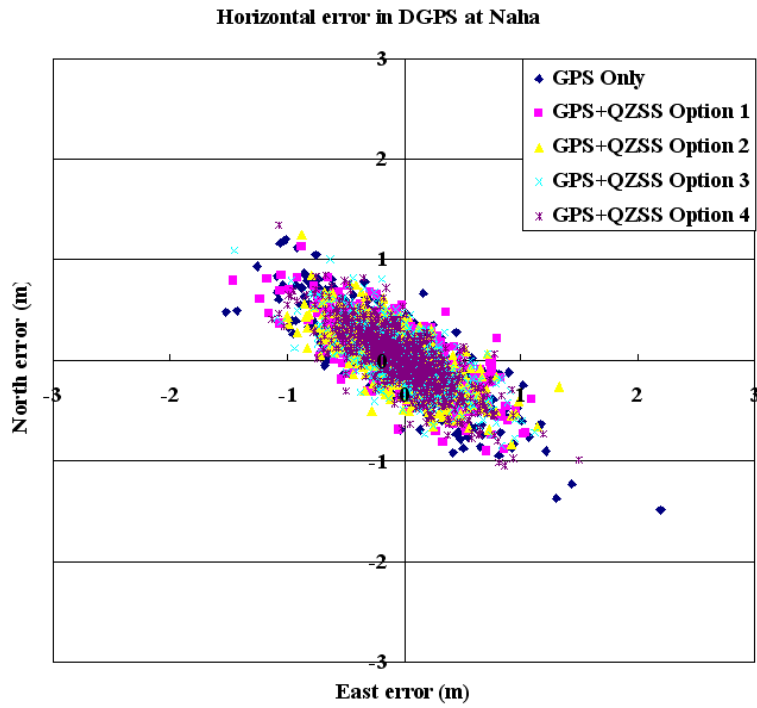
**Figure 4.13.3 DGPS results at Naha with four QZSS options or without QZSS**

(mask angle is 15º)

Horizontal error in DGPS at Jakarta
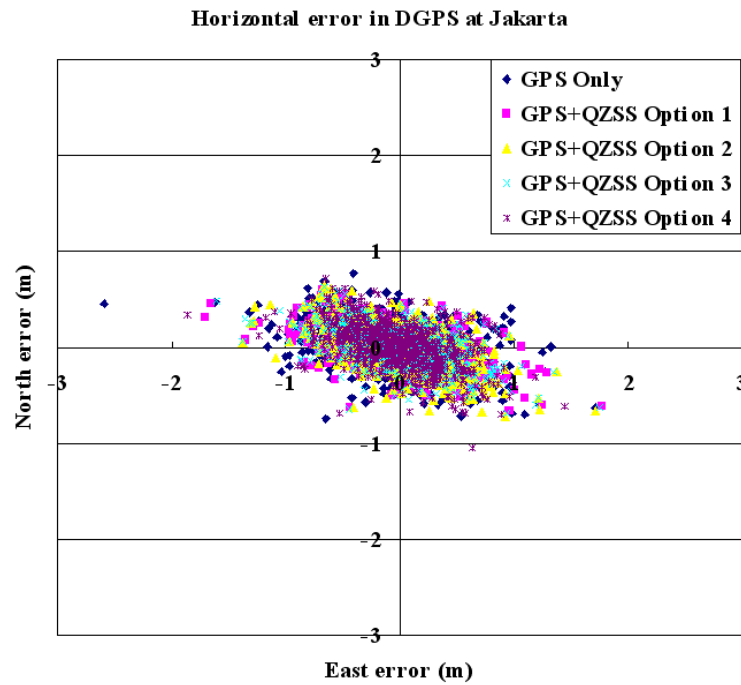
Figure 4.13.4 DGPS results at Jakarta with four QZSS options or without QZSS
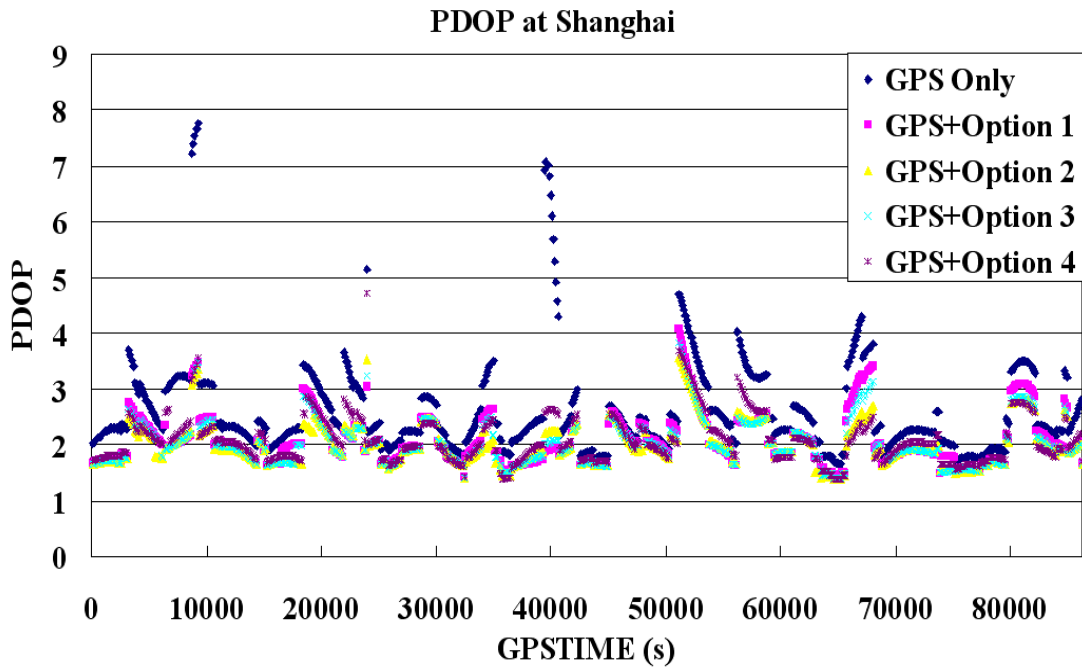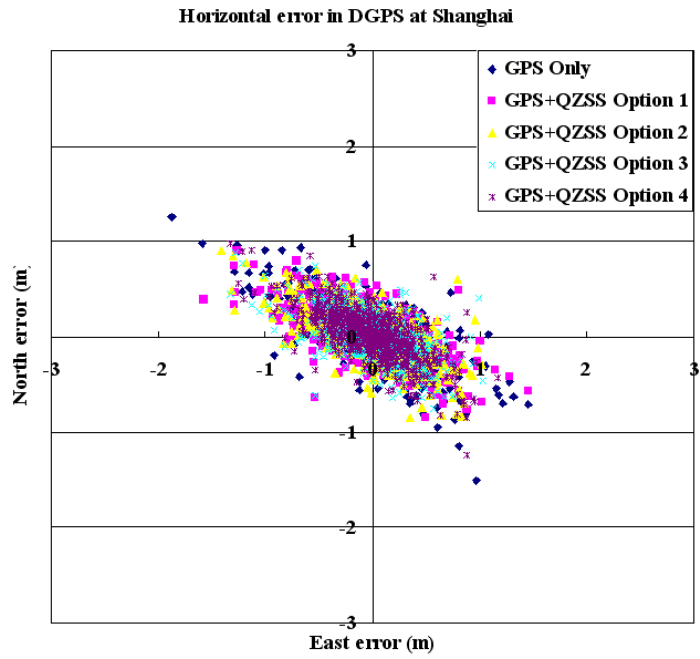
(mask angle is 15º)

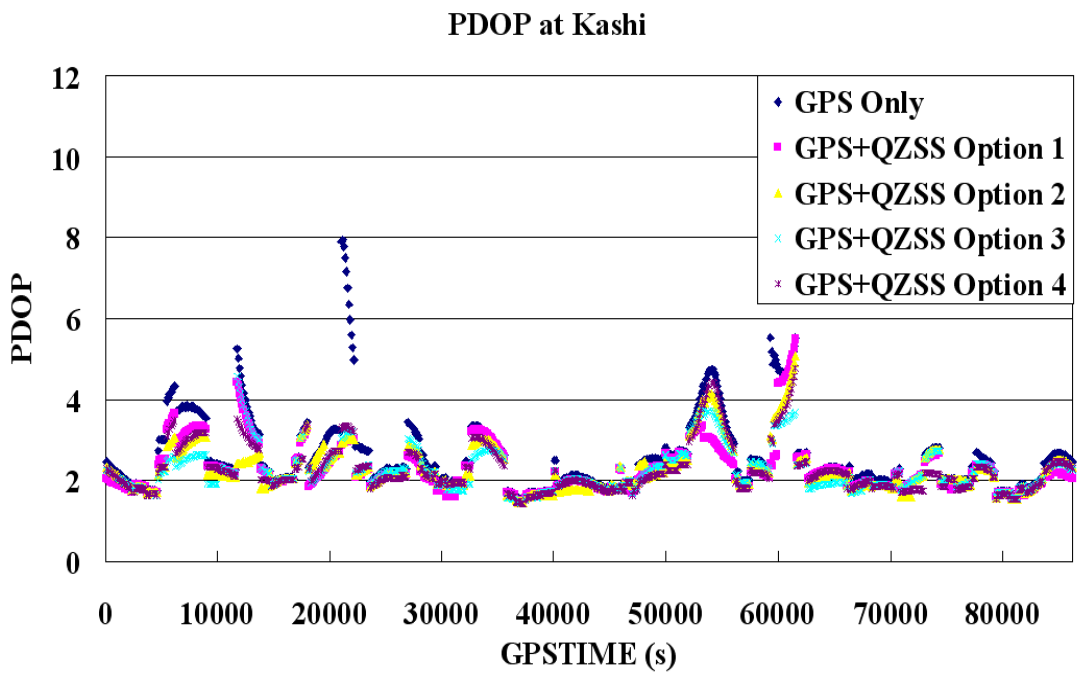**Figure 4.13.5 DGPS results at Shanghai with four QZSS options or without QZSS**
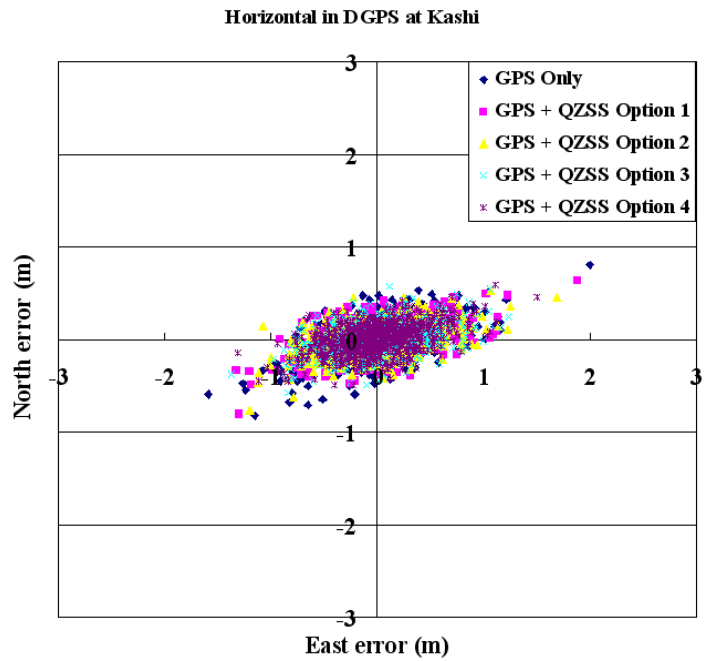
(mask angle is 15º)

Figure 4.13.6 DGPS results at Kashi with four QZSS options or without QZSS

(mask angle is 15º)

Area		Opt. 1 +GPS	Opt. 2 + GPS	**Opt. 3 + GPS**	Opt. 4 + GPS	GPS Only
Sapporo	X (m)	0.31	0.31	**0.31**	0.32	0.53
	Y (m)	0.26	0.26	**0.26**	0.27	0.52
	2drms (m)	0.81	0.81	**0.81**	0.98	1.48
Tokyo	X (m)	0.32	0.31	**0.31**	0.33	0.53
	Y (m)	0.28	0.27	**0.27**	0.28	0.53
	2drms (m)	0.85	0.82	**0.82**	0.87	1.50
Naha	X (m)	0.28	0.26	**0.28**	0.31	0.34
	Y (m)	0.36	0.32	**0.33**	0.36	0.41
	2drms (m)	0.91	0.82	**0.87**	0.95	1.07
Shanghai	X (m)	0.25	0.25	**0.24**	0.26	0.29
	Y (m)	0.38	0.36	**0.34**	0.36	0.40
	2drms (m)	0.91	0.88	**0.83**	0.89	0.99
Kashi	X (m)	0.16	0.16	**0.16**	0.16	0.20
	Y (m)	0.38	0.38	**0.36**	0.36	0.40
	2drms (m)	0.82	0.82	**0.79**	0.79	0.89
Jakarta	X (m)	0.20	0.22	**0.21**	0.23	0.24
	Y (m)	0.42	0.42	**0.41**	0.38	0.45
	2drms (m)	0.93	0.95	**0.92**	0.89	1.02

Table 4.16 Standard deviation (m) in L1 code DGPS positioning with or without QZSS

(mask angle is 15º)

4.4.5 ASR in 24hr

Single epoch L1 signal AR in short baseline (mask angle is 15º) was estimated here. WL method which was introduced in chapter 3 was proposed here. GPS with QZSS was considered as triple frequency system, GPS only was considered as dual frequency system. In the case of GPS with QZSS, triple frequency WL method was used, and in the case of GPS only, dual frequency system WL was proposed.

Table 4.17 gives the ASR of the L1 signal in 24 hr with or without QZSS. Table 4.17 shows that integrating QZSS with GPS, epoch when common NVS at each city was all more than five in all of the day. Epoch of common NVS more than five could be improved about 1.5% in Sapporo, 0.3% in Tokyo, 0.0% in Naha, 0.7% in Shanghai, 2.4% in Kashi, and 0.0% in Jakarta. The basic requirement for RTK positioning could be offered in 24 hours using GPS with QZSS.

At six cities, ASR (common NVS > 4) using four QZSS options in 24 h were all more than 99.0%. Using

orbit option 3 (QZSS orbit), ASR could be improved about 5.95% in Sapporo, 5.28% in Tokyo, 5.28% in Naha, 5.06% in Shanghai, 5.41% in Kashi, and 5.62% in Jakarta. Therefore, the time of AR could be reduced. From ASR results, the efficiency and reliability for highly precise positioning could be improved after integrating QZSS with GPS.

Signal		Triple-frequency				Dual-frequency
Satellite		Opt.1 +GPS	Opt.2 +GPS	**Opt.3 + GPS**	Opt.4 +GPS	GPS Only
Sapporo	Epoch common NVS < 5	0	0	**0**	0	11
	Success epoch number	718	717	**718**	715	667
	Common NVS > 4	100%	100%	**100%**	100%	98.5%
	ASR (common NVS > 4)	**99.7%**	**99.6%**	**99.7%**	**99.3%**	**94.1%**
Tokyo	Epoch common NVS < 5	0	0	**0**	0	2
	Success epoch number	718	718	**718**	715	680
	Common NVS > 4	100%	100%	**100%**	100%	99.74%
	ASR (common NVS >4)	**99.7%**	**99.7%**	**99.7%**	**99.3%**	**94.7%**
Naha	Epoch common NVS < 5	0	0	**0**	0	0
	Success epoch number	717	717	**718**	714	682
	Common NVS > 4	100%	100%	**100%**	100%	100%
	ASR (common NVS >4)	**99.6%**	**99.6%**	**99.7%**	**99.2%**	**94.7%**
Shanghai	Epoch common NVS < 5	0	0	**0**	0	5
	Success epoch number	717	718	**717**	715	678
	Common NVS > 4	100%	100%	**100%**	100%	99.3%
	ASR (common NVS >4)	**99.6%**	**99.7%**	**99.6%**	**99.3%**	**94.8%**
Kashi	Epoch common NVS < 5	0	0	**0**	0	17
	Success epoch number	714	716	**715**	716	662
	Common NVS > 4	100%	100%	**100%**	100%	97.6%
	ASR (common NVS >4)	**99.2%**	**99.4%**	**99.3%**	**99.4%**	**94.2%**
Jakarta	Epoch common NVS < 5	0	0	**0**	0	0
	Success epoch number	716	717	**717**	714	679
	Common NVS > 4	100%	100%	**100%**	100%	100%
	ASR (common NVS >4)	**99.4%**	**99.6%**	**99.6%**	**99.2%**	**94.3%**

Table 4.17 ASR of L1 signal at six cities for 24 hr (mask angle is15º)

4.5 SUMMARY

In this section, triple frequency simulator was introduced. Noise and error models in the simulator were presented here. Performance of QZSS was evaluated using data from simulator.

From spatial and temporal numerical analysis, it was shown that QZSS not only improves the availability and geometry of satellites using NVS and PDOP estimation, but also enhances the reliability and efficiency of GPS positioning, using DGPS positioning and ASR estimation, in the near Japan area, and also in most of the East Asian region.

Feature of QZSS orbit (Asym-8-shape) was also discussed here. Using QZSS in East Asian region, that geometry position condition was improved significantly when longitude of location is close to Japan center longitude could also be concluded.

From analysis of NVS and PDOP in the East Asian and Japan regions, among four optional QZSS, Option 3 (Asym-8-shape) constellation is the best option for the local Japan region, and Option 2 (Egg-shaped 1 constellation is the best option for East Asian region.

CHAPTER 5
POSITIONING WITH QZSS

In this chapter, L1 code DGPS positioning and single epoch DD L1 signal ASR estimation in different baseline with or without QZSS were measured to prove impact of accuracy and efficiency with QZSS. Various AR methods, which have been introduced in Chapter 3, were also offered in this chapter.

5.1 PARAMETERS IN POSITIONING ANALYSIS

In this section, parameters in positioning analysis were introduced. L1 code DGPS positioning was measured and AR for carrier base positioning was performed in different baseline distance. ASR was estimated to prove the performance of AR.

Five Japanese cities (ICHIKAWA1, ICHIKAWA2, ADACHI, IWAKI and KUJI) were chosen as reference and rover stations. Figure 5.1 shows locations of five cities in positioning analysis. Short distance (about 0.7km), medium distance (about 14.2km), long distance (about 190.9km) and extra-long distance (521.7km) were considered here. Estimation time was 24 hours, and mask angle was 15 degree at each station. Height at each station was 100m.
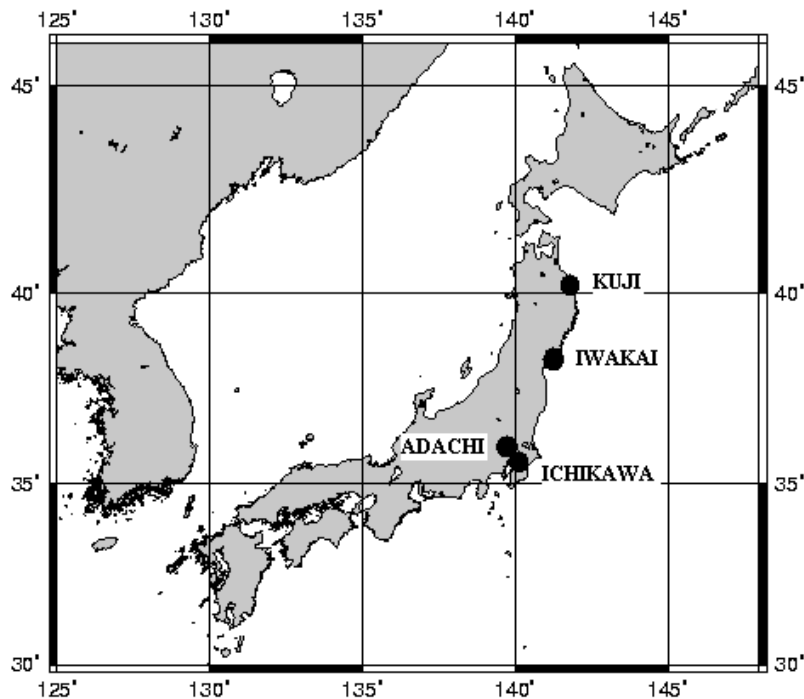
Figure 5.1 Locations of each station in positioning analysis

Baseline	Position	Height (m)	Distance (km)
Reference	ICHIKAWA1	100	
Short	ICHIKAWA2	100	0.698
Medium	ADACHI	100	14.167
Long	IWAKI	100	180.871
Extra-long	KUJI	100	521.715

Table 5.1 Locations of reference and rover stations

Multi-path error on code and carrier signal were only simulated as deflecting from ground, because environment of each station was not considered. Cycle slip was also not considered, single epoch ASR was estimated. Parameters of numerical estimation were shown as following:

- L1, L2 and L5 Signals were generated from GPS triple simulator in 1 Hz,

- GPS Ephemeris: YUMA191 file

- QZSS Orbit: Asymmetric 8-shape orbit option,

- Estimation time: 00:00 UTC - 24:00 UTC, April 21, 2003,

- Satellite Numbers : GPS+QZSS 29+3 ; GPS Only 29

- Mask angle: 15° (Both base and rover stations),

- Antenna carrier offset was simulated as NOVATEL antenna GPS702, c/n0 was calculated from OEM3 receiver,

- No Carrier Smoothing in DGPS positioning and AR

- Ambiguity of L1 signal estimated by using WL OTF algorithm in Dual frequency AR, and EWL method in Triple frequency AR,

- Ambiguity of L5 signal estimated by using GF method was used in triple frequency AR in long and extra long baseline cases, because cycle slip is ignored, 120 second time average of continuous signal was used in GF method

- In AR, with a sampling interval of 2 minutes, total estimation epoch number is 720. After each interval of 2 minutes only one epoch of data is taken processed and analysis. ASR was given in Equation (4.3) in the last chapter.

5.2 NVS & PDOP

As introducing in the last section, NVS and PDOP were important parameters in positioning. Before positioning analysis, NVS and PDOP with or without QZSS at each station were estimated in this section.

5.2.1 NVS at Base and Rover Stations

Table 5.2 gives temporal variations of NVS for 24 hours at each station when mask angle was 15 degree.

	NVS in 24 hours	
	GPS + QZSS	GPS Only
ICHIKAWA1 (Reference Station)		
Min NVS	**7**	4
Max NVS	**14**	11
Mean NVS	**9.71**	7.38
ICHIKAWA2		
Min NVS	**7**	4
Max NVS	**14**	11
Mean NVS	**9.71**	7.38
ADACHI		
Min NVS	**7**	5
Max NVS	**14**	11
Mean NVS	**9.71**	7.40
IWAKI		
Min NVS	**7**	5
Max NVS	**14**	11
Mean NVS	**9.65**	7.37
KUJI		
Min NVS	**6**	4
Max NVS	**14**	11
Mean NVS	**9.52**	7.33

Table. 5.2   NVS in 24 hr at each station

From Table5.2, at least 2 more satellites could be tracked by using QZSS than without QZSS at each station in one day. After using QZSS, mean NVS for 24 hours can be improved about 31.57% at ICHIKAWA1 (Reference Station), 31.57% ICHIKAWA2, 31.22% at ADACHI, 30.94% at IWAKI, 29.88% at KUJI.

5.2.2 PDOP at Base and Rover Stations

Table 5.3 give and PDOP (NVS > 3) when mask angle is 15 degree for 24 hours at each station when mask angle was 15 degree.

	PDOP (NVS > 3) in 24 hours	
	GPS + QZSS	GPS Only
ICHIKAWA1 (Reference Station)		
Min PDOP	**1.30**	1.45
Max PDOP	**4.04**	6.18
Mean PDOP	**1.98**	2.49
ICHIKAWA2		
Min PDOP	**1.30**	1.45
Max PDOP	**4.04**	6.19
Mean PDOP	**1.98**	2.49
ADACHI		
Min PDOP	**1.30**	1.45
Max PDOP	**4.04**	6.19
Mean PDOP	**1.98**	2.49
IWAKI		
Min PDOP	**1.31**	1.47
Max PDOP	**4.03**	6.18
Mean PDOP	**2.00**	2.50
KUJI		
Min PDOP	**1.37**	1.53
Max PDOP	**4.01**	6.18
Mean PDOP	**2.02**	2.52

Table. 5.3 PDOP (when NVS > 3) in 24 hr at each station

According to table 5.3, after using QZSS,

- min. PDOP for 24 hours could be improved about 10.34% at ICHIKAWA1 (Reference Station), 10.34% at ICHIKAWA2, 10.34% at ADACHI, 10.88% at IWAKI, and 10.46% at KUJI. Max. PDOP for 24 hours could be improved about 34.62% at ICHIKAWA1, 34.62% at ICHIKAWA2, 34.73% at ADACHI, 34.79% at IWAKI, and 35.11% at KUJI;
- mean PDOP for 24 hours could be improved about 20.48% at ICHIKAWA1, 20.48% at ICHIKAWA2, 20.48% at ADACHI, 20.0% at IWAKI, and 19.84% at KUJI.

It indicates that position geometry condition was improved using QZSS at each station.

From NVS and PDOP analysis, after using QZSS, NVS and PDOP cold all are improved at base and rover baselines, performance of positioning was expected to be enhanced.

5.3 DGPS POSITIONING IN DIFFERENT BASELINE

In this section, L1 code positioning with or without QZSS in short, medium, long and extra-long baseline was estimated. Carrier smoothing was not used here. Common NVS between reference and rover stations was also discussed.

5.3.1 Common NVS

Common NVS is the important function in differential positioning. Figure 5.2 shows common NVS with or without QZSS for 24 hours in different baseline when mask angle is 15 degree. Figure 5.2.1 indicates in short baseline, figure 5.2.2 indicates in medium baseline, figure 5.2.3 indicates in long baseline, and figure 5.2.4 indicates in extra-long baseline. Table 5.4 summarized temporal variations of common NVS for 24 hours in different baseline cases.
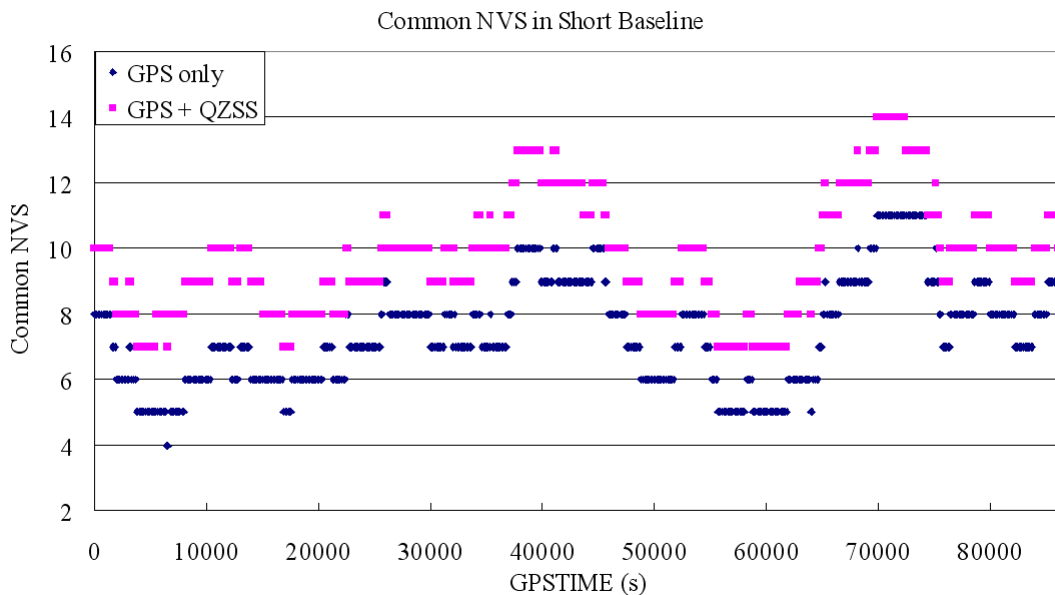
Figure 5.2.1 Common NVS for 24 hr with or without QZSS in short baseline

(mask angle is 15 degree)
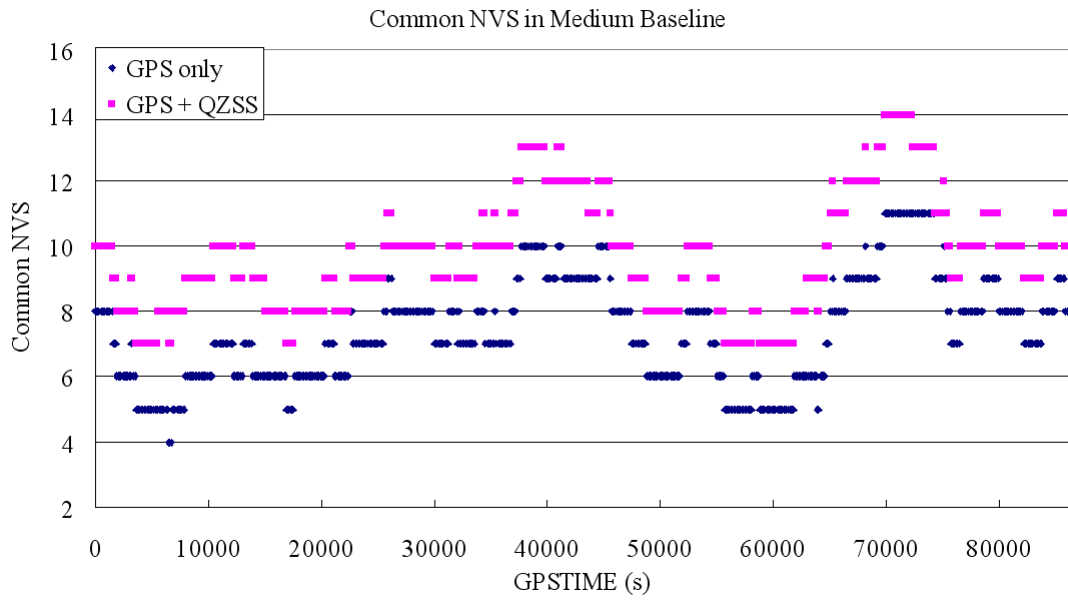
Figure. 5.2.2 Common NVS for 24 hr with or without QZSS in medium baseline (mask angle is 15 degree)
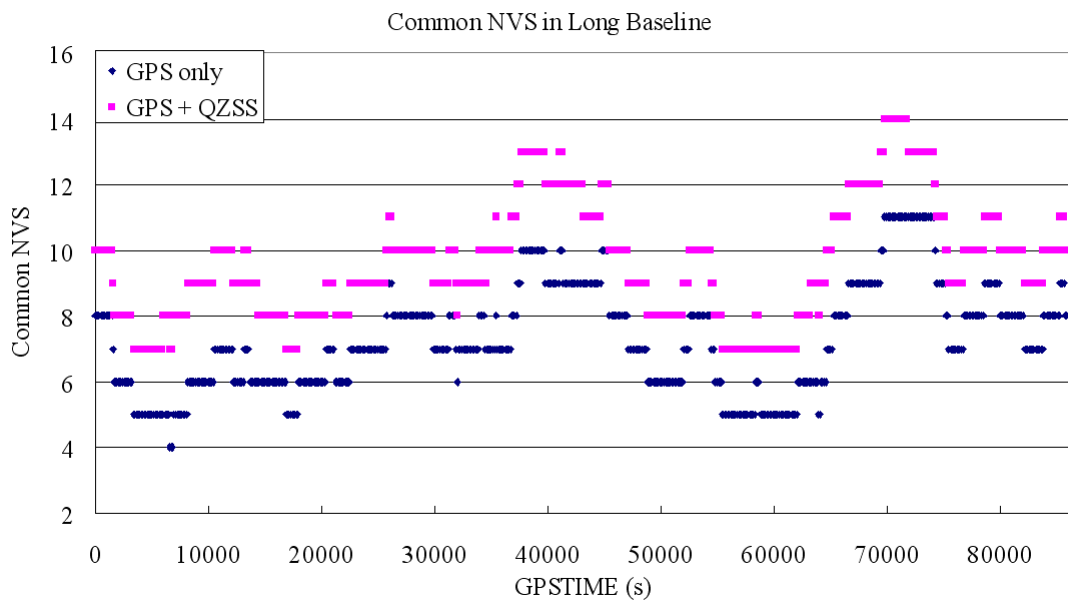
Figure. 5.2.3 Common NVS for 24 hr with or without QZSS in long baseline (mask angle is 15 degree)
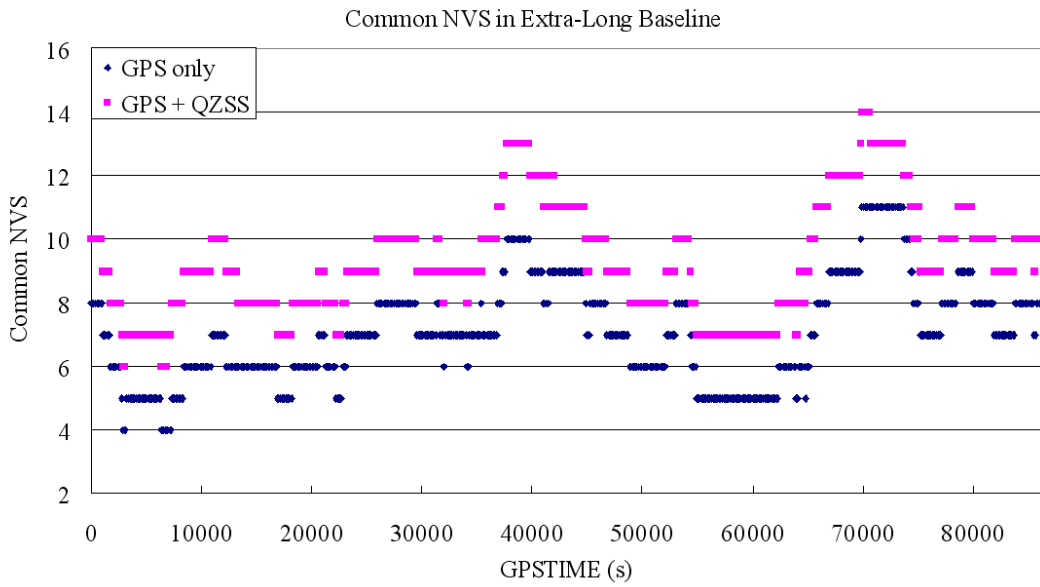
Figure. 5.2.4 Common NVS for 24 hr with or without QZSS in extra-long baseline

(mask angle is 15 degree)

Form figure 5.2 and table 5.4, it was shown that at least **6 common NVS** can be tracked by using QZSS in each cases, mean common NVS for 24 hours can be improved 31.40% in short baseline, 31.57% in medium baseline, 31.55% in long baseline, and 28.45% in Extra long base line. From analysis of NVS, PDOP and common NVS, it indicates that available time for differential positioning, visible satellites and geometry of satellites could all be improved in each baseline or at each station.

Base Line		GPS + QZSS	GPS Only
	Min Comm. NVS	**7**	4
Short	Max Comm. NVS	**14**	11
	Mean Comm. NVS	**9.71**	7.39
	Min Comm. NVS	**7**	4
Medium	Max Comm. NVS	**14**	11
	Mean Comm. NVS	**9.71**	7.38
	Min Comm. NVS	**7**	4
Long	Max Comm. NVS	**14**	11
	Mean Comm. NVS	**9.59**	7.29
	Min Comm. NVS	**6**	4
Extra-long	Max Comm. NVS	**14**	11
	Mean Comm. NVS	**9.32**	7.10

Table. 5.4 Common NVS with or without QZSS in different baseline distance for 24 hr

5.3.2 DGPS Positioning

L1 Code Positioning in Short Baseline
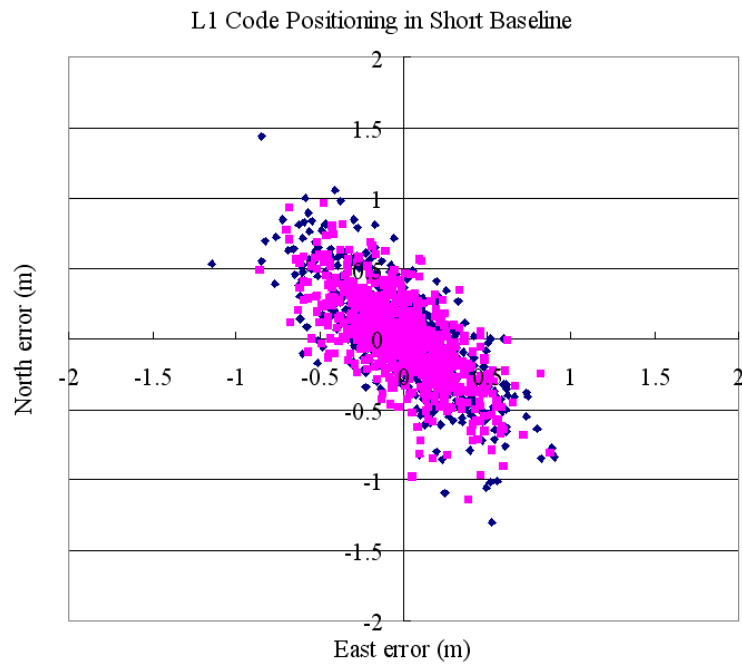
Figure. 5.3.1 L1 code positioning in short baseline

L1 Code Positioning in Medium Baseline

Figure. 5.3.2   L1 code positioning in Medium baseline

L1 Code Positioning in Long Baseline
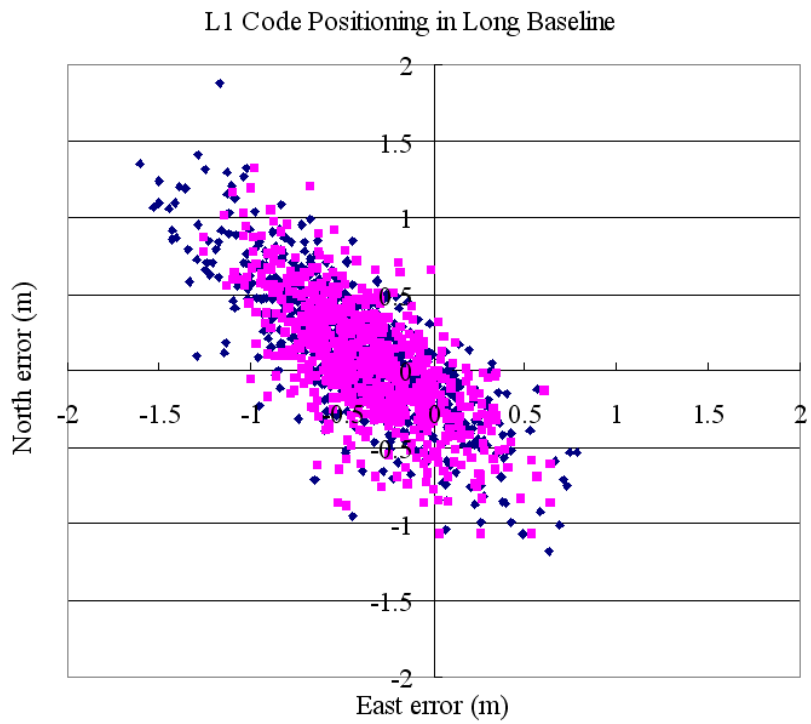
Figure. 5.3.3   L1 code positioning in long baseline

L1 Code Positioning in Extra-Long Baseline
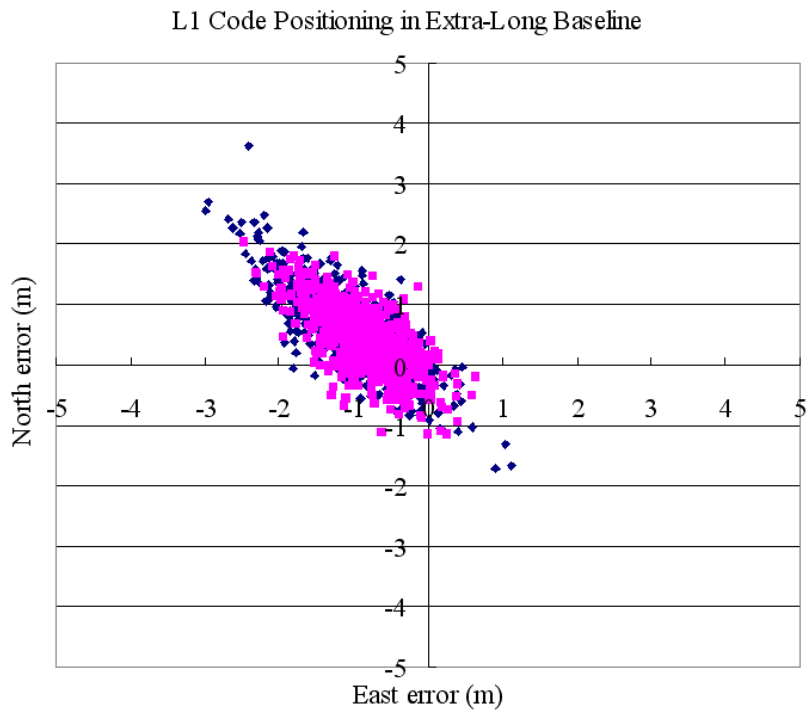
Figure 5.3.4 L1 code positioning in extra-long baseline

In this part, L1 code positioning for 24 hr (Comm. NVS > 4) with or without QZSS in each baseline was estimated when mask angle was 15 degree. Figure 5.3 shows DGPS results in different baseline (Comm. NVS > 4), figure 5.3.1 shows which in short baseline, figure 5.3.2 shows which in medium baseline, figure 5.3.3 shows which in long baseline and figure 5.3.4 shows which in extra-long baseline.

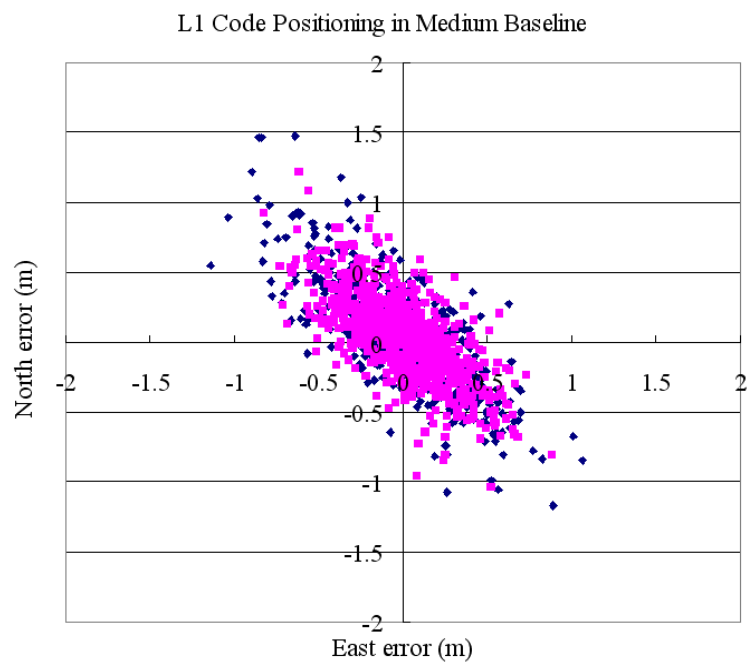Table 5.5 summarized the L1 code DGPS positioning results when Comm. NVS > 4. Because using extra satellite with QZSS, accuracy of DGPS can be improved 9.0% in horizontal direction and 10.20% in vertical direction in short baseline, 10.64% in horizontal direction and 13.46% in vertical direction in medium baseline, 15.83% in horizontal direction and 16.92% in vertical direction in long baseline, 19.21% in horizontal direction and 26.32% in vertical direction in extra long baseline. After using QZSS with GPS, availability time for DGPS and accuracy of DGPS could be improved in each baseline, obviously in long and extra long distance.

Baseline		GPS + QZSS	GPS Only
Short	CommNVS > 4	**100%**	99.72%
	X (m)	**0.30**	0.34
	Y (m)	**0.27**	0.29
	2drms (m)	**0.81**	0.89
	H (m)	**0.44**	0.49
Medium	CommNVS > 4	**100%**	99.58%
	X (m)	**0.31**	0.35
	Y (m)	**0.28**	0.31
	2drms (m)	**0.84**	0.94
	H (m)	**0.45**	0.52
Long	CommNVS > 4	**100%**	99.58%
	X (m)	**0.38**	0.44
	Y (m)	**0.33**	0.41
	2drms (m)	**1.01**	1.20
	H (m)	**0.54**	0.65
Extra-long	CommNVS > 4	**100%**	98.47%
	X (m)	**0.53**	0.64
	Y (m)	**0.48**	0.61
	2drms (m)	**1.43**	1.77
	H (m)	**0.70**	0.95

Table 5.5 Standard deviation (m) in L1 code DGPS positioning (CommNVS > 4)

with or without QZSS when mask angle is 15 degree

5.4 ASR IN DIFFERENT BASELINE

In this section, L1 signal AR with or without QZSS in different baseline was performed when mask angle was 15 degree. The case of GPS with QZSS was considered as triple frequency system, and the case of GPS only was considered as dual frequency system. ASR in 24 hours with or without QZSS in different baseline was estimated here. Higher number of ASR means more reliable and more efficient in AR.

Three triple frequency AR methods which were proposed in this chapter, WL method, GF method and IF method, have been introduced in chapter 3.

5.4.1 ASR in Short or Medium Baseline

WL method was used in short and medium baseline. In case of GPS with QZSS, triple frequency WL method was proposed, and in case of GPS only, dual frequency WL method was used.

Table 5.6 gives ASR of primary signal (common NVS > 4) in 24 hour in short and medium baseline when mask angle was 15 degree. From Table 5.6, using GPS with QZSS, epoch of common NVS mort than 5 in one day could be improved about 0.28% in the case of short baseline, and about 0.42% in the case of medium baseline, available time for carrier based positioning was improved to be all of the day. RTK positioning could be possible in 24 hours.

	GPS+QZSS (triple frequency system)	GPS Only (dual frequency system)
Short baseline		
Epoch CommNVS < 5	0	2
Success	**719**	711
CommNVS >4	100.0%	99.72%
ASR (CommNVS >4)	**99.87%**	99.03%
Medium distance		
Epoch CommNVS < 5	0	3
Success	**699**	651
CommNVS >4	100.0%	99.58%
ASR (CommNVS >4)	**97.08%**	90.79%

Table 5.6 ASR of primary signal for 24 hour in short or medium baseline (CommNVS >4)

ASR (common NVS > 4) in 24 hours could be improved about 0.85% in short baseline, and about 6.93% in medium baseline. Especially, it could be improved to be more than 99.5% when in short base line in case of GPS with QZSS.

5.4.2 ASR in Long or Extra-long Baseline

GF AR method and IF AR method was proposed for long and extra long baseline in GPS with QZSS. Evaluating impact of GF and IF methods in longer baseline, WL method was also estimated here. In the case of AR with GPS only, dual frequency WL method was used. Table 5.7 gives ASR of primary signal (common NVS > 4) in 24 hour in short and medium baseline when mask angle was 15 degree.

From Table 5.7, using GPS with QZSS, epoch of common NVS mort than 5 in one day could be improved about 0.42% in the case of long baseline, and about 1.53% in the case of extra-long baseline, available time for carrier based positioning could also be improved to be all of the day in longer baseline, obviously in extra-long baseline.

ASR using WL method could not be improved obviously using GPS with QZSS, however, using proposed triple frequency GF and IF methods, ASR could be improved at more than 80% in long baseline, and to be at more than 60.0% in extra-long baseline. That proposed GF method and IF method was effective in longer baseline AR could be concluded.

	GPS+QZSS (triple frequency system)			GPS Only (dual frequency system)
Long baseline				
Epoch CommNVS < 5	0			3
CommNVS >4	100.0%			99.58%
	WL	GF	IF	
Success	63	**602**	**635**	45
ASR (CommNVS >4)	8.75%	**83.61%**	**88.19%**	6.28%
Extra-long distance				
Epoch CommNVS < 5	0			11
CommNVS >4	100.0%			98.47%
	WL	GF	IF	
Success	4	**434**	**473**	2
ASR (CommNVS >4)	0.55%	**60.28%**	**65.69%**	0.28%

Table 5.7 ASR of primary signal for 24 hour in long or extra-long baseline (CommNVS >4)

Between two long baseline AR methods, ASR estimated in IF method was higher than which in GF method in both of long and extra-long baseline cases, it indicates that IF method could estimate ambiguity more accuracy and effectively.

5.5 SUMMARY

In this section, positioning in short, medium, long or extra-long baseline with or without QZSS was discussed. After using QZSS, NVS and PDOP could all be improved at each station.

In different baseline L1 code DGPS positioning, after using QZSS,
- in short baseline, accuracy could be improved 9.0% in horizontal direction, 10.20% in vertical direction
- in medium baseline, accuracy could be improved 10.64% in horizontal direction,13.46% in vertical direction,
- in long baseline, accuracy could be improved 15.83% in horizontal direction and 16.92% in vertical direction,
- in extra-long baseline, accuracy could be improved 19.21% in horizontal direction and 26.32% in vertical direction.

It indicates that accuracy of DGPS could be improved at each baseline, obviously in longer baseline.

In different baseline RTK positioning, after using GPS with QZSS,
- in short baseline, epoch of common NVS more than 5 could be improved about 0.28%, ASR could be improved at more than 99.5% using triple frequency WL method,
- in medium baseline, epoch of common NVS more than 5 could be improved about 0.42%, ASR could be improved about 6.93% using triple frequency WL method,
- in long baseline, epoch of common NVS more than 5 could be improved about 0.42%, ASR could be improved at more than 80.0% using GF or IF method,
- in extra-long baseline, epoch of common NVS more than 5 could be improved about 1.53%, ASR could be improved at more than 60.0% using GF or IF method.

Because using extra satellites with QZSS, there are at least 6 common NVS at each baseline, RTK positioning could be performed in all of one daytime, which was the most influence in extra-long baseline. Using extra signal (L5 signal) and better geometry positioning with extra satellite integrating with QZSS, AR could all be improved at each baseline using proposed AR methods, even if in the case of longer baseline.

From different baseline positioning with QZSS analysis in this chapter, reliability and efficiency of QZSS could be proved.

CHAPTER 6
CONCLUSION AND RECOMMENDATION

The major of this thesis is to prove impact from integrating GPS and Japanese QZSS. The thesis is composed three parts. The first part shows the various AR methods using linear combination with three frequencies signals, the second part indicates performance of QZSS, and the third part points on the impact in positioning with QZSS.

6.1 CONCLUSION

1. Because now the third frequency signal (L5) has not been transmitted and QZSS is also under the preparation stage, triple frequency simulator, which was based on several range error and noise model, was developed for numerical analysis.

2. Performance with QZSS in East Asian region or in local Japan and surrounding region was shown in this research. It has been shown that QZSS not only improves the availability and geometry of satellites, but also enhances the reliability and efficiency of GPS positioning in the near Japan area, and also in most of the East Asian region.

3. Because the QZSS satellite orbit was Asym-8-shaped satellite orbit, the feature of Asym-8-shaped satellite orbit was shown in this research. From analysis among four optional QZSS, that Asym-8-shaped satellite orbit is best for Japan region could be concluded.

4. L1 code DGPS positioning with QZSS in different baseline was estimated in this research. After using QZSS, accuracy of positioning could be all improved in each baseline positioning, obviously in longer baseline.

5. Primary signal AR in different baseline was interested in this research. After using QZSS, with extra satellite, it was possible that RTK positioning could be performed in all time of the day, and with extra signal, more linear combination signal could be developed, ASR could be improved in each baseline using proposed AR method.

6.2 RECOMMENDATION

Here are some recommendations for the future work on the study of QZSS:

1. Study on integrating QZSS and European Galileo is the next stage in the research.

2. In this research, numerical estimation was used data from triple simulator. When QZSS becomes available, it is necessary to evaluate efficiency of proposed AR methods.

3. It is necessary to study how to shorten the initial time in triple frequency GF or IF AR method in longer baseline.

REFERENCE

Alfred Leick, (1995): "*GPS Satellite Surveying*", A WILEY-INTERSCIENCE PUBLICATION, New York, 1995.

Frank Czopek, Gerald Mader, (2002): "*Calibrating Antenna Phase Centers*", GPS World, May, 2002.

GSI (2004): "*GEONET New Services*" Geographical Survey Institute, Japan
http://www.gsi.go.jp/WNEW/PRESS-RELEASE/2004/0329-1.htm

GPS World, (2007): "*GPS Modernization Fits and Starts*", GPS World, Sep 2007

H.Isshiki (2003): "*An Approach to Ambiguity Resolution in Multi Frequency Kinematic Positioning*", Proceedings of 2003 International Symposium on GPS/GNSS, 545-552

International GPS Service (IGS), (2005): "IGscb.ttp://igS Product Table",
from http://igscb.jpl.nasa.gov/components/prods.html, Feb, 2005

Inside GNSS, (2007): "*Successful GPS Block IIR-M Spacecraft Launch*", *Gibbons Media & Research LLC,* Inside GNSS, 2007

Japan Aerospace of Exploration Agency, (2007): "Interface Specification of QZSS (IS-QZSS) Ver. 0.1" http://qzss.jaxa.jp/is-qzss/IS-QZSS_01_E.pdf, June, 2007

Jayanta Kumar Ray (1999). "*Mitigation of GPS Code and Carrier Phase Multipath Effects Using a Multi-Antenna System*" UCGE Reports Number 20136, 1999

Jon Person, (2004): "*Writing Your Own GPS Applications: Part 2 - Causes of Precision Error*", 2004

Jung, J, P. Enge, and B. Pervan (2000): "*Optimization of Cascade Integer Resolution with Three Civil GPS Frequencies*". Proceedings of the ION 2000, 19-22 Sep, Salt Lake City, UT, pp.2191-2201

Kaplan, E. D. (1996). "*Understanding GPS - Principles and Applications*", Artech House Publisher, Boston, London, 1996

Klobuchar, John (1996). "*A. Ionospheric Effects on GPS, in global positioning system: Eheory and Applications*", Vol. I, B. Parkinson, J Spilker, P. Axelrad, and P. Enge. American Institute of Aeronautics and Astronautics, pp.485-515, 1996

Kogure, S., Kawano, I., and Kajii, M. (2003): "The Status and Experiment Plan for GPS Augmentation Using Quasi-Zenith Satellite System (QZSS)." Presentations at 4th CGSIC IISC Asia Pacific Rim Meeting, Tokyo, Japan, 2003

Lt Col John Wilt, (2001): "*GPS Modernization*", Civil GPS Service Interface Committee (CGSIC), Salt Lake City, UT, 2001

Miyano Tomoyuki, Kawano Isao, Mokuno Masaaki, Suzuki Takashi, (2000): "I*mprovement of Navigation accuracy for Spaceborne GPS Receiver without SA(Selective Availability)*", Vol.100, No.244(20000721) pp. 49-52, 2000

Navigation Center., (2006). "*YUMA Almanacs.*" U.S. Coast Guard Navigation Center, 2006 (http://www.navcen.uscg.gov/gps/almanacs.htm)

Parkinson, B. W., Spilker, J. J., Axelrad, P., and Enge, P. (1996): "*Global Positioning System: Theory and Applications*", American Institute of Aeronautics and Astronautics, Inc., 370 L'Enfant Promenade, SW, Washington, DC 20024-2518., 1996

Petrovski, I. G., Ishii, M., Torimoto, H., Kishimoto, H., Furukawa, T., Saito, M., Tanaka, T., and Maeda, H., (2003): "*QZSS - Japan's New Integrated Communication and Positioning Service for Mobile Users*". GPS World, pp.24-29., 2003

Richard D. Fontana, Wai Cheung, Tom Stansell, (2001): "*The modernized L2 Civil Signal: Leaping Forward in the 21st Century*", Richa*GPS Modernization Fits and Starts*", GPS World, pp 29—34, Sep 2001

Ronald R. Hatch, (1982): "*Synergism of GPS Code and Carrier Measurements, Proceedings of the Third International Geodetic Symposium on Satellite Doppler Positioning*", New Mexico State University, pp.1213-1232. 1982

Ronald R. Hatch, (2006): "*A New Three-Frequency, Geometry-Free, Technique for Ambiguity Resolution*", ION GNSS 2006 proceedings, Fort Worth, U.S., Sep. 2006

Sakai Takeyasu, Fukushima Sonosuke, Takeichi Noboru, Aramaki, Masae, Ito Ken, (2007): "*Observation of the GPS Second Civil Signal (L2C)*", Technical report of IEICE, Vol. 106. No.471, pp(20070112), pp. 75-80, 2007

Saastamoinen, J. (1973). "*Contribution to Theory of Atmospheric Refraction*", Bulletin Geodesique, Vol. 105, Sep. 1972, Vol. 106, Dec. 1972, Vol.107, March 1973

Satoshi Kogure, Mikio Sawabe, Motohisa Kishimoto, (2006): "*Status of QZSS Navigation System in Japan*", ION GNSS 2006 proceedings, Fort Worth, U.S., Sep. 2006

Satoshi KOGURE, (2007): "*QZSS/MSAS Status*", Civil GPS Service Interface Committee (CGSIC), Salt Lake City, UT, 2001

Swider, (2001): "*GPS Policy Update*", Civil GPS Service Interface Committee (CGSIC), Salt Lake City, UT, 2001

T. Tsujii, M. Murata, M. Harigae, T. Ono and T. Inagaki, (1998): "*KINGS and Flight Test Evaluation*", Technical Report of National Aerospace Laboratory, TR-1357T, 1998

THE WHITE HOUSE, (2000): "*STATEMENT BY THE PRESIDENT REGARDING THE UNITED STATES' DECISION TO STOP DEGRADING GLOBAL POSITIONING SYSTEM ACCURACY*", Office of the Press Secretary, THE WHITE HOUSE, 2000

U.S. Department of Transportation (DoT), (2003): "*Notational Civil GPS Service   GPS Augmentations & GPS Modernization* ", Technical Brochure, "http://www.igeb.gov//outreach//civil-gps-brochure.ppt", 2003

U.S. DoD., (2007): "*DoD Permanently Discontinues Procurement Of Global Positioning System Selective Availability*", U.S. Department of Defense, IMMEDIATE RELEASE, No. 1126-07, Sep 2007

Verhagen, S. (2002). "*Studying the Performance of Global Navigation Satellite Systems - A New Software Tool.*" GPS World, pp60-65, 2002

Wu, F., Kubo, N., and Yasuda, A., (2004): "*Performance Analysis of GPS Augmentation Using Japanese Quasi-Zenith Satellite System. Earth*", Planets and Space, 56(1), pp.25-37., 2004

Yun Zhang, Falin Wu, Nobuaki Kubo, Akio Yasuda, (2003): "*TEC measurement by single dual-frequency GPS receiver*", Proceedings of the 2003 International symposium on GPS/GNSS, pp351-358, Nov. 2003

Yun Zhang, Nobuaki Kubo, Akio Yasuda. (2005): "*The Benefit from Triple Frequencies in Ambiguity Resolution*" The Journal of Japan Institute of Navigation, Vol.112 pp219-227. March 2005

Yun Zhang, (2005): "*The Benefit of Triple Benefit of Triple Frequency System in Ambiguity Resolution*", Master Thesis, 2005

Yun Zhang, (2006): "*Performance Analysis of GPS Augmentation Using Quasi-Zenith Satellite System in Local Japan Area*", ION GNSS 2006 proceedings, Fort Worth, U.S. Sep. 2006

Yun Zhang, Falin Wu, Akio Yasuda (2007): "*Impact of Integrated GPS and The Quasi-Zenith Satellite System in the East Asian Region*", Transactions of the Japan Society for Aeronautical and Space Sciences, Vol.50 No.168, pp105-112, 2007